Hamburg University of Applied Sciences

Faculty of Life Sciences

Modelling the integration of heat pumps for large heating applications into the power grid

Master's Thesis submitted in partial fulfillment of the requirements for the academic degree

Master of Science (M.Sc.)

in the degree program Renewable Energy Systems – Environmental and Process Engineering

submitted by

Lukas, Eisenbarth

[redacted]

Hamburg, July 27, 2025

Supervisor: Prof. Dr. Hans, Schäfers (HAW Hamburg)

Supervisor: Master-Ing. Martin, Grasenack (CC4E)

The thesis was written in collaboration with the CC4E.

Summary

Name of Student

Lukas Eisenbarth

Title of the Paper

Modelling the integration of heat pumps for large heating applications into the power grid

Keywords

Large-scale heat pump modelling, power grid analysis, district heating grid, grid support, heat pump design, techno-economic optimisation

Abstract

This thesis investigates the impact of large-scale heat pump operation on the energy infrastructure in the city of Hamburg. The objective is to determine how the operation of the large-scale heat pumps can be optimised economically, with respect to grid support and the fulfilment of heat demand requirements. For this purpose, a Python-based model was developed, and the system characteristics of the large-scale heat pumps and the surrounding infrastructure were mapped and linked to various input data regarding heat demand, price signals and grid data. The simulation results show that a price-led operation performs better than a heat-led operation when compromising between operating costs and district heat demand coverage. Furthermore, the results indicate the future potential for large-scale heat pumps in Hamburg to replace conventional power plants in the context of redispatch interventions. Here, in a simplified approach a maximum coverage rate of 51.9 % of redispatch-related energy in Hamburg is achieved by adjusting the large-scale heat pump operation in response to grid signals in 2024.

Table of contents

List of Figures

List of Tables

List of abbreviations

HP	heat pump
LSHP	large-scale heat pump
$\boldsymbol{COP}$	coefficient of performance
CHP	combined heat and power
HTHP	high temperature heat pump
SLP	standard load profil
$\boldsymbol{KW}$**-value**	'Kundenwert'
TSO	transmission system operator
BGM	balancing group managers
CHP	combined heat and power
CC4E	Competence Center für Erneuerbare Energien und EnergieEffizienz

1 Introduction

1.1 Motivation and Preface

In the best interests of our society, the transition to a fully renewable energy supply must be driven forward as quickly as possible. This is illustrated by the latest AR6 Synthesis Report published in 2023 by the IPPC, which according to Chairman Housung Lee conveys a clear message for action: “We are walking when we should be sprinting”, he commented at the press conference launch [1, 2]. Furthermore, the shift to sustainable energies is not only essential for environmental protection, but also plays a major role in breaking free from geopolitical ties and laying the foundations for peaceful global structures by reducing the potential of conflicts. The latest edition of the conflict barometer published by the Heidelberg Institute for International Conflict Research in 2023 shows resources, including those used for nuclear and fossil energy, as the second most common cause of political conflicts globally [3, 4]. To ensure an independent energy supply, the European Commission presented the REPowerEU plan in May 2022, which aims to mobilize up to 300 billion Euros to increase the share of renewable energies in the energy mix up to 45 % by 2030 [5, 6, 7]. In addition, it is targeted to realize the project “Fit for 55” by reducing the CO_2 emissions until 2030 by 55 % compared to 1990 and reaching climate neutrality by 2050 in line with the European Green Deal [7]. The national climate targets in Germany are even more ambitious and mandate a reduction in greenhouse gases of 65 % by 2030 compared to the reference year 1990 and net greenhouse gas neutrality by 2045 (KSG, 2020, § 3 (1) No. 1). While the share of renewable energies in electricity consumption had risen to 54.4 % in 2024 and is set to rise further to 80 % by 2030, the share of renewable energies in final energy consumption for heating and cooling was only 18.1 % in 2024 (EEG, 2023, § 1 (2)) [8]. Considering the fact that consumption in the heating and cooling sector accounted for more than half of total final energy consumption in Germany in 2023, there is a pressing need to expand renewable energies in the heating sector to reach the objectives according to the REPowerEU plan [9]. For this reason, the previous German government set the target in its coalition agreement 2021 of generating 50 % of heat from renewable energy sources by 2030 [10]. An essential part of achieving this goal is the expansion of district heating supply and increasing the share of renewable energy generation in district heating [11, 12]. Since the production of district heat from renewable energy sources peaked in 2021 with 24.3 TWh_{th} and did not increase thereafter [8], the need for development in this area is urgently. In the transformation process the integration of large-scale heat pumps (LSHPs) in the district heating grid is a key factor [11, 13]. It is assumed that LSHPs will provide approximately 58 to 70 % of the district heating supply in 2045. Therefore, an average expansion of the capacity provided by LSHPs from 4.0 up to 4.9 GW per year is required by 2045 [11, 13]. To enable a rapid roll-out of LSHPs a holistic system integration into the energy infrastructure including the precise coordination and communication between the power grid and district heating network is necessary [14, 15]. Thus, sector coupling

between the electricity and heating sector plays a major role in achieving a technically successful and economically most profitable operation. This is crucial to reduce energy costs and increase the social acceptance of the population for progress in the energy transition [16]. To accelerate the transformation process, the Heat Planning Act, which came into force on 1 January 2024, requires all existing municipalities with a population of over 100,000 to develop municipal heating plans at the latest by 30 June 2026 (WPG, 2024, § 4 (2) No. 1). Here, the city of Hamburg – which has with 860 km one of the biggest district heating networks in Germany – takes a pioneering and leading position [17]. The city's municipal heat planning stipulates the construction of two river-source LSHPs with a total capacity of around 225 to 255 MW_{th} and a wastewater LSHP with a capacity of 60 MW_{th} to supply its district heating network [18, 19, 20]. The announced projects are the largest heat pump (HP) projects in Germany to date. Therefore, they are in special focus and have a trend-setting effect on future project planning in Germany.

1.2 Objective of the Work

The objective of this study is to simulate the operation of the LSHPs planned in the district heating network of Hamburg and to analyze their interactions with the energy infrastructure – in particular, the electricity sector and the power grid. In this context, the plant design including technical operational management as well as the external operating conditions through the energy infrastructure shall be represented as realistically as possible. First, the important system properties and input parameters shall be determined, and time series shall be created to enable a simulation of one year in 15-minute resolution. In this regard, both the demands of the heating sector and the requirements of the electricity sector – shaped by market signals and grid operation factors – shall be taken into account. Subsequently, a simulation framework will be constructed which reads in the data time series and enables the simulation of heat pumps (HP) operation over the course of one year. As part of this process, different operating strategies shall be developed and implemented into the simulation framework. Thereafter, the HP design shall be refined, and the operating strategies shall be simulated considering various scenarios. Their impacts on HP operation as well as on the heating and electricity sector shall be analysed regarding heat demand coverage, cost-effective operation, contribution to grid support and further criteria.

The simulation framework including the HP model is to be designed to allow flexible configuration of system properties, so that single parameters such as thermal storage size, compressor efficiency, or economic factors can be adjusted, and the integration of new time series data is facilitated. This shall enable the modelling of different scenarios and support future development of the model beyond the scope of this work.

2 Context and Framework

In the following sections, the impact of the rollout LSHPs on both the heating sector and the electricity sector is discussed. Furthermore, the interactions between LSHPs and the electricity sector, as well as the factors for successful integration of LSHPs into the electricity sector, are analyzed. This is crucial for operating strategies of LSHPs. In addition, the development status of Hamburg's district heating network and the integration of LSHPs within it is described. Embedding the system within the existing infrastructure is essential to identify the operational constraints and requirements for LSHPs.

2.1 Impact of LSHPs in Heat Transition

The subsequent chapter outlines the role of LSHPs in heat transition.

The heating sector is the sector with the largest share of final energy consumption in Germany. At 1,259 TWh_{th}, heating and cooling consumption in Germany accounted for around 55.5 % of final energy consumption (2,268 TWh) in 2023 [9]. In the same year the district heating demand in turn accounted with 100.0 TWh_{th} for 8.0 % of the total heat and cooling demand with only 21.1 % of district heat being generated from renewable energies [8, 21]. According to the latest long-term O45-scenarios developed by Fraunhofer ISI the district heat demand will increase to a range between 140 to 150 TWh_{th} by 2045 [22]. Considering the fact that the national target of Germany is to reduce the total final energy demand by 45 % to reach a minimum of approx. 1,400 TWh by 2045 compared to the reference year 2008 (2,550 TWh) the share of district heating in total final energy demand is expected to increase from 4.4 % to around 10 – 11 % (EnEfG, 2023, § 4 (2)). This development is illustrated in Figure 1.

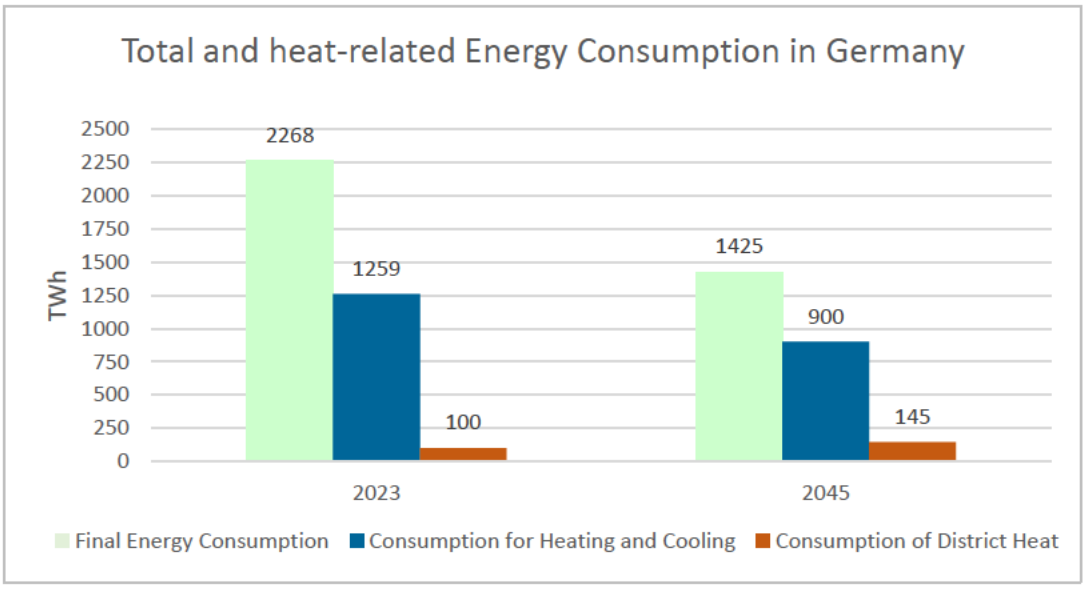

Figure 1: Development of total and heat-related energy consumption [9, 21, 22, 23] (own illustration)

Therefore, the importance of district heating in the heat transition is growing. In 2020, around 465 district heating network operators and numerous local and neighbourhood heating providers were

documented as operating nearly 3,800 heating networks with a total pipeline length of 31,252 km [13]. However, district heating networks are expected to be significantly expanded in the future. The number of newly connected buildings ranges from 72,000 to 140,000 per year, and an average of approximately 800 km of new pipeline is assumed to be laid annually until 2045. A key factor for the expansion process of heating networks is the successful increase of energy production by LSHPs. Currently, the heat generation from LSHPs still covers only 0 to 1 % of the whole district heat demand [13, 21]. But until 2045 LSHPs shall dominate the district heating sector and cover 58 to 70 % of its demand [11, 13]. According to the O45-scenarios the district heat generation will increase to a range between 156 and 167 TWh_{th} by 2045 [11, 24]. The forecast of rising installed capacity by LSHPs is shown for the scenario of the electricity-based future energy supply in Figure 2.

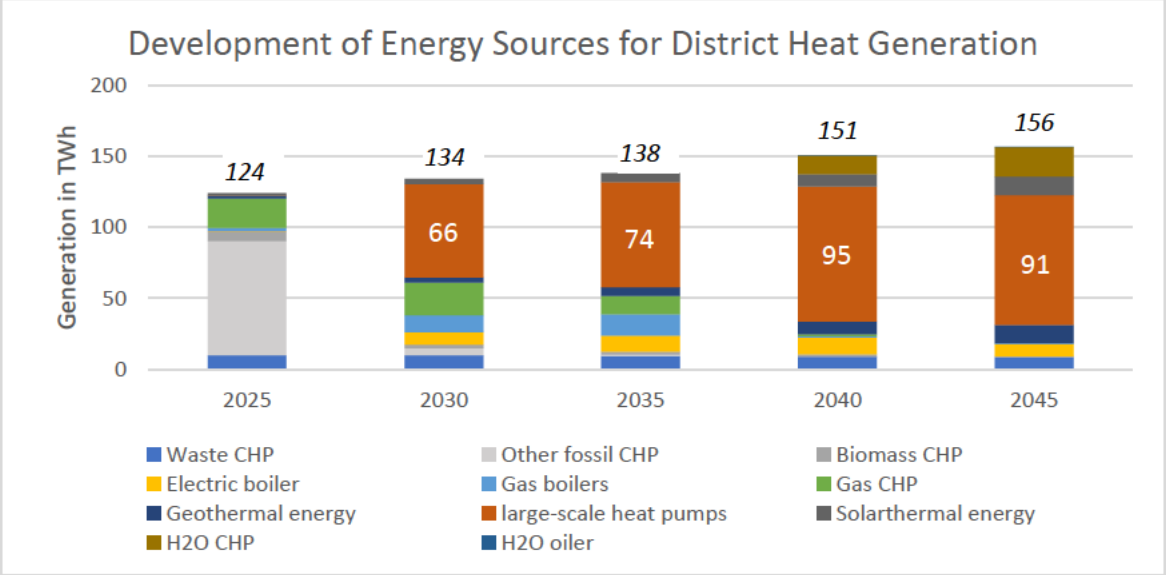

Figure 2: Development of energy sources for heat generation in German heating grids [11]

Anticipating this increase in energy production by LSHPs an annual growth of 4.0 – 4.9 GW_{th} installed is expected [11, 13]. Here economic viability for new projects is essential. To secure the necessary capital for the investments, certain risks, such as connection rates for the expansion of heating networks, are hedged by the public sector [13]. However, the state's intervention in determining district heating connections for customers raises concerns and challenges in terms of consumer protection, as each district heating network is a local monopoly and consumers have no option to switch providers in the event of price increase [25, 26, 27]. The planned price regulation measures to avoid disproportionately high prices contain a lot of potential for conflict between providers and consumers [28]. Therefore, ensuring a cost-optimized operation of LSHPs is crucial for gaining public acceptance of the district heating transition. Hence, a successful LSHP roll-out requires integrated planning across heat and electricity sectors, along with technically optimized system designs.

2.2 Interaction of LSHPs with the Power Grid and Electricity Market

The following section analyses the interactions between the electricity grid, the electricity market and the operation of LSHPs. Here, it is examined how price signals and grid-supportive requirements influence the operation of LSHPs and which effects must be considered during the modelling process.

The German electricity grid operates with alternating current and is divided into four voltage levels: extra-high, high, medium, and low voltage [29]. It is part of the European interconnected grid, which must be kept constant at 50 Hz to ensure stable grid operation. In this system, the power fed into the grid must always match the power withdrawn, as any imbalance can lead to frequency deviations, which – if not corrected – can ultimately cause a grid collapse. Due to the volatile operation of renewable energy generators, maintaining the correct balance between feed-in and withdrawal of power in the electricity grid is one of the greatest challenges of the energy transition [30]. Electric heat generators such as LSHPs can be controlled flexibly and are capable of compensating fluctuations in the power grid. If the low electricity generation costs of renewable energies lead to low electricity procurement costs for LSHPs, the LSHPs can be primarily operated during periods of high renewable electricity production [13]. Excess heat that is not immediately needed is stored in large thermal storage systems. During periods of heat demand when renewable electricity generation is low – and market electricity prices are usually higher – this demand is covered by the previously charged heat storage and other heat generation technologies. This flexible operation of LSHPs supports the power grid, reduces the curtailment of renewable electricity, and improves the carbon footprint of heat generation, thus lowering the operational costs [31]. To make optimum use of favourable electricity prices and the supply of renewable electricity, it is anticipated that in the future the share of LSHPs in heat generation will rise sharply at moments when the residual load is low [13]. Therefore, the installed capacity of LSHPs is intended to be oversized to enable this operational flexibility. However, it must be considered that an insufficient number of full-load hours leads to higher specific heat generation costs, as investment costs then have a disproportionately large impact [13, 31, 32]. A precise balance between system serviceability and economic efficiency is therefore crucial. In general, it is assumed that the most important factor for a successful market ramp-up of LSHPs is a favourable ratio between electricity procurement costs to gas prices on the market [13]. Therefore, in the scope of this work a price-driven operation strategy based on electricity market signals is investigated.

The German electricity market is essentially divided into two areas, the energy-only market and the market for system services, including the capacity markets [33]. The energy-only market trades solely electricity that is produced, while capacity markets, such as the balancing services market, remunerate the provision of capacity or the readiness to deliver power when needed for interventions that safeguard security of supply. Thus, the energy-only market is supplemented by the market for system services which ensures system stability and security of supply [33]. To ensure optimal grid planning,

balancing group managers (BGMs)[1] must submit accurate quarter-hourly forecasts of generation and consumption for the following day to the transmission system operator (TSO) [29, 30]. Deviations from forecasts require immediate corrective actions by the TSO to maintain system stability, especially regarding frequency and voltage control (EnWG, 2025, §§ 13, 14). These actions are carried out by the activation of positive and negative control energy, which is procured via the balancing services market [33]. Positive control energy is the electricity that is fed into the grid to counteract falling grid frequency and negative control power is electricity that is taken from the grid to prevent excessively high grid frequencies. Control energy is divided into primary control power, which balances fluctuations in the grid within seconds, secondary control power, which intervenes within five minutes, and minute reserve, which is used to balance the grid frequency within quarter hours [29, 33]. To date, LSHPs are not known to be used for system services for the provision of control energy, as they usually do not fulfil the required response times for primary and secondary control. In principle, however, the provision of minute reserve by LSHPs is expected in the future [13, 34]. Another system service that is regulated by the system service market is the capacity to compensate for grid congestion [33]. If the cross-section of the power cable in one area is too small to transport a large amount of electricity, this leads to an overload and a bottleneck in the power grid in this area. In such cases, the grid operator must take measures aimed at changing the geographical distribution of electricity feed-in while keeping the total feed-in volume constant to ensure the security of supply for customers located downstream of the congestion point [35]. This means that electricity production must be reduced upstream of the congestion point and increased downstream of it. Measures to eliminate grid bottlenecks include redispatch interventions, feed-in management, and the regulation of controllable consumption units – also including LSHPs (§13 EnWG). To date during a redispatch intervention, mostly two conventional power plants with matching adjustment capacity are involved. One plant, located upstream of the anticipated bottleneck, is instructed to reduce its power output, while the second plant, situated downstream of the bottleneck, is instructed to increase its power production. Here operators of affected plants are entitled to compensation for economic disadvantages caused by redispatch. The costs for redispatch interventions are currently covered by grid usage fees, which are ultimately borne by the end users [33]. However, the issue of grid congestion could be addressed much more efficiently through the integration of grid-supportive, flexible assets. In this context, LSHPs may replace conventional power plants in future redispatch operations, thereby contributing to a more cost-effective and sustainable grid management. As the energy-only market in Germany operates within a single national price zone [36], while grid congestion is inherently a local phenomenon, a discrepancy arises between the economic incentives of the electricity market and the physical requirements of the power grid [33]. If LSHPs are operated purely based on market signals – producing heat when there is a general electricity surplus – a cost-optimized operation can be achieved. However, this does not necessarily imply that their operation is beneficial from a grid stability perspective at their specific location. For instance, the electricity price may remain high due to an overall low generation level in

[1] A balancing group or balancing area represents the smallest unit in the energy market model and functions as a virtual energy account managed by a BGM, comprising various injection and withdrawal points.

Germany, thereby preventing an economically viable operation of LSHPs in Hamburg and at the same time, a local grid bottleneck might occur due to high wind generation in northern Germany, necessitating increased electricity transport to the south. In such a case, operating LSHPs in Hamburg could help relieve the local congestion, even though market signals from the energy-only market alone would discourage their use. In the context of this study, however, the operation of LSHPs is not only analyzed from an economic perspective but also regarding their potential for grid-supportive operation, with a particular focus on redispatch interventions.

2.3 Embedding LSHPs into Hamburg's Energy Infrastructure

This chapter describes the role of the planned LSHPs in the transformation process of the Hamburg's district heating network. Furthermore, the site allocation of the LSHPs is described. This is essential for the local integration into Hamburg's electricity grid and the associated requirements for grid compatibility, which are investigated in chapter 4.1.6 and 5.2.2.

As part of the second update of the Hamburg Climate Plan in 2022 the city raised its climate targets and aims for a reduction of greenhouse gas emission of 70 % by 2030 compared to 1990 [37, 38], even exceeding the national targets (KSG, 2020, § 3 (1) No. 1). In September 2019, Hamburg was able to fully purchase back the city's largest district heating network from the Swedish energy company Vattenfall. It is now operated by the 'Hamburger Energiewerke GmbH' which is a company completely owned by the city of Hamburg. Recent scenario analyses predict an additional connection of 49,000 consumers to the district heating network of Hamburg by 2030 and 72,000 by 2045 [39]. The city plans to shift the district heating supply to renewable energies, biomass and waste heat [40]. This shall be realized by shutting down the 423 MW_{th} coal-fired CHP plant in Wedel and expanding the district heating grid through a crossing of the Elbe to harvest the energy potentials in the port [40, 41, 42]. The project to harness the port's energy potential for district heating, called 'Energiepark Hafen', is scheduled to begin operations by the end of the year [43]. One of the core components of the 'Energiepark Hafen' is the wastewater heat pump at the Dradenau sewage treatment plant with a heat capacity of approx. 60 MW_{th} [20, 44]. Furthermore, the 300 MW_{th} CHP plant in Tiefstack shall be replaced due to the project 'Tiefstack Energy Park' [44, 45]. Among others the most essential centerpieces in the 'Tiefstack Energy Park' are two water heat pumps with heat capacities of approx. 60 MW_{th} and 195 MW_{th} [19, 20]. The 60 MW_{th} water heat pump will be located at the location of the recent CHP plant in Tiefstack and the larger one probably at the location of the recent CHP plant in Wedel [20]. In Figure 3 the most relevant heat generation units in Hamburg's future district heating grid including the LSHPs are shown.

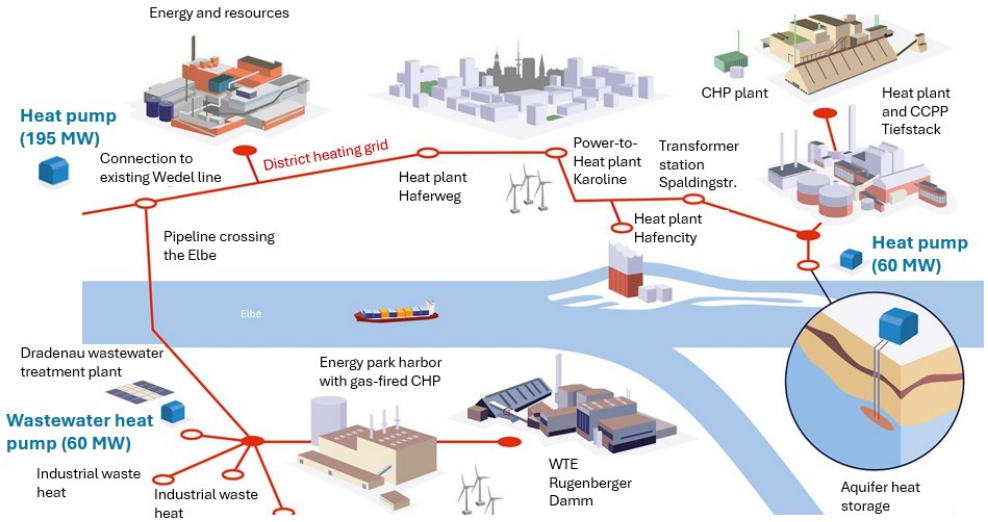

Figure 3: Simplified schematic of district heating network in Hamburg [44]

Modelling the wastewater and river heat pumps planned in the projects ‘Energiepark Hafen’ and ‘Energiepark Tiefstack’, taking into account the effects on the Hamburg power grid, is the subject of this work.

3 The Heat Pump Concept

In the following segment the working principle of a compression heat pump (HP) is explained, and key aspects of HP modelling are outlined. In this context performance parameters are introduced to evaluate the efficiency of a heat pump system. This is essential for comparing different HP systems with respect to the requirements they must meet in large-scale applications.

HPs can be fundamentally categorized between sorption and compression HPs, whereby a further distinction between transcritical and subcritical HPs is made for the compression HPs [46, 47]. Since sorption heat pumps are not suitable for large-scale water-source applications and transcritical systems require complex modeling, this work focuses mostly on modeling LSHPs as subcritical compression systems. Currently subcritical compression HPs are the most common and technically feasible option for large-scale use.

3.1 How the Compression Heat Pump works

This chapter explains the heat pump cycle and uses the equivalent thermodynamic ideal cycle – the reversed Carnot cycle – to support the understanding.

A HP transports heat from a cold reservoir with the temperature T_{low} to a hot reservoir with the temperature T_{high}, whereby $T_{high} > T_{low}$. For this purpose, electrical energy W_{el} is required according to the second law of thermodynamics [48] In contrast to a heat engine, which converts heat into work, a heat pump uses work to move heat against the natural temperature gradient [49]. Therefore, the reverse Carnot cycle which runs in the opposite direction compared to a heat engine is often used for performance indicators for real heat pump cycles [50].

3.1.1 Carnot Cycle

To understand the concept of a HP system and in particular those aspects thereof which result in efficiency losses the concept of the equivalent ideal thermodynamical – the Carnot cycle – is important. The Carnot cycle is the process that can be operated with the least energy input and thus has the maximum achievable efficiency. The reserve Carnot cycle for heat pump processes consists of four reversible steps [50, 51].

1 - Isothermal expansion and heat exchange at T_{low}:

The medium absorbs heat energy from the heat source Q_{source} at low temperature level T_{low}. Since the process is ideal the temperature difference between the reservoir and the medium is infinitesimal small and the heat exchange must take place very slowly (quasi-static). The absorbed heat Q_{source} is entirely converted into volume work W_V, which the system is performing. As a result, the temperature of the medium stays constant at T_{low}.

2 - Isentropic compression:

Electrical energy W_{el} is used to compress the working medium. As the internal energy increases and no heat is exchanged with the environment, the temperature of the medium rises from T_{low} to T_{high}. The process is adiabatic [52].

3 - Isothermal compression and heat exchange at T_h:

Heat energy $Q_{provide}$ is transferred from the medium to the high-temperature reservoir at a constant temperature level T_{high} in a very slow (quasi-static) process. During the heat exchange, volume work is performed on the medium by isothermal compression, where $W_V = Q_{provide}$ so that the temperature of the medium remains constant [52].

4 - Isentropic expansion:

The medium expands and performs mechanical work due to a turbine or an expander in an isentropic expansion. The energy for the work performed is provided by the internal energy of the medium. As a result, the medium cools down from T_{high} to T_{low} in an adiabatic process [50].

Figure 4 shows the reverse Carnot cycle as a component diagram and plots the process in a T-S diagram. The work required for the process is shown in the T-S diagram by the enclosed area of the process vectors.

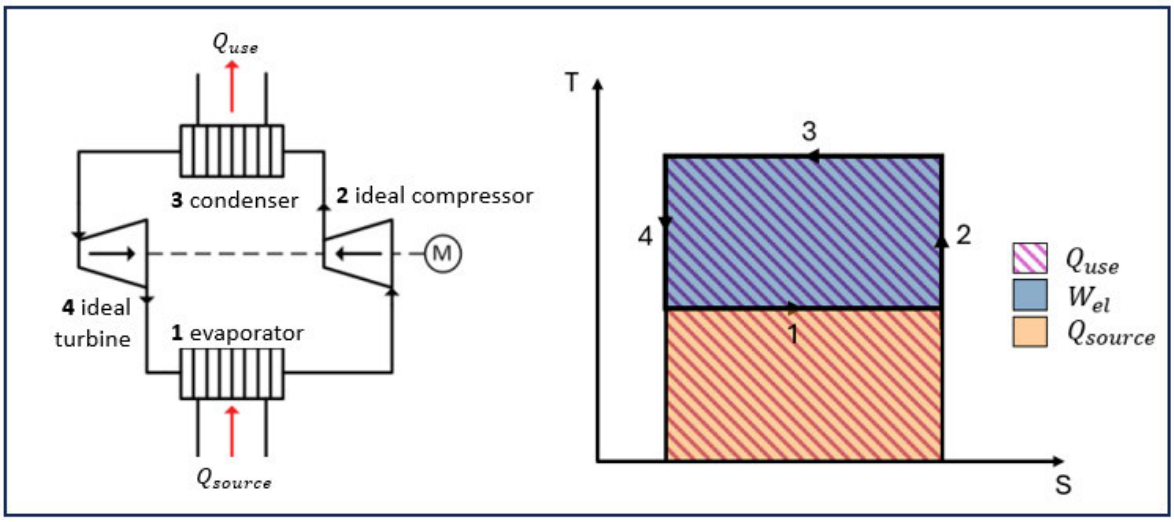

Figure 4: Topology and T-S diagram of reverse Carnot cycle [50, 51] (own illustration)

The Carnot process cannot be operated economically in practice for various reasons [50]. One reason is that the Carnot cycle assumes an isentropic expansion, where the medium performs work due to a turbine. Since the turbine used to expand the medium could only cover a small portion of the compressor work and, in practice, is associated with high costs and mechanical losses, an expansion valve is used in HP systems [50]. By using an expansion valve the expansion takes place without performing work, thus the process becomes irreversible due to an increase in entropy. The expansion is now no longer isentropic, but isenthalpic. Furthermore, the isothermal heat transfers assumed in the Carnot cycle are not possible in practice, as they would take an infinitely long time [51]. The heat exchange in a real heat pump happens due to a temperature gradient and therefore leads to rising

entropy as it is an irreversible process. In addition, isentropic compression would only take place in an ideal compressor, which does not exist in real HP systems. Moreover, dissipation and friction losses occur due to the mechanical movements of the compressor and during the flow of the refrigerant in all components. All process deviations described cause an increase in entropy [53]. As a result, part of the energy required to move heat against its natural gradient can no longer be used to drive the process since it is used for entropy production. This means more electrical energy is needed to drive the process.

3.1.2 Real Compression Heat Pump Cycle

The following chapter describes the relevant process steps for thermodynamic modelling. In a HP cycle three circuits are involved in the working mechanism.

The first circuit obtains the heat source medium, the second circuit the refrigerant as HP working medium and the third circuit belongs to the user side [54, 55]. The topology and the working cycle in the p-h diagram are shown in Figure 5.

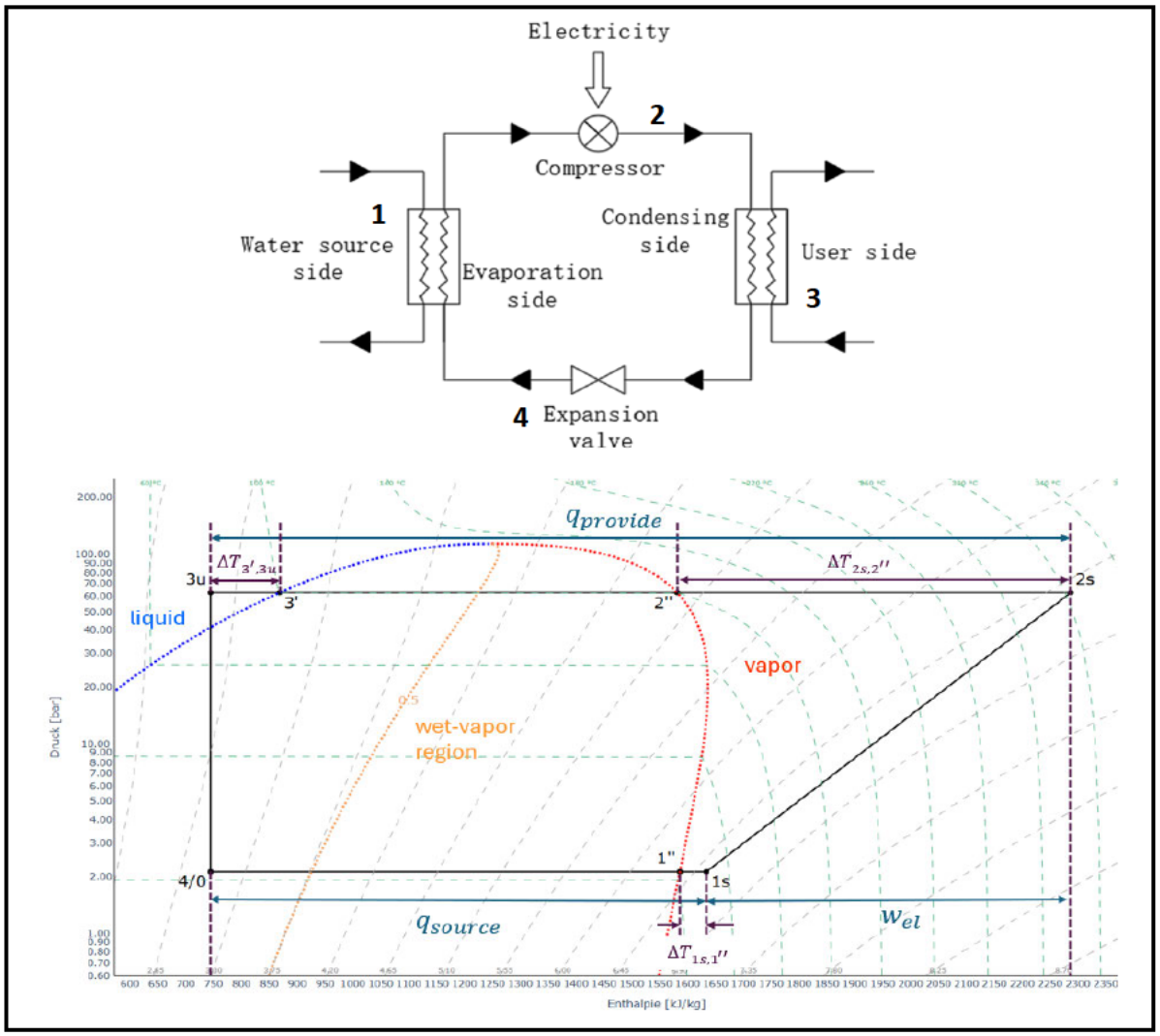

Figure 5: Topology and HP working cycle in the p-h diagram [56] (own illustration)

As illustrated, the working principle of a single-stage heat pump cycle consists of four main steps, involving the components: evaporator, compressor, condenser, and expansion valve [57]. Although the HP cycle is a closed system, open systems must be assumed for the energy balances of the individual process steps, as a mass flow beyond the system boundaries takes place in each step and thus flow work is performed [52, 58].

Step 1 – Evaporator

$\mathbf{4/0 - 1''}$: Heat is transferred from the heat source medium to the refrigerant through a heat exchanger. In a model-idealistic process the refrigerant enters the evaporator as a liquid-vapor mixture and then evaporates completely due to its low boiling point at a constant evaporation temperature $T_{vap} = T_{4/0} = T_{1''}$ and a constant pressure $P_{vap} = P_{4/0} = P_{1''}$ [59]. The energy for vaporization is obtained by cooling the heat source medium.

$\mathbf{1'' - 1s}$: The saturated vapor gets overheated by an isobaric heat exchange until it leaves the evaporator with a temperature of $T_{1s} > T_{1''}$. Overheating is necessary to prevent liquid drops from entering the compressor, which could cause damage and reduce the technical lifetime of the compressor [50]. To transfer the heat to the refrigerant in a finite time, the source medium must be slightly warmer than the refrigerant $T_{Source} > T_{1s,ref.}$. If the temperature of the heat source is not sufficient for superheating, waste heat from the compressor could be used through an internal heat exchanger or hot steam from the compressor outlet could be returned through a bypass line to increase the temperature at the compressor inlet [50, 55]. The absorbed heat from the heat source is defined by [60]:

$$Q_{source} = m \cdot \left(h_{1s} - h_{4/0}\right) \tag{1}$$

Step 2 – Compressor

$\mathbf{1s - 2s}$: In the compressor, the overheated refrigerant vapor is raised to a higher pressure and a higher temperature level by adding mechanical work. In an ideal process the compression would be isentropic, and the specific work could be calculated simply by [50, 51]:

$$w_{el,isentrop} = h_{2s,isentrop} - h_{1s} \tag{2}$$

However, since the entropy increases in a real compression process due to dissipation, mechanical friction and irreversible processes, the actual specific work is:

$$w_{el,real} = h_{2s} - h_{1s} \tag{3}$$

The ratio between the specific work in the isentropic process and the real process is expressed with the isentropic efficiency or compressor efficiency [50, 51]:

$$\eta_{comp} = \frac{w_{el,isentrop}}{w_{el,real}} = \frac{h_{2s,isentrop} - h_{1s}}{h_{2s} - h_{1s}} \tag{4}$$

Step 3 - Condenser

$\mathbf{2s - 2''}$: After leaving the compressor the superheated steam is cooled down in an isobaric process $P_{2s} = P_{2''}$ until it reaches the condensation temperature $T_{cond} = T_{2''}$. It must be ensured that the temperature T_{2s} is slightly higher than the condensation temperature $T_{2s} > T_{cond} = T_{2''}$. This is necessary to provide that the refrigerant is in the phase of superheated vapor without any liquid components throughout the entire compression process [55].

$\mathbf{2'' - 3'}$: The refrigerant condensates with release of condensation enthalpy at a constant temperature $T_{con} = T_{2''} = T_{3'}$ until the state of boiling liquid is reached.

$\mathbf{3' - 3u}$: Due to further heat exchange the liquid refrigerant cools down even more $T_{3'} > T_{3u}$ until it leaves the condenser and enters the expansion valve. The purpose of subcooling is to avoid vapor formation in front of the throttle, since the expansion valve only functions properly when at the inlet the refrigerant is completely in the liquid phase.

Analogous to the evaporator the total released heat in the condenser is calculated by [60]:

$$Q_{provide} = m \cdot (h_{2s} - h_{3u}) \tag{5}$$

Step 4 – Expansion valve

$\mathbf{3u - 4/0}$: After the condensation the refrigerant passes a throttle valve where an isenthalpic and adiabatic expansion takes place. The lowering of pressure causes the refrigerant to start boiling and a part of the refrigerant spontaneously evaporates thus constantly lowering its temperature level. Since the pressure before the expansion valve is higher than behind the expansion valve $p_{3u} > p_{4/0}$, the medium naturally flows in the direction of decreasing pressure. However, the process would never run against the pressure gradient from low pressure to higher pressure. Thus, the process is irreversible, and entropy is generated $s_{3u} < s_{4/0}$ [50, 52]. In the first stage of the expansion the refrigerant stays in the liquid phase until saturation temperature is reached due to pressure reduction and the partial evaporation starts.[2] In the second stage after reaching the boiling point the energy required for spontaneous evaporation is provided by the internal energy of the refrigerant itself by dropping its temperature.

Daviations from idealized assumptions:

To better classify the results of thermodynamic modeling, it is important to be aware of the process deviations. The real HP cycle differs from model idealized assumptions in the process steps described above in several aspects [55]:

[2] To describe the temperature change during the first stage the Joule-Thomson-coefficient $\mu_{JT} = \left(\frac{\partial T}{\partial p}\right)_H$ is introduced. It indicates the temperature change during an isenthalpic pressure drop in single-phase systems. The effect results from intermolecular interactions: when expansion requires overcoming strong attractive forces, kinetic energy is reduced, leading to a temperature drop. For liquids the Joule-Thomson-coefficient is usually very small, meaning the temperature change before evaporation is minimal. This is reflected in the p-h diagram, where isenthalpic and isothermal lines run nearly parallel in the liquid region.

- Heat losses to the environment occur, which reduces the usable heating output [57]
- Pressure losses occur in the main components and in the pipes [55]
- For zeotropic refrigerants a so-called temperature glide occurs during condensation and evaporation [55]
- In the compressor, the refrigerant reaches a higher temperature due to polytropic compression than the refrigerant wetted surfaces of the compressor, resulting in a specific entropy and enthalpy decrease of the refrigerant [55]. At the beginning of the compression process, the specific entropy of the refrigerant increases because it enters the compressor at a suction gas temperature T_{1s} that is colder than the temperature of the refrigerant wetted surfaces of the compressor.

In Figure 6 the model-idealized HP cycle (green dashed line) and the HP cycle with process deviations considering real operation effects (yellow line) are depicted. The process deviations, such as pressure losses, are illustrated in an exaggerated manner for illustrative purposes.

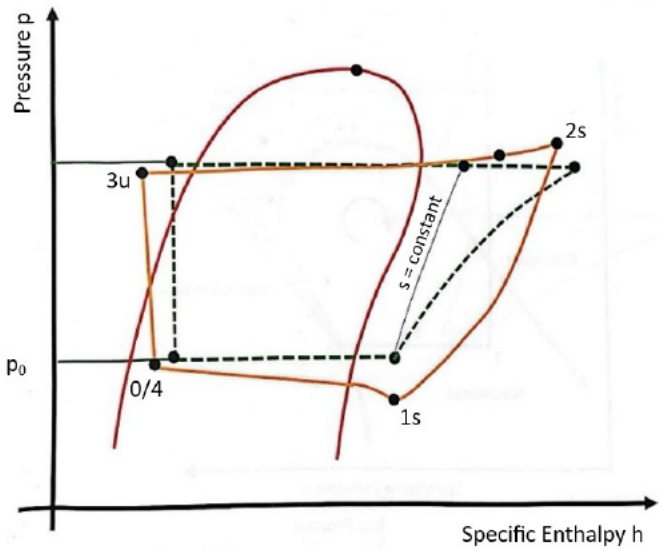

Figure 6: p-h diagram of HP cycle with exaggerated process deviations [55]

3.2 Regulation of Operating Parameters

In the following, the control circuit is outlined that governs the HP operation in response to fluctuating environmental parameters.

Besides controlling the compressor power, the expansion valve is a key component in regulating the system operation. Its task is to adjust the refrigerant mass flow in the evaporator so that the refrigerant evaporates completely and no liquid droplets are drawn in by the compressor [47, 55]. Thus, the expansion valve tunes the superheating of the saturated vapor after evaporation by maintaining the temperature difference $\Delta T_{1'',1s}$ constant at a minimum of 3 to 5 °C or more. In modern HP technology, electronic expansion valves are commonly used due to their superior precision and adaptability. The pressure and temperature at the evaporator gas outlet are measured by sensors and compared with

the setpoints. A controller evaluates the information and commands the expansion ventil for adjustment, thus closing the feedback loop. Figure 7 shows the integration of the expansion ventil into the HP control circuit.

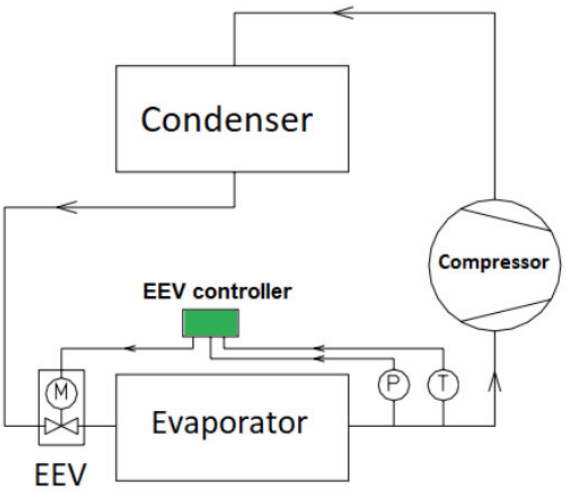

Figure 7: Control circuit of HP systems [61]

Considering the HP control circuit and aiming for a realistic implementation in the thermodynamic model, additional system parameters – such as the size of the heat exchangers – would need to be known. As this system parameters are unknown, a simplification of the control circuit is done as explained in chapter 4.7.1.

3.3 Key Performance Indicators

In the subsequent chapter the key performance indicators used to evaluate the system performance are introduced. The right use of performance indicators is essential to evaluate the process of the system according to the desired outcome. This is applied in the thermodynamic modeling of the HP system described in chapter 4.7.

If the HP is considered under model-idealized assumption that no energy losses to the environment occur, then according to the first law of thermodynamics the energy balance is [46]:

$$Q_{provide} = Q_{source} + W_{el} \tag{6}$$

The most common quantity to evaluate the efficiency of a HP process is the coefficient of performance (COP) which is defined as the ratio of heating output to electrical input power [50]:

$$COP = \frac{\dot{Q}_{provide}}{\dot{W}_{el}} \tag{7}$$

The Carnot process is the process with the highest efficiency and thus reaches the highest COP. According to the second law of thermodynamics and the definition of entropy the heating power transferred in a reversible process is [52]:

$$\dot{Q}_{rev} = \dot{m} \cdot T \cdot (s_{high} - s_{low}) \tag{8}$$

If this equation is inserted into the definition of the COP and the energy balance of an ideal lefthand Carnot cycle is considered as shown in the T-s diagram in Figure 4, it follows [50]:

$$COP_{Carnot} = \frac{\dot{Q}_{provide}}{\dot{W}_{el}} = \frac{\dot{Q}_{provide}}{\dot{Q}_{provide} - \dot{Q}_{source}}$$
$$= \frac{\dot{m} \cdot T_{high} \cdot (s_{high} - s_{low})}{\dot{m} \cdot T_{high} \cdot (s_{high} - s_{low}) - \dot{m} \cdot T_{low} \cdot (s_{high} - s_{low})} = \frac{\boldsymbol{T_{high}}}{\boldsymbol{T_{high} - T_{low}}} \tag{9}$$

Paraphrased, the COP_{Carnot} indicates how much heat output can be transferred to the temperature level T_{high} per electrical input power $\dot{W}_{el}$ when heat is absorbed from a source at the temperature level T_{low} [57]. When defining the COP_{Carnot}, it is crucial to know which temperature levels is being referred to. The $COP_{interior}$ is defined for the temperature difference between the evaporation and condensation temperature. Thus, it applies [50]:

$$COP_{Carnot,interior} = \frac{T_{con}}{T_{con} - T_{vap}} \tag{10}$$

However, if the heat gradients in the heat exchangers are considered and it is referenced to the temperature of the heat source and the heating grid, then it is defined [50, 57]:

$$COP_{Carnot,exterior} = \frac{T_{grid}}{T_{grid} - T_{source}} \tag{11}$$

For the thermodynamic modelling of an HP cycle as done in chapter 4.7, the real COP_{real} is calculated using enthalpy balances [50, 54]:

$$COP_{real} = \frac{\dot{Q}_{provide}}{\dot{W}_{el}} = \frac{\dot{m} \cdot (h_{2s} - h_{3u})}{\dot{m} \cdot (h_{2s} - h_{1s})} \tag{12}$$

To rate the quality of a HP cycle, the so-called quality factor is introduced $\eta_{quality}$ [62]. The quality factor is the ratio of the COP_{real} in the real HP process to the one of the Carnot cycle COP_{Carnot}:

$$\eta_{quality,interior} = \frac{COP_{real}}{COP_{Carnot,interior}} \tag{13}$$

$$\eta_{quality,exterior} = \frac{COP_{real}}{COP_{Carnot,exterior}} \tag{14}$$

Since the Carnot cycle always assumes heat exchange at constant temperatures T_{high} and T_{low}, the process steps of superheating in the evaporator and subcooling in the condenser distort the significance of the $\eta_{quality}$, as they result in a deviation from the constant evaporation or condensation temperature and thus change the temperature lift $T_{high} - T_{low}$. For example, the COP_{real} would increase with significant subcooling after the expansion valve, as the resulting lower heat flow weighted mean temperature in the condenser reduces the effective temperature lift [50]. To ensure the significance of the quality factor with large proportions of superheating or subcooling in the heat exchangers, the COP_{Lorenz} is introduced [46, 63]:

$$COP_{Lorenz} = \frac{\bar{T}_{high}}{\bar{T}_{high} - \bar{T}_{low}} \tag{15}$$

Where $\bar{T}_{high}$ is the heat flow weighed mean temperature or entropic mean temperature on the condenser or user side and $\bar{T}_{low}$ the heat flow weighed mean temperature on the side of the evaporator or heat source [64]. If no phase changes take place, then the heat flow weighed mean temperature can simply be assumed by [58]:

$$\bar{T} = \frac{T_{in} + T_{out}}{2} \tag{16}$$

However, when a phase change takes place, a differentiated consideration must be made through integration along the heat exchanger [64]:

$$\bar{T} = \frac{1}{\dot{Q}} \cdot \int_{x_{start}}^{x_{end}} T(x) \cdot \frac{d\dot{Q}}{dx} dx \tag{17}$$

Here x is a placeholder for the integration parameter along which temperature and heat flow change in the heat exchanger. The Lorenz quality grade $\eta_{quality,Lorenz}$ is calculated analogous to the other quality factors and indicates the ratio between COP_{real} and COP_{Lorenz}. The use of $\eta_{quality,Lorenz}$ is purposeful when large proportions of superheating or subcooling phases in the evaporator or condenser occur as described in chapter 4.7.

While the COP is only determined for a specific set of operating conditions, the so-called annual performance factor represents the operation under real conditions for an entire year. The APF is defined by:

$$APF = \frac{\int_{t_1}^{t_2} Q_{use}}{\int_{t_1}^{t_2} W_{el}} \tag{18}$$

Here t_1 is the time at the beginning of the year and t_2 is the time at the end of the year [65, 66]. The quality factor $\eta_{quality,Lorenz}$ and the APF can be applied for HP modelling in alternate mode as explained in chapter 4.8.

3.4 Preselection of Refrigerants

In the subsequent chapter the characteristics of different refrigerants are investigated to enable a preselection of feasible HP designs for the planned LSHPs. This serves as a basis for further refining the HP model and identifying which system designs should be compared in the final evaluation done in chapter 5.1.

The refrigerant is the HP's working fluid. Refrigerants are substances that evaporate at low temperatures and possess high internal energy [47, 55]. Table 1 lists the refrigerants currently utilized and planned to use in LSHP projects in Germany. All refrigerants with a low global warming potential (GWP) and low ozone depletion potential (ODP) are marked in green, while refrigerants to be avoided in future projects are marked in orange.

Table 1: LSHP projects in Germany categorized by refrigerants [19, 67][3]

Refrigerant	Type	Total power planned [MW]	Total Power in Op. [MW]	In Op. with Water-Source [MW]
Unknown	Unknown	1379.36	73.39	not clearly stated
R717	Natural	49.81	49.81	7.08
R1234ze(Z)	HFO	20.20	20.20	/
R134a	HFC	10.23	10.23	1.5
HFC	HFC	8.00	8.00	/
R1234ze(E)	HFO	2.20	1.10	/
R1233zd(E)	HCFO	0.88	0.88	/
R600, R717 (ammonia)	HC	0.50	0.50	/

The existing and planned projects in Germany provide a useful indication for the selection of refrigerants for LSHPs in Hamburg. However, not all the refrigerants listed in Table 1 are suitable for the planned LSHPs in Hamburg considering the temperature levels of the heat source and the district heating grid. Figure 8 shows various refrigerants for LSHP applications and their possible temperature ranges.[4]

[3] The information on projects with specific refrigerants includes only those projects which explicitly documented the refrigerant used. Many projects do not specify the refrigerant used. Therefore, the actual installed or planned capacity of LSHPs with a specific refrigerant may be significantly higher than indicated in the table.

[4] The upper temperature range is shown 15 °C below critical temperature here. Thus, the upper range might be slightly higher for specific refrigerants

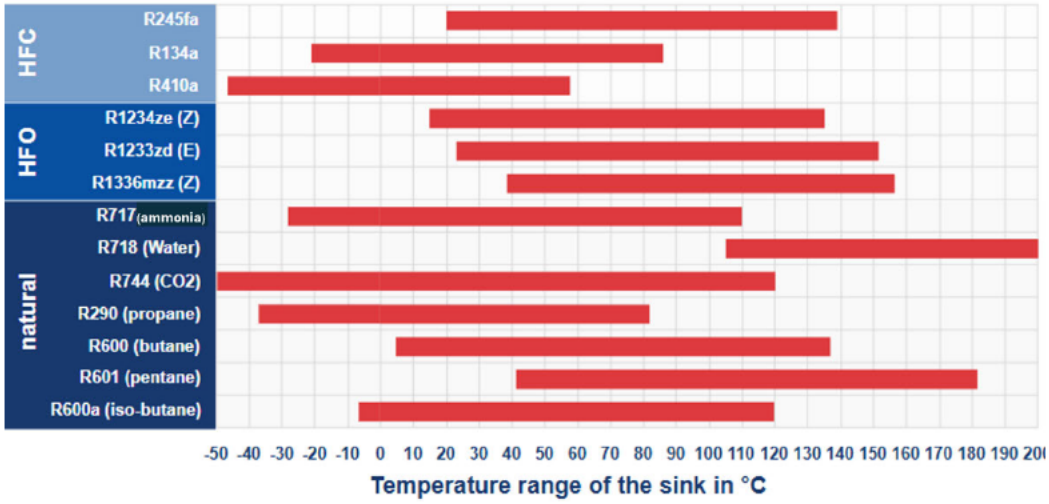

Figure 8: Temperature range of refrigerants used for LSHPs [68]

Figure 9 shows the wet-vapor curves of possible refrigerants in the p-H and T-s diagrams.[5] The refrigerants that generally fulfil the requirements for river-source LSHPs as planned in Hamburg are shown in solid lines and the remaining in dashed lines.

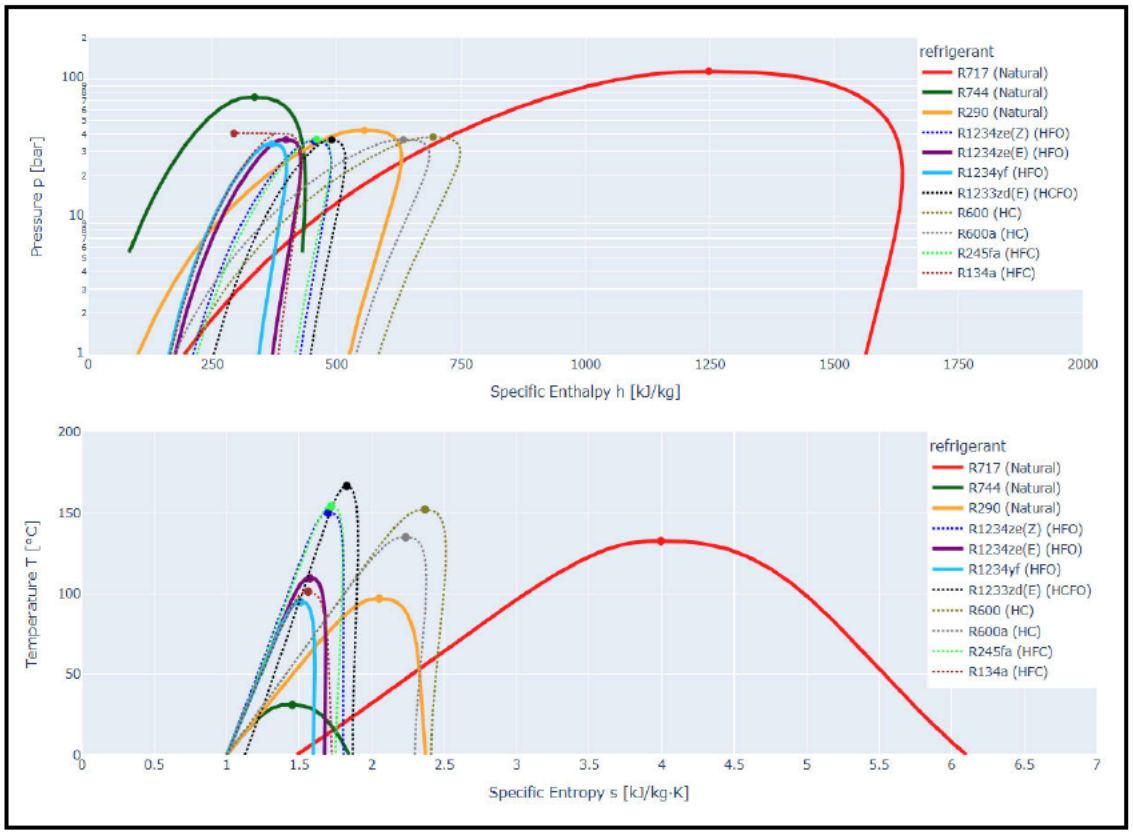

Figure 9: Wet-vapor curves of possible refrigerants (own illustration)

[5] The distortion of the wet steam curve of R134a in the p-h diagram is due to a calculation error in CoolProp. In addition, the saturated vapor curve of water was omitted due to its deviations from the other curves. Thus, the other curves can be better visualized.

“HFCs (Hydrofluorocarbons)” In 2024, the European Union banned the production of new HPs using HFCs due to their high GWP (Regulation (EU) 2024/573) [69]. Hence, R245fa (lime) and R134a (brown) are not an option.

“HFOs (Hydrofluoroolefins)” The refrigerants R1234ze(Z) (blue) R1234ze(E) (purple) and R1234yf (light blue) are considered environmentally friendly alternatives for HFCs [47, 70], since their critical temperatures and pressures are very similar as shown in Figure 9. The boiling point of R1234ze(Z) at ambient pressure is approx. 9.8 °C which restricts their use to the second stage of a multiple-stage HP. The critical temperature of the refrigerant R1234yf at its critical point is 94,7 °C [71], thus limiting the operation for sink temperatures below 90 °C. The critical temperature of R1234ze(E) is 109,4 °C and therefore more favorable.

“HCFOs (Hydrochlorofluoroolefins)” The refrigerant R1233zd(E) (black) has the highest critical temperature, which makes it attractive for HTHPs [47]. But the boiling point at ambient pressure is above 18 °C and therefore too high for the first stage of a river-source HP [70].

“HCs (Hydrocarbons)” R600a (grey) and R600 (olive) have high flammability, which is why they are only suitable for smaller systems with small filling quantities of maximum 2.5 kg [47].

“Natural” When considering natural refrigerants, R718 (water), R744 (carbon dioxide, green), R290 (propane, organge) and R717 (ammonia, red) are generally used [47]. Due to its significantly high boiling point water would just be an option for the upper stage of a cascaded HP. R744 (green line) works in transcritical operation due to its low critical point as shown in Figure 9. Especially for large temperature lifts with high supply temperatures as they occur in the LSHPs in Hamburg, it is a suitable option. Propane is generally well suited for LSHPs due to its low boiling point at high pressure levels, but it is highly flammable and thus very strict safety instructions apply. Furthermore, its critical point is at a temperature of 96.7 °C, therefore limiting the operation for heating network temperatures below 90 °C. R717 enables large evaporation and condensation enthalpies as illustrated in Figure 9. This is a key advantage, as R717 facilitates high volumetric heating output with small filling quantities. Nevertheless, at high temperatures the available compressor technology is limited due to the high pressure levels, thus restricting the use of R717. Thanks to special cast steel designs compressors can withstand approx. maximum operating conditions at 76 bar and grid temperatures of 110 °C [13, 47, 72] Here special safety precautions must be taken due to the toxicity of ammonia.

As a result of the analysis the refrigerants R717, R1234ze(E), R290 and R1234yf are selected for further consideration of subcritical HP modelling, whereby in real-world operation R290 and R1234yf are only options for supply temperatures below 90 °C.

4 Design of Simulation Framework and HP Modell

The following section describes the development of the model used to simulate LSHPs in Hamburg's power grid. The modelling approach is outlined in several steps. First the input parameters are introduced. Then the general structure of the algorithm and the system characteristics of the LSHPs are described. Thereafter, the specific segments of the algorithm are highlighted. Here, the operating modes of the LSHPs and the corresponding technical control strategies are detailed. Consequently, the model-based heat output calculation depending on the operating mode is explained and the performance of thermodynamic modelling for calculating the electrical input power is presented.

Various factors must be taken into account when developing the HP model. Here, a distinction is made between assumptions on the technical design of the HP and input parameters outside of the system based on real measured values. Figure 10 shows an overview of the different parameters considered to calculate the electrical input power of the river-source LSHPs in Hamburg.

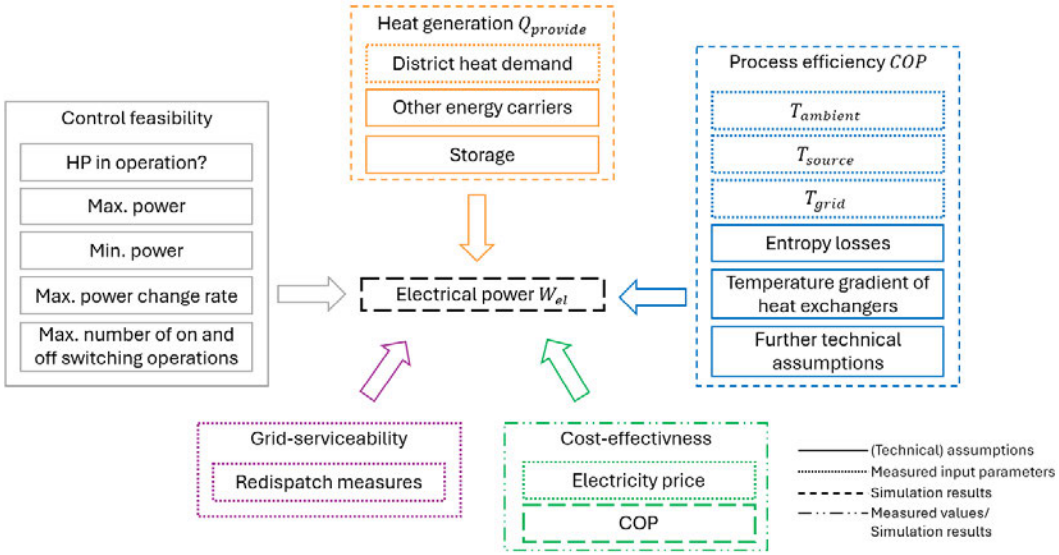

Figure 10: Parameters for modelling river-source LSHPs in Hamburg (own illustration)

When determining the heat output and the electrical input power, the individual parameters and their interdependencies must be considered across consecutive timesteps. Figure 11 illustrates the key parameter interdependencies governing the specification of the heat pump's electrical input and thermal output, which are explained in more detail in the following chapters.

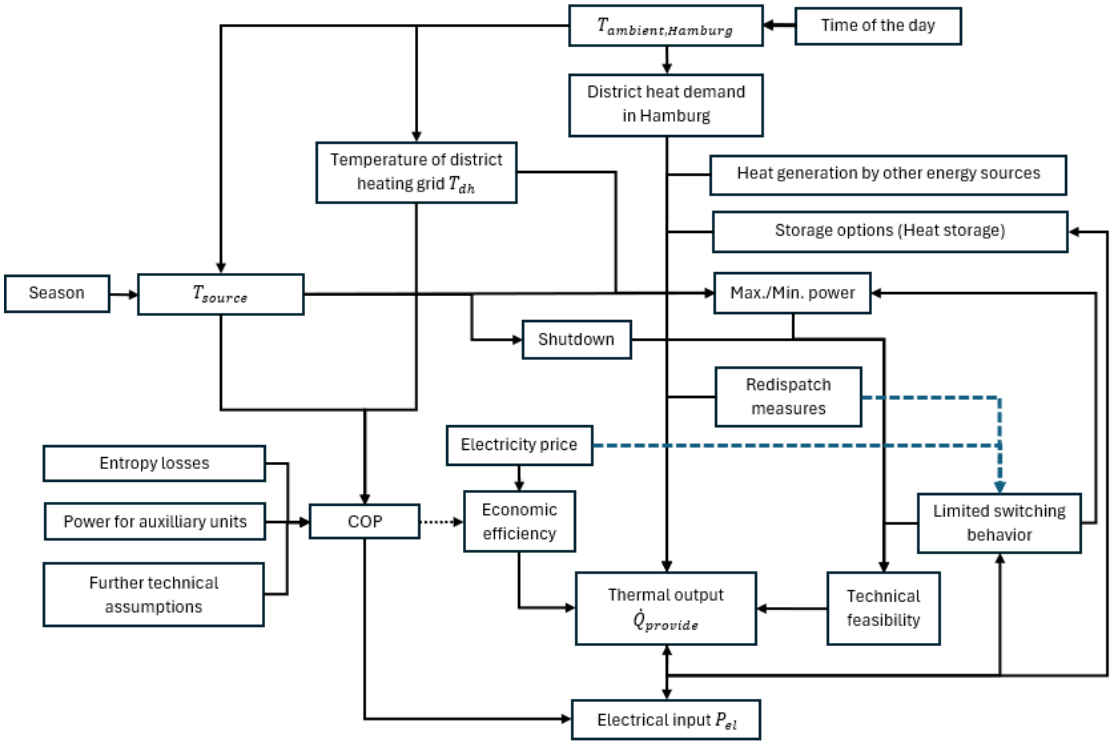

Figure 11: Causal dependencies among the model parameters (own illustration)

The targeted thermal output resulting from the heat demand, the economic efficiency and the redispatch measures is further narrowed down in each step by checking the technical feasibility. Here, the defined parameter states of one step including the number of modules in power are the initial state for the next step and therefore impacting the technical feasibility to fulfil upcoming demands. Furthermore, the storage level, resulting from the cumulative energy balance of all previous steps, influences the thermal output in the current timestep. The temperature of the district heating grid T_{dh} and the source temperature T_{source} are affecting the COP and the maximum thermal output due to maximum compressor power, as discussed in chapter 4.3.4. In addition, shutdowns are carried out in case of too low source temperature as described in chapter 4.3.5 [20].

4.1 Measured Input Parameters

This section describes the creation of the input data series and presents the corresponding results.

The simulation is performed for a selected year using a 15-minute time resolution. Accordingly, time series with the same resolution are generated for all input parameters, including ambient temperature $T_{ambient}$, water temperature T_{source}, heating grid temperature T_{grid}, heat demand, electricity prices and redispatch measures. Many raw data sets for core input data such as the ambient temperature and the water temperature were not complete or had faulty and unplausible values. Furthermore, the format of raw data from every category was not consistent. Thus, the data had to be processed in several steps. Here, faulty values were filtered, missing values were supplemented due to interpolation, the resolution of the data series were adjusted, and the validity and quality of the data were checked.

Moreover, the process of data preparation was tracked to evaluate if a data series has too many artificially supplemented values.

4.1.1 Ambient Temperature in Hamburg

The ambient temperature of Hamburg is required as it affects the temperature of the heating grid as well as the heat demand. The German weather service 'deutsche Wetterdienst' does record the ambient temperature at two measuring points in Hamburg, in Fuhlsbüttel and Neuwiedenthal [73]. The data is available for the last decades in a 10-minute resolution at a ground level of 2 meters [74]. When choosing the weather year to create the time series for district heating it is considered that the simulation of LSHPs in this work is also used in a wider context for further simulations of the 'Competence Center für Erneuerbare Energien und EnergieEffizienz' (CC4E), which are based on the weather data from 2012. Thus, for reasons of consistency, the year 2012 is used here as the weather year as well. The ambient temperature data series for 2012 was verified as error-free.

4.1.2 Water Temperature of the Elbe

The data series for the water temperature of the Elbe is needed as it serves as the source temperature for the HP model. The institute of 'Hygiene und Umwelt' operates several measuring stations on the Elbe. In correspondence with the head of the department of the 'Wassergütemessnetz', measurement data with a 10-minute resolution is provided for the locations Blankenese, Bunthaus and Seemannshöft [75, 76]. The data series of 2012 had some missing measurements, which were supplemented by linear interpolation. However, since only less than 3 % of the measurement data were supplemented, the data series is considered reliable. Figure 12 shows the 15-minute temperature profiles of the Elbe water in Blankenese and the ambient air in Fuhlsbüttel for the year 2012.

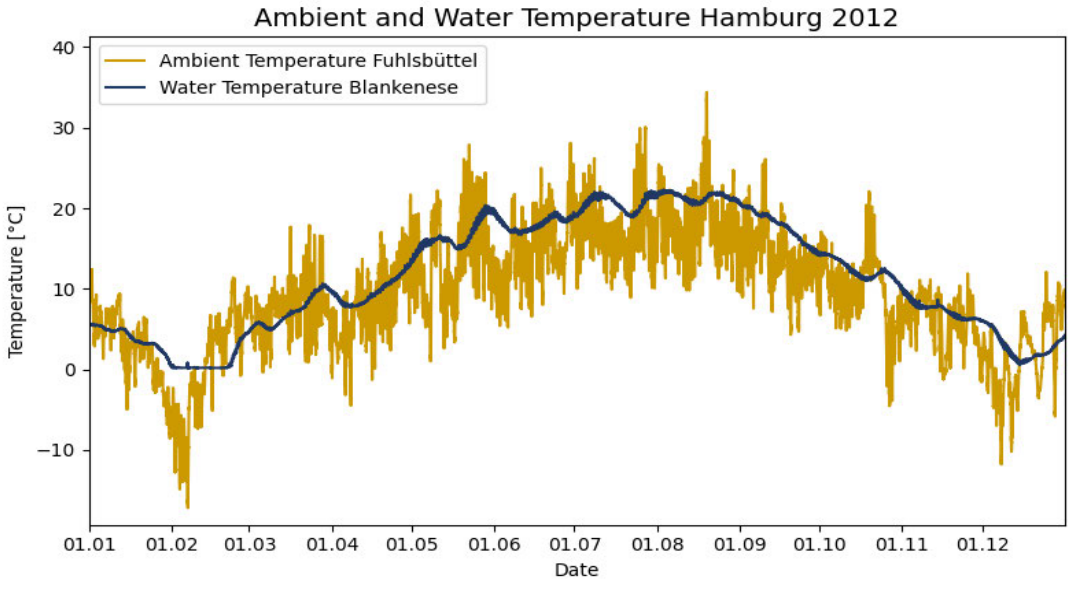

Figure 12: Ambient and water Temperature in Hamburg 2012 [77, 76] (own illustration)

As expected, the water temperature follows the ambient temperature with a time delay [78], whereby the water temperature of the Elbe does not drop below 0 °C.

4.1.3 Temperature of the Heating Grid

The temperature of the heating grid is essential for heat pump operation, as it defines the supply temperature level at which the LSHPs are expected to provide heat. The temperature of the heating grid in Hamburg varies depending on the ambient temperature. Using the diagram provided in the documents from the 'Hamburger Energiewerke' and manually determining value pairs, the heating grid temperature at every timestamp is determined due to interpolation between the given value pairs [79]. The temperature of the heating grid even rises to over 130 °C during very cold temperatures below -10 °C. However, higher sink temperatures require more complex HP designs to reduce extensive material stress due to high temperatures at the outlet of the compressor. Furthermore, the COP decreases with higher supply temperatures, thus affecting economic efficiency. Since the planned LSHPs are currently just supplemental heat generators in the heating grid, it is assumed that the energy at higher temperature levels can be provided by other sources. For the wastewater HP in Dradenau, which does not feed directly into the district heating network but into an intermediate hydraulic circuit, maximum supply temperatures between 95 and 98 °C are planned [20, 80]. For the other LSHPs, maximum supply temperatures of just below 100 °C are planned according to the specifications of 'Hamburg Energiewerke' [20]. Therefore, in the default scenario it is assumed the LSHPs support the district heating grid with supply temperatures between 90°C and 100°C depending on the current temperature level needed. Figure 13 shows the temperature profiles of the heating grid in Hamburg and the supply temperature of the LSHPs as a function of the ambient temperature and Figure 14 shows the temperature development in the district heating grid and the supply temperature of the LSHPs as a function of the ambient temperatures recorded in 2012.

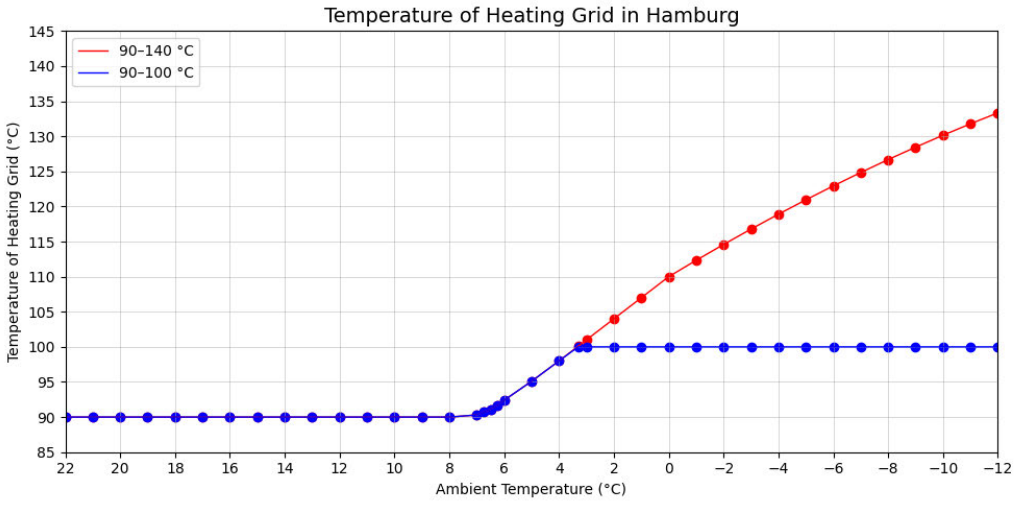

Figure 13: Temperature dependency of the heating grid on ambient temperature [79] (own illustration)

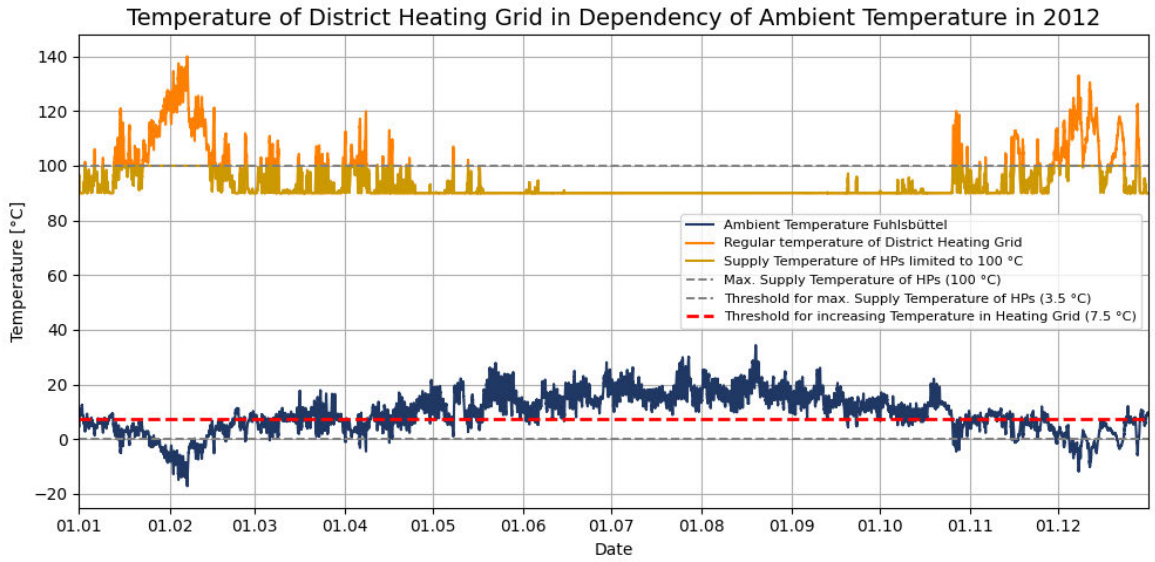

Figure 14: Ambient temperature and temperature of heating grid in Hamburg 2012 [76, 79] (own illustration)

The temperature curve shows that the temperature in the heating grid increases for cold ambient temperatures below 7.5 °C. If the temperature is limited to 100 °C no further increase occurs after the ambient temperatures drops below 3.5 °C.

4.1.4 District Heat Consumption in Hamburg

The temperature of the heating grid in Hamburg is necessary to adapt the targeted heat output of the LSHPs. As there is neither a 15-minute time series nor a sufficient data basis to derive one for district heat consumption in Hamburg, standard load profiles (SLPs) for gas customers are used to map the consumption behaviour instead. This approach assumes that the consumption patterns for district heating in households and commercial buildings are comparable to those of gas consumption. Likewise, no 15-minute consumption data is available for gas consumption. However, as shown in previous studies [81], the hourly factors used by gas network operators to estimate future consumption behavior can be used to generate a corresponding 15-minute time series. Here, the first step is to create a daily consumption time series. This can be achieved due to the process that gas network operators use to forecast the future consumption of their customer groups as a function of ambient temperature and past consumption behavior (GasNZV, 2005, § 24). Here, the different customers are assigned to an SLP, so that every SLP represents a certain costumer group. In accordance with the guidelines for processing SLPs [82], the forecast for daily gas consumption of a customer group is calculated as follows:

$$Q_{daily,SLP} = KW_{SLP} \cdot h_{SLP}(T_{allo}) \cdot F_{day,SLP} \tag{19}$$

Here Q_{daily} is the forecast for daily gas consumption for a certain SLP, $F_{day,SLP}$ is the factor for the day of the week, the value KW_{SLP} is the average daily consumption at 8°C for this SLP and $h_{SLP}(T_{allo})$ is the profile function value of the SLP in dependency of the allocation temperature T_{allo}. Currently the profile function value h is calculated by using the profile functions of the TU München and the

'Gasprognosetemperatur' as T_{allo} provided by the DWD, which is estimated considering various parameters to optimize the forecast for the daily heat consumption Q_{daily} [82, 83, 84]. Until 2022 the gas operator 'Hamburger Energienetze' used the FfE SigLinDe profiles and the temperature for the next day estimated due to the geometric series of the temperatures of the last days. To enable an independent calculation without relying on the 'Gasprognosetemperatur' as T_{allo} the FfE SigLinDe profiles are used in combination with the daily average temperatures from the weather year considered. This aligns with the method the 'Hamburger Energienetze' applied until 2022 since they also used the FfE SigLinDe profiles with linear extension as seen in Figure 15 [82, 85]. Thus, the profile function value h is calculated by:

$$h(T_{allo}) = \left[\left(\frac{A}{1+\left(\frac{B}{T_{allo}-T_0}\right)^C} + D\right)\right] + \left[max\begin{Bmatrix} m_H \cdot T_{allo} + b_H \\ m_W \cdot T_{allo} + b_W \end{Bmatrix}\right] \tag{20}$$

Here, A, B, C, and D are the coefficients of the Sigmoid function as part of the SLP, the reference temperature is fixed with $T_0 = 40\ °C$ and m_H, m_W, b_H, b_W are the coefficients for the linear part of the profile function where m represents the slope of the line and b the function value of the linear part at 0 °C. The linear extension increases the accuracy of the function value $h(T_{allo})$ at very low or high temperatures to counteract the systematic underallocation in the area of very cold temperatures and to represent the remaining consumption through hot water in the area of hot temperatures, as shown in Figure 15 [82, 86].

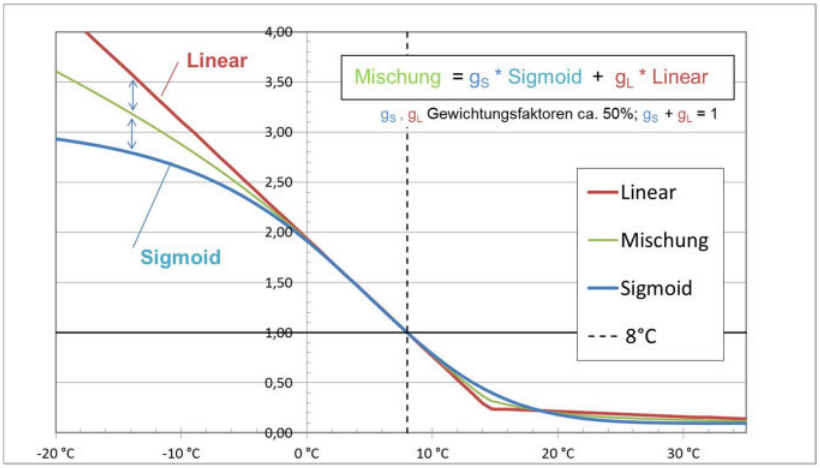

Figure 15: Scheme for deriving the SigLinDe profiles with linear extension [82]

The 'Kundenwert' KW-value is defined due to past consumption behavior of the customer group in a certain period [82]. It applies:

$$KW = \frac{Q_N}{\sum_{i=1}^{N}\left(h\left(\vartheta_{D_i}\right) \cdot F(D_i)\right)} \tag{21}$$

Due to the correspondence with the energy supplier BDEW and the gas network operator of Hamburg, the 'Hamburger Energienetze', the monthly KW-values for the SLPs used in 2022 are obtained. The monthly KW-values were calculated by the 'Hamburger Energienetze' according to equation (21) based on the annual consumption of the customers of the SLP that were billed in this month or, if a delay occurs, with a monthly offset [85]. Thus, the arithmetic mean KW-value is the annual KW-value which describes the annual consumption of the SLP most accurately. Using the KW-values and the time series for the daily temperature of the weather year considered, the daily gas consumption for each SLP is determined according to equation (22)[6]. The daily consumption values are used to forecast the annual gas consumption for each SLP and, subsequently, to determine the total annual gas consumption grouped by SLPs representing households and commercial customers, respectively. It applies:

$$Q_{gas,annual,group} = \sum_{i=1}^{i=365} \sum_{n}^{n=a} Q_{gas,D_i,SLP_n} \tag{22}$$

Adopting the concept of SLPs to the district heating sector and considering the data available for the district heat consumption regarding households and commercial customers [87], the daily district heat consumption of each SLP is defined using proportionality factors as shown in equation (23) and (24). Here the district heat demand of 2023 is chosen for the district heat consumption analysis, as 2023 is the most recent year with available data [87]. Depending on whether the SLP belongs to household or commercial customers, the district heat consumption is determined by scaling the calculated gas consumption. It applies:

$$Q_{daily,dh,SLP(household)} = \frac{Q_{dh,annual,households}}{Q_{gas,annual,households}} \cdot KW_{SLP} \cdot h_{SLP}(T_{allo}) \cdot F_{day,SLP} \tag{23}$$

$$Q_{daily,dh,SLP(commercial)} = \frac{Q_{dh,annual,commercial}}{Q_{gas,annual,commercial}} \cdot KW_{SLP} \cdot h_{SLP}(T_{allo}) \cdot F_{day,SLP} \tag{24}$$

In 2022 the SLPs with the following nomenclature have been used by 'Hamburger Energienetze' to allocate gas consumption: DE_HKO03 (cooking gas), DE_HKO03 (single-family home), DE_HMF33 (multi-family home), DE_GHA34 (retail), DE_GKO34 (local authorities), DE_GMK34 (metal and automotive) [82, 85]. The SLP used for the customer group of cooking gas (DE_HKO03) can be neglected since district heating supply is not used for cooking [79]. Based on the daily consumption values, the daily mean temperatures and the hourly factors of the individual SLPs, which were developed in 2002

[6] In the simulation the monthly KW-values were used depending on every month instead of the arithmetic mean KW-value (annual KW-value) for the whole year. The use of the annual KW-value would be mor accurate as it compensates for the customer shifts that took place during the year. This error only became apparent towards the end of the work and was therefore not corrected. Since the monthly KW-values of every SLP are almost constant during the year the error can certainly be considered negligible.

on behalf of the BDEW and VKU, an hourly consumption profile is generated for each SLP [88, 89, 90, 91].[7] The hourly factors of every SLP indicate a percentage value of the total daily consumption for the respective hours, depending on the day of the week and the average daily temperature. As the factors are only specified for certain daily temperatures, the averaged values are determined by linear interpolation. In addition, the hourly factors are only dependent on the average daily temperature, which means that no temperature fluctuations during the day that deviate from the assumptions contained in the hourly factors are considered. Based on the hourly district heat consumption profiles for each SLP, 15-minute consumption time series are generated using weighted interpolation. Summing up the quarter-hourly consumption values across all SLPs results in the final 15-minute district heat demand time series. Since the values from different years are used, the annual district heat consumption from 2023, the KW-values from 2022 and the daily temperatures from 2012, it is important to understand what the result of the calculated 15-minute district heat consumption series represents. The generated quarter-hourly time series distributes the already defined amount of district heat consumption in 2023 across the individual 15-minute intervals of the year, based on the temperature conditions of 2012 and assuming a customer profiling that corresponds to the one of gas customers in 2022.

To create a sustainable structure which enables providing a heat demand time series based on different simulation conditions a class 'SLP_simulation_conditions' is set up such that the simulation conditions regarding the heat demand time series are stored as an object of the class. By creating a new object, a new district heat demand time series relying on different input data – such as another weather year, a different total demand, other KW-values or different hourly factors – can be generated. To facilitate the future use of the data generation structure for upcoming simulations with different input data, the process of data generation through the class 'SLP_simulation_conditions' is illustrated by flowcharts in the appendix A.

In 2023 district heat consumption in Hamburg by households and commercial customers totaled 15,797 TJ [92]. The households consumed 9,524 TJ and the sector of business and services consumed 6,272 TJ [92]. In Figure 16 the 15-minute time series for district heat consumption of 2023 in dependency of the weather in 2012 and an assumed consumption profile of 2022 is shown.

[7] In 2007 new hourly factors for the SLPs have been developed by the BGW and VKU also containing city-specific factors for certain SLPs such as DE_HKO03 (single-family home), DE_HMF33 and (multi-family home). This was only recognized at a later stage of the work process. Therefore, the hourly factors developed in 2007 were not used to generate the results; instead, those developed in 2002 were applied. The daily load peaks from the hourly factors developed in 2007 are slightly lower compared to the hourly factors of the SLPs developed in 2002.

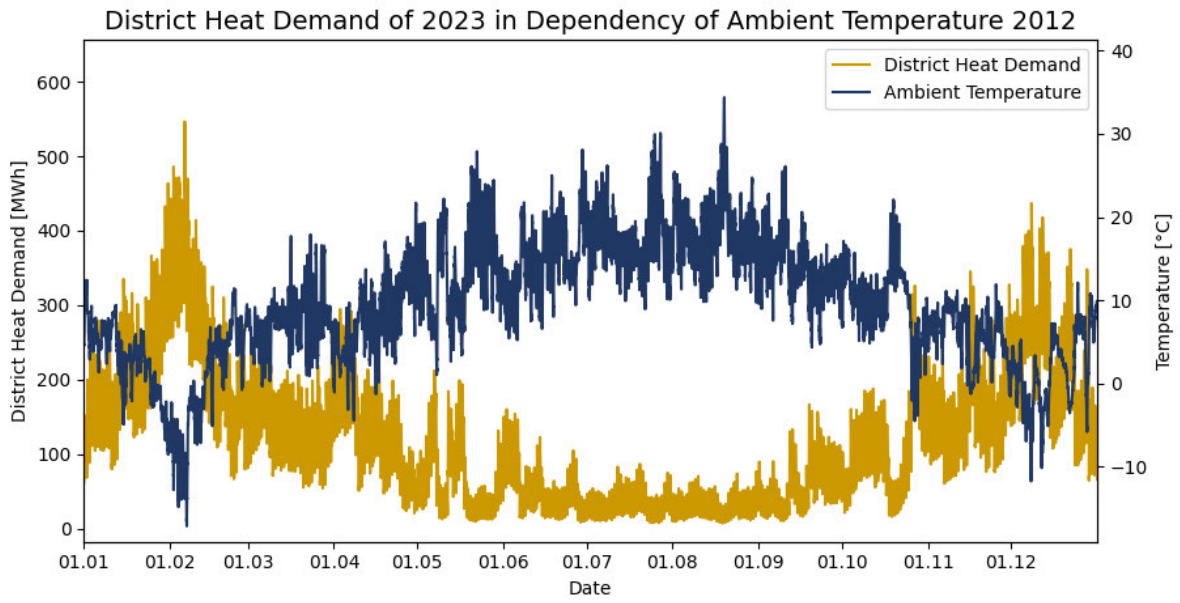

Figure 16: District heat demand 2023 in dependency of temperature 2012 [77] [85] [88] [92] (own illustration)

As expected, the district heat consumption decreases with an increase of temperature, which reflects a usual consumption behavior [93, 94, 95, 96]. Comparative literature shows that the curve of the district heat load in Germany in 2012 has a very similar progression [81]. The fluctuations during the day in different seasons depend on the hourly factors used. Figure 17 illustrates the hourly fluctuation of the SLPs developed in 2002 for single-family homes and local authorities, to which the largest consumption was allocated in 2022.

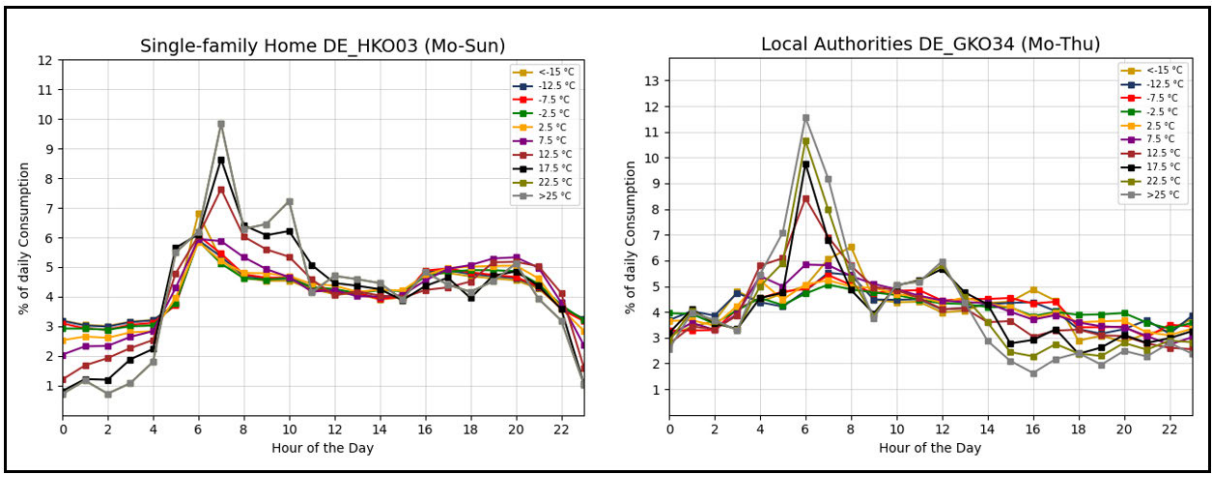

Figure 17: Hourly factors for single-family homes and local authorities during weekdays [88] (own illustration)

While consumption is more evenly distributed at colder daily average temperatures the percentage peak values increase with rising temperatures. It must be noted that in the hourly demand factors, there is no such explicit distinction between space and water heating. Assuming there is no space heating at high ambient air temperatures, the hourly demand factors for the highest temperature range are related to water heating [97]. Hence, the daily fluctuations regarding the average consumption

during the day are higher in summer than in winter seasons. Figure 18 compares the district heat demand for a week in winter season with the one during summer season.

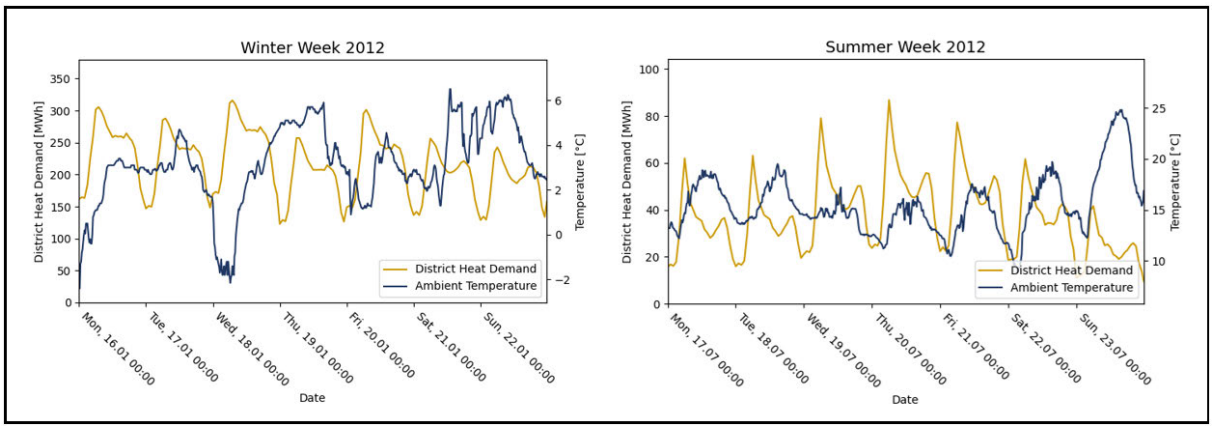

Figure 18: Comparison of district heat demand for winter and summer weeks [88] (own illustration)

The days in winter show a higher daily average consumption but smaller peak values compared to the daily average consumption. This behavior is consistent and very similar to the profile behavior described in comparable literature using the SLPs developed in 2007 [81, 97]. The generated time series for the quarter-hourly district heat consumption is therefore deemed valid and plausible.

4.1.5 Electrictiy Price

The adaption of the HP operation according to market signals is pivotal for cost-optimization. Here solely the energy-only-market is considered since LSHPs are not used to date to provide control energy due to their insufficient response time as described previously in chapter 2.2. In Germany, day-ahead electricity market prices are published daily at 12:00 p.m. for the following day. This allows LSHPs to align their operation and optimize electricity procurement accordingly. The day ahead market prices of the previous years in Germany are provided by the ‘Bundesnatzagentur’ in an hourly resolution [98]. The data files were also already provided by the CC4E. The files are transformed, and the data is processed using interpolation to generate a time series with a 15-minute resolution. For reasons of actuality the day-ahead market prices of 2024 are considered in this work. The course of the prices is shown in Figure 19.

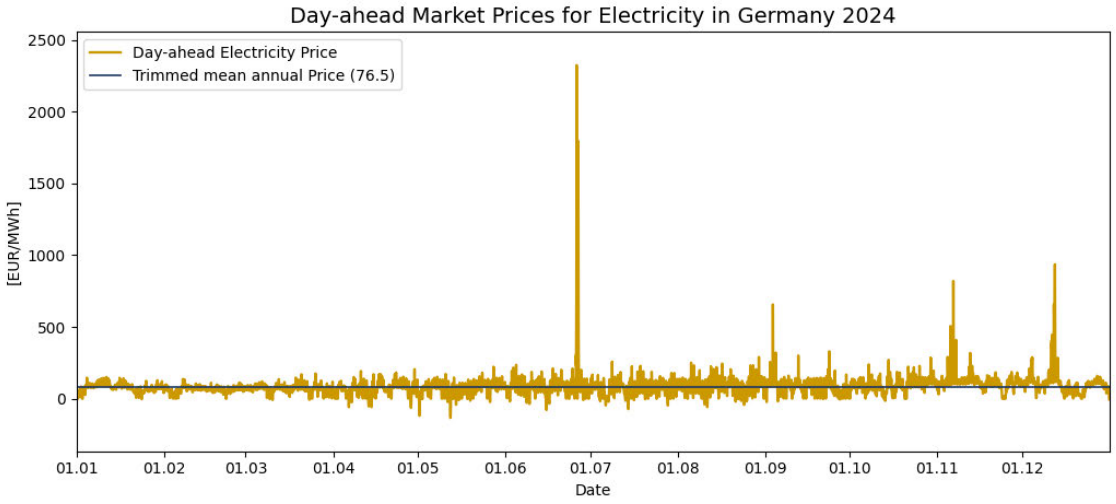

Figure 19: Day-ahead Electricity Prices in Germany 2024 [98] (own illustration)

4.1.6 Redispatch Interventions

As described in chapter 2.2 it is anticipated that LSHPs have the potential to compensate for grid congestion by adapting their electricity consumption behavior when a grid bottleneck occurs. The redispatch measures carried out in recent years are documented by the grid operators and published by the grid operator '50Hertz' [35]. Here, the period of the redispatch measure, the average output and the affected power plants are documented. Filtering for power plants in Hamburg, the data for 2024 shows when and which power plant carried out redispatch measures.[8] The data is processed in such a way that the reduction or increase in active power feed-in from all power plants in Hamburg is allocated to the individual 15-minute timesteps. Moreover, the data is inverted so that the data series already contains the data with the power direction showing in the same direction to which the LSHPs shall adapt their consumption behavior. Thus, a quarter-hour time series of reverse redispatch intervention is generated which shows adjustments of electricity consumption the LSHPs need to perform to avoid the redispatch measures proceeded. Due to the simplified modeling approach of summarizing all planned LSHPs in one representative unit, as it is explained in chapter 4.3.2, the generation of individual data series of redispatch intervention for each individual power plant in Hamburg has been omitted. However, when scanning the data for redispatch interventions in Hamburg in 2024, it was found that opposing redispatch measures occurred only during 5 hours on 7 December and 1 hour on 29 December. Therefore, the aggregated data series, which sums up all redispatch measures in 15-minute intervals, is considered representative of the redispatch measures in Hamburg in 2024. In Figure 20 the time series of aggregated reverse redispatch measures is illustrated for 2024.

[8] Only those power plants are filtered which are explicitly labelled with 'Hamburg' in their name. It cannot be ruled out with certainty that additional Hamburg-based plants were omitted due to the absence of this designation.

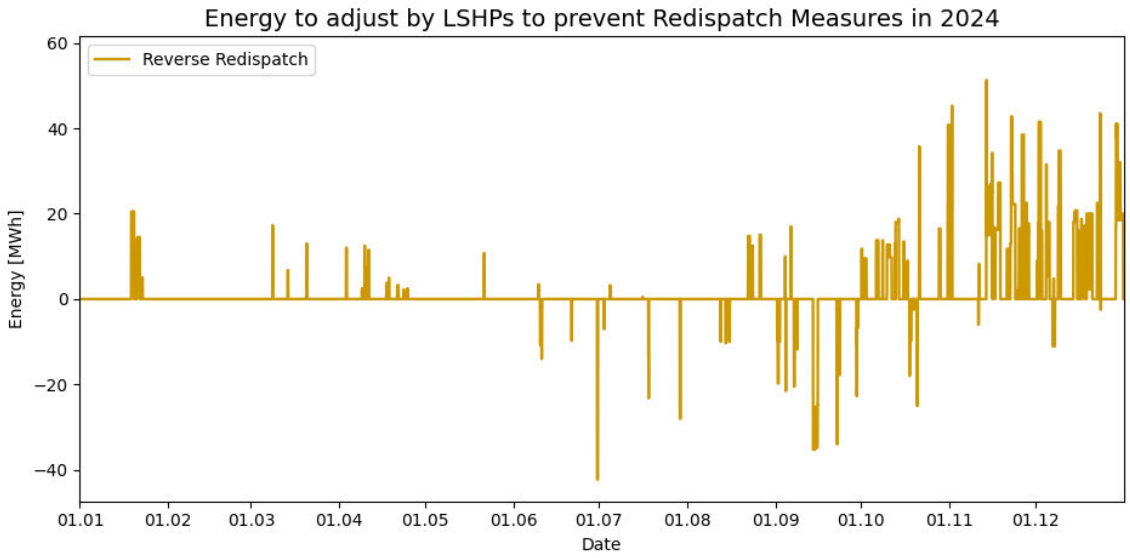

Figure 20: Aggregated reverse Redispatch Measures 2024 [35] (own illustration)

If the curve is above zero, it means that a redispatch measure takes place due to reduction in power generation. The assumption is that if the LSHPs consume that amount of energy additionally to their regular consumption then there would be no need to reduce the output of power plants. On the other hand, if the curve is below zero then an increase in power due to reserve energy is necessary. Here, the decrease of LSHPs power consumption of that amount in regard to their regular consumption could prevent the need for additional reserve power. However, this is a simplification, which assumes that the power consumption of the LSHPs takes place exactly at the location in Hamburg's power grid where redispatch measures would otherwise be required. Based on the data for power imports in Hamburg in 2024 [99], it suggests that changes in electricity consumption within the city—without further spatial resolution—do not affect redispatch measures in a correlated manner. It is observed that redispatch interventions occur independently of the magnitude of power imports at a given time, i.e. adjustments to the electricity imports are not inevitably used to compensate for redispatch actions. Figure 21 shows the hourly real redispatch volumes plotted against the corresponding power imports.

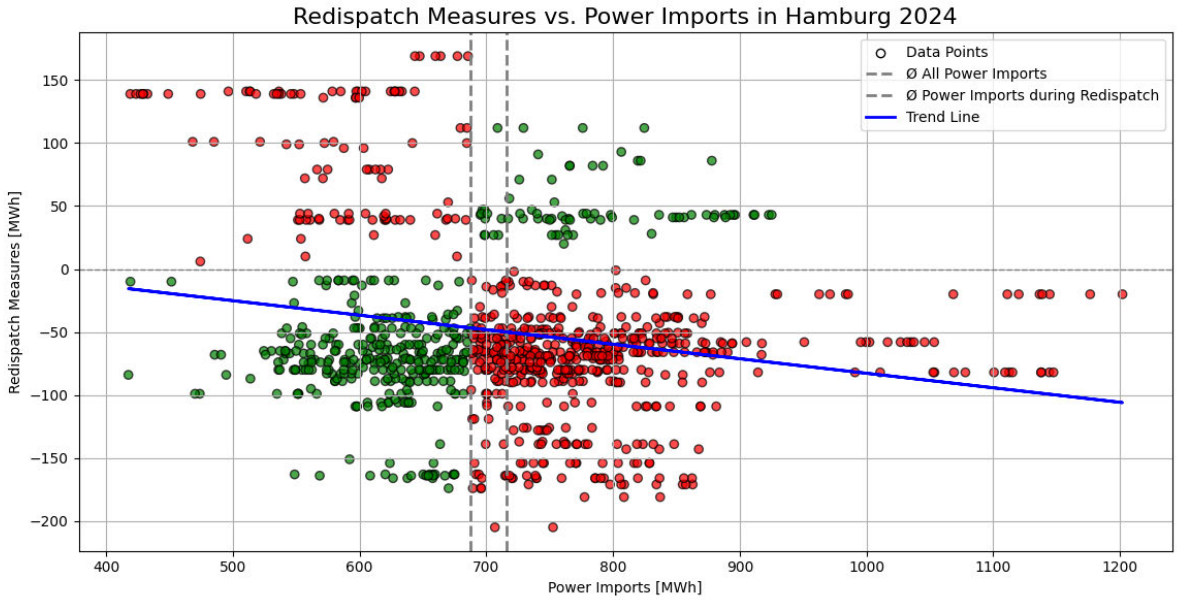

Figure 21: Correlation between Redispatch Measures and Electricity Import 2024 [35, 99] (own illustration)

In 304 hours of the year, a reduction in power due to redispatch measures coincides with a decrease in power imports regarding the average power import during the whole year (bottom left), while in 75 hours, an increase in power due to redispatch is accompanied by an increase in power imports (top right). Conversely, in 553 hours, a reduction in redispatch power coincides with an increase in power imports (bottom right), and in 103 hours, an increase in redispatch power occurs alongside a decrease in power imports (top left). The Pearson correlation coefficient for the correlation between the power for redispatch intervention x_i and the imported power y_i only considering the hours where redispatch intervention took place is calculated to:

$$r = \frac{\sum_{i=1}^{n}(x_i \cdot y_i) - n \cdot \bar{x} \cdot \bar{y}}{\sqrt{\sum_{i=1}^{n}(x_i^2) - n \cdot \bar{x}^2} \cdot \sqrt{\sum_{i=1}^{n}(y_i^2) - n \cdot \bar{y}^2}} = -0.197 \qquad (25)$$

The correlation coefficient implies a weak negative correlation between the power used for redispatch intervention and the imported power in Hamburg in 2024. Since only those points were considered where redispatch interventions actually took place, and it is not evident how electricity imports may have influenced the potential prevention of such interventions, no further conclusions can be drawn regarding the control of electricity imports to influence redispatch interventions. The fact that no direct influence of electricity imports on redispatch interventions can be identified should raise awareness that assuming a grid-supportive operation of heat pumps solely by compensating the energy involved in redispatch actions is a simplification that requires further refinement. This again leads to the conclusion that the local positioning of the grid-serving flexibilities plays a very important role. The LSHPs in Wedel and Tiefstack are planned to be installed at the same locations where the power plants are intended to be replaced [20]. Among the 146 redispatch measures recorded in 2024, 88 were attributed to the CHP plant in Wedel, 48 to units located at the Tiefstack site, and 10 to the CHP plant

in Moorburg, which is located near the site of the planned wastewater HP in Dradenau [35]. Therefore, the assumption that the LSHPs adjust their power consumption according to the redispatch interventions carried out by these power plants is a valid approximation to capture the effects of a grid-supportive operation. Nevertheless, to accurately determine the interactions between the electricity grid and the operation of LSHPs in a grid-supportive approach, an actual load flow analysis of the Hamburg electricity grid with the assignment of the LSHPs to specific grid nodes would be necessary.

4.2 General Structure of the Simulation

In the following chapter the general structure of the simulation and the concept of data processing during modelling is depicted. This is fundamental to comprehend how the following subsequent parts of the model are interconnected.

To enable the modelling of different LSHPs a class “hp” is created for the simulation, in which individual HP objects can be created with their respective attributes. The fundamental process for simulating each timestep in the year for each individual HP object is illustrated in Figure 22.

Figure 22: Core structure of the model's algorithm (own illustration)

Before the individual timesteps are simulated, all input data frames are prepared and the HP objects with their attributes are created. Then the parameters for the simulation are set and lists are initiated to store the simulation results of each HP object. Subsequently, all timesteps of a selected time period are run through in a for-loop by iterating the data frame 'df_dates'. Here, the input data for each timestep is loaded first and then the simulation steps for each HP object are performed in a nested for-loop. To run a simulation step, the nested for-loop retrieves the necessary parameters from the previous simulation step, and the available switches for the current simulation step are calculated. Then the function 'state_calculation_hp' of the class 'hp' is called and the parameters of the timestep are calculated for the respective object. The simulation of a timestep due to the function 'state_calculation_hp' essentially consists of two parts, the determination of the heat output and the calculation of the electrical input power through thermodynamic modeling. Thereafter, all parameters are stored in a dictionary called 'dic_states_hp' and appended to the list rows_Sim1[index], which collects the dictionaries for each timestep of the HP object at the respective index. At the end of the simulation, Excel files are created for each HP object, containing the simulation results of all timesteps.

When access parameters from previous timesteps during the simulation and when saving the simulation results at the end of the simulation, it is crucial to understand the memory structure correctly of the list 'rows_Sim1'. The structure is shown in Figure 23.

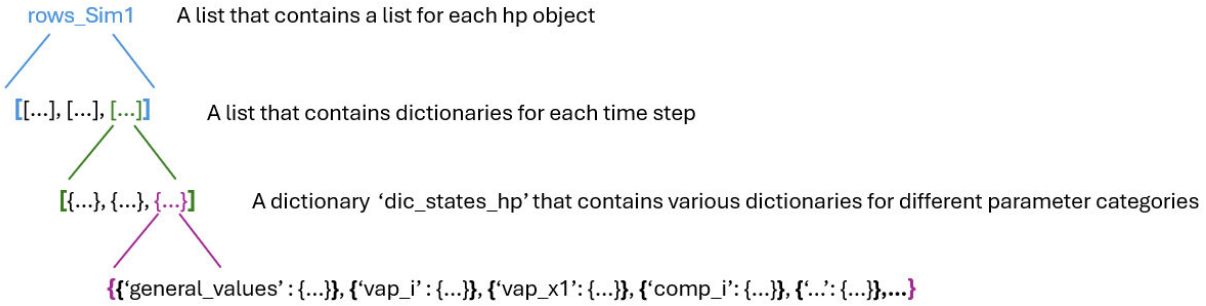

Figure 23: Memory structure of main list containing the simulation results of one HP object (own illustration)

The list 'rows_Sim1' contains a list for each hp object. One list of each hp object in turn includes the dictionaries 'dic_states_hp' of each timestamp. That's why at the end of one simulation step the dictionary 'dic_states_hp' gets added to the respective list of the hp object with the index 'index', as shown in Figure 22. The dictionary 'dic_states_hp', which contains all parameters of one timestep for an HP object is separated into subordinated dictionaries. The subordinated dictionary with the main key 'general_values' includes all the general parameters and the other subordinated dictionaries include the thermodynamic quantities of each state of the thermodynamic modeling.

4.3 System Characteristics and Operational Constraints

This chapter defines the framework conditions on which the model is based. The modelling assumptions described in this chapter set the foundation for further model refinement and must be considered when evaluating the results.

4.3.1 System Size and Control

The system size of the LSHPs planned in Hamburg includes a 60 MW_{th} HP in Tiefstack, a 60 MW_{th} wastewater HP at the wastewater treatment plant in Dradenau, and a 165 to 195 MW_{th} HP in Wedel. In a past interview with Ulrich Liebenthal from the 'Hamburger Energiewerke' at the beginning of this study, the heat output of the planned HP in Wedel was estimated to be between 150 and 165 MW [20]. However, the current database for LSHPs projects provided by the 'LandesEnergieAgentur Hessen' indicates a capacity of 200 MW_{th} for the LSHPs in Wedel [19]. Since it was also informed that all LSHPs consist of smaller 15 MW_{th} modules which can be controlled separately, a total power of 195 MW_{th} is anticipated for the Wedel site. Thus, in total 315 MW_{th} divided into 21 modules with 15 MW_{th} each are assumed to be installed in Hamburg at three different locations. Here, the modules can be operated independently and ideally achieve part-load operation at 50% of their nominal power [20].

4.3.2 Simplified Modelling Approach

Even though the model enables modelling different LSHPs as different HP objects, for reasons of simplification it is decided to cover the properties of the three LSHPs planed in one single representative HP object. This enables a more streamlined evaluation, better visualization of the results and a time-optimized simulation. This approach is supported by the modular design of the HPs, which are planned in 15 MW_{th} units. Since the LSHPs are expected to communicate with each other and operate in a coordinated manner to meet thermal demand, this assumption is considered acceptable within the intended accuracy of this study. The extent to which this simplification may influence the accuracy of the results, particularly regarding the contribution to grid support, is discussed in chapter 6.

4.3.3 Storage System

According to the information provided by 'Hamburger Energiewerke', a thermal storage tank with a capacity of 40,000 m^3 is planned at the Tiefstack site, and a storage tank with a capacity of 55,000 m^3 is planned at the Dradenau site [20]. No storage facility is currently planned at the Wedel site, but this has not been ruled out yet. With a supply temperature between 90 and 100°C and the temperature profile presented in chapter 4.1.3, the average sink temperature of the LSHPs in 2012 is 92.7 °C. With a total storage tank size of 95,000 m^3 and an assumed return temperature of the water in the heating grid of 45 °C [79], this results in a heat energy storage capacity of:

$$Q = V \cdot \rho \cdot c_p \cdot \Delta T = 95{,}000\, m^3 \cdot \frac{1000\, kg}{m^3} \cdot 4{,}18 \frac{kJ}{kg \cdot K} \cdot (92.7 - 45)K = 18{,}94\, TJ = 5262\, MWh \quad (26)$$

Thus, with a nominal thermal output of 315 MW_{th}, the storage can be fully charged in about 16 hours and 42 minutes.

4.3.4 Output Limitation due to Compressor Power

The maximum thermal output of the LSHPs is restricted by the nominal power of the compressor. Since the compressor's maximum power cannot be exceeded, the maximum heat output varies depending on the operating conditions. The nominal thermal output of 15 MW_{th} per module is therefore tied to specific operating conditions. As these exact conditions are not publicly available, it is assumed in this study that the published heat output specifications have been chosen in such a way that the resulting public perception reflects the actual physical performance of the HP operation. Consequently, the nominal thermal output of 15 MW_{th} per module is considered to be achievable under average operating conditions. To determine the average operating conditions, the average $\overline{COP}_{Carnot,exterior}$ is calculated using the input data for the water temperatures and the district heating supply temperatures of the LSHPs, analogous to equation (11) in chapter 3.3. The module's nominal thermal

output in each simulation timestep is then scaled by the $\overline{COP}_{Carnot,exterior}$ and the average nominal thermal power $\bar{\dot{Q}} = 15\ MW$. It applies:

$$\dot{Q}_i = \frac{COP_{Carnot,exterior,i}}{\overline{COP}_{Carnot,exterior}} \cdot \bar{\dot{Q}} \qquad (27)$$

Since the development of the COP_{real} is typically proportional to the $COP_{Carnot,exterior}$ in practical applications, scaling the nominal thermal output in this manner is a reasonable approach. This assumption is further supported by the model simulations, which also show a direct correlation between the COP_{modell} resulting from the modelling and the $COP_{Carnot,exterior}$ based solely on the external conditions. Figure 24 shows the time series of the COP values and the theoretically maximum total heat output assuming an operation of all modules under standard operating conditions for 2012. As in this figure, all subsequent figures displaying energy flows show the energy amounts per 15-minute time interval on the y-axis, unless explicitly stated otherwise.

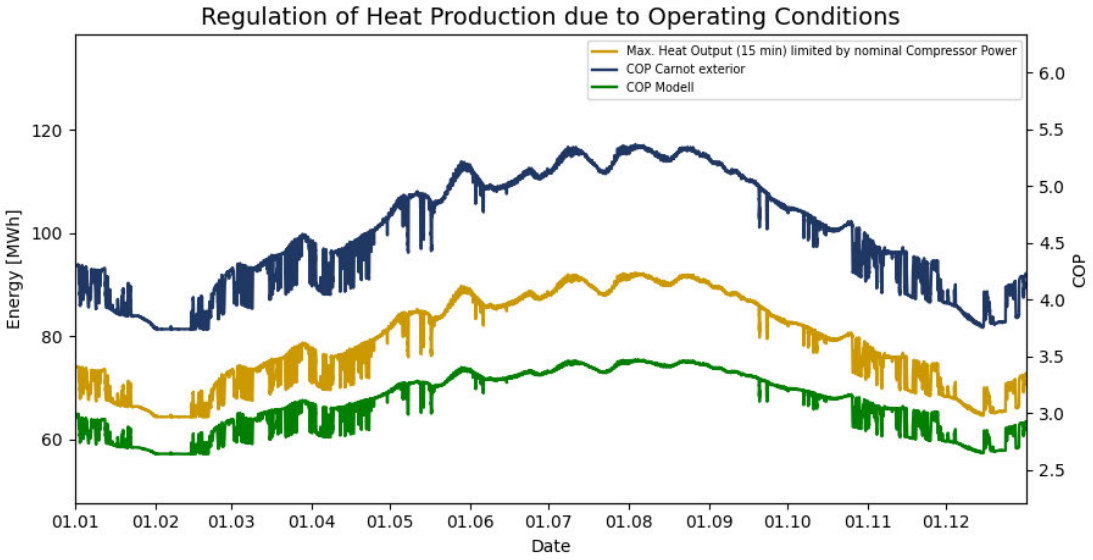

Figure 24: Heat output regulation due to nominal compressor power (own illustration)

It should be noted that with the current method of scaling, the nominal thermal output is always scaled to the average operating conditions that are set in the simulation. It is assumed that if the operating conditions change, the published data for the rated thermal output remains as a fixed scaling factor for heat output determination in regard to the new average operating conditions. For example, if a simulation is conducted under the assumption of reduced district heating supply temperatures, the resulting increase in the average $\overline{COP}_{Carnot,exterior}$ will still lead to an average nominal thermal output of 15 MW_{th} per module over the period of one year. This occurs despite the fact that a compressor operating at the same nominal electrical input would generate different heat outputs under such altered conditions. Accordingly, the assumed nominal compressor power is also effectively modified depending on the input data series, but constant within a simulation run. This also applies to changes due to the time series of water temperatures when simulating different weather years. An adaptation

to this scaling method in future simulations would be easily possible by tying the nominal power of 15 MW_{th} per module to fixed set of operating conditions $(T_{source}|T_{sink})$. Then a constant maximum compressor power would be maintained even in different simulation runs with different input data series.

4.3.5 Operational Limits at Low Source Conditions

At too low source temperatures, the operation of LSHPs is technically and economically unfeasible. According to the Information from the 'Hamburger Energiewerke' an operation of the LSHPs at source temperature below 5 °C is not intended [20]. This constraint is taken into account in the model and a shutdown of the LSHPs is executed if the source temperature drops below 5 °C. Nevertheless, since the HP in Dradenau uses wastewater from the wastewater plant as heat source, it is assumed that the HP at this site can stay in operation, even if the water temperature of the Elbe falls below 5 °C. This is realized by specifying the number of wasterwater modules in the attributes of the heat pump object. However, even though different source temperatures occur at the site in Dradenau compared to the water temperatures of the Elbe, in the current model no distinction is made between those source temperatures due to a lack of data for the wastewater temperature at the Dradenau site. Thus, the operation of the wastewater modules is simulated in the same way as the operation of all other modules based on the source temperatures of the Elbe, except that the wastewater modules remain in operation even at source temperatures below 5 °C. Figure 25 shows the operation of the LSHPs under the source temperature conditions of the year 2012 in 15-minute timesteps with simulation mode 1 optimized for maximum heat output.

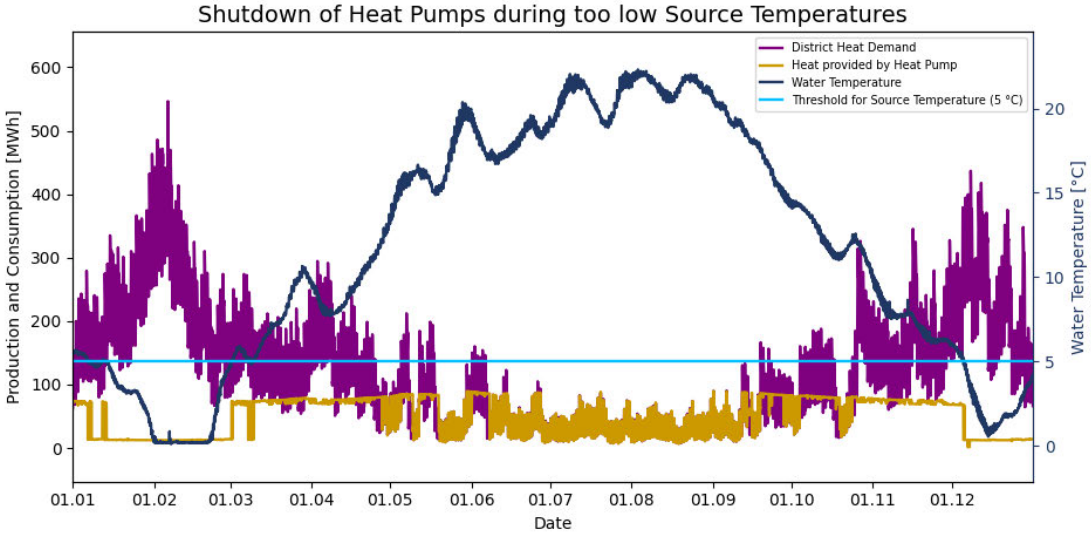

Figure 25: Shutdown of LSHPs due to source temperatures below 5 °C (own illustration)

It becomes evident that the shutdown of the HP modules supplied by the Elbe occurs at times when district heating demand is highest due to low ambient temperatures. In transitional periods it can occur that the source temperature hovers around the defined threshold. Here, intermittent fluctuations can

be observed which result in modules switching on and off in short periods of time, as shown in Figure 26.

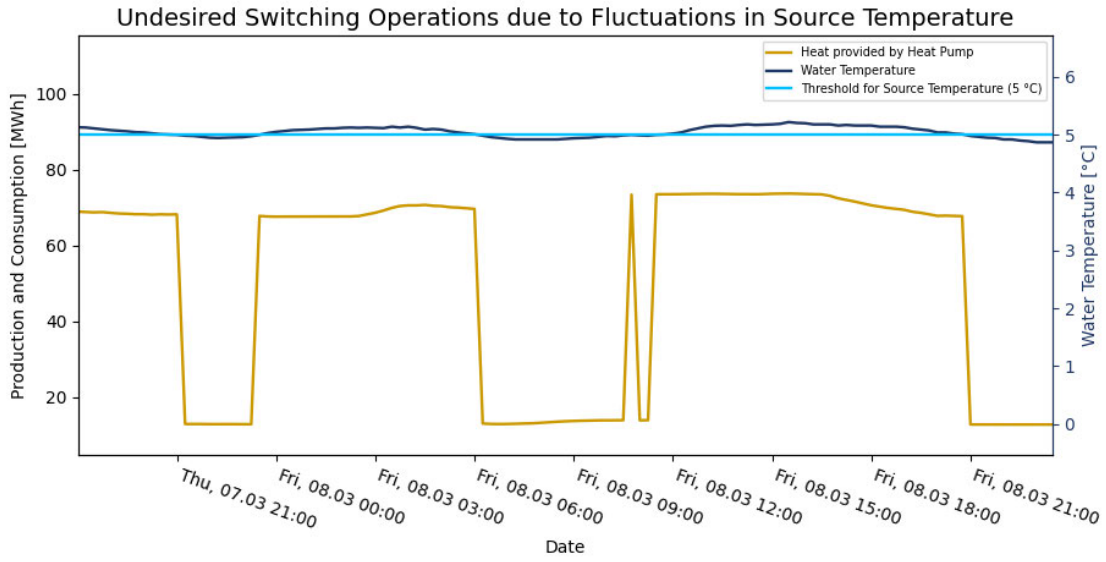

Figure 26: Undesired switching operations due to fluctuations in source temperature (own illustration)

A mechanism that only causes shutdowns if the source temperature remains below the threshold value for a longer period of time has not yet been established in the current algorithm. However, as threshold crossings only occur very rarely during the year, the impact of unnecessary switch-offs can currently be considered negligible. Nevertheless, the implementation of a mechanism to prevent such short-term fluctuations from triggering shutdowns is regarded as a necessary step in further model development to reflect operational realism.

4.4 Operating Modes for Heat Generation

The subsequent section depicts the different operating modes according to which the heat output of the LSHPs is determined. Each operating mode aims for different operating objectives. Thus, the selection of the operating mode is key to optimizing the operation for the desired requirements. In general, three basic operating modes are available in the HP model. The working principle of these modes is compared in the following chapters for the period between 25 April and 30 April 2024.

4.4.1 Mode 1

Mode 1 aims to maximize the HPs' heat coverage of district heat consumption regardless of the current electricity procurement costs. Figure 27 illustrates the operating principle.

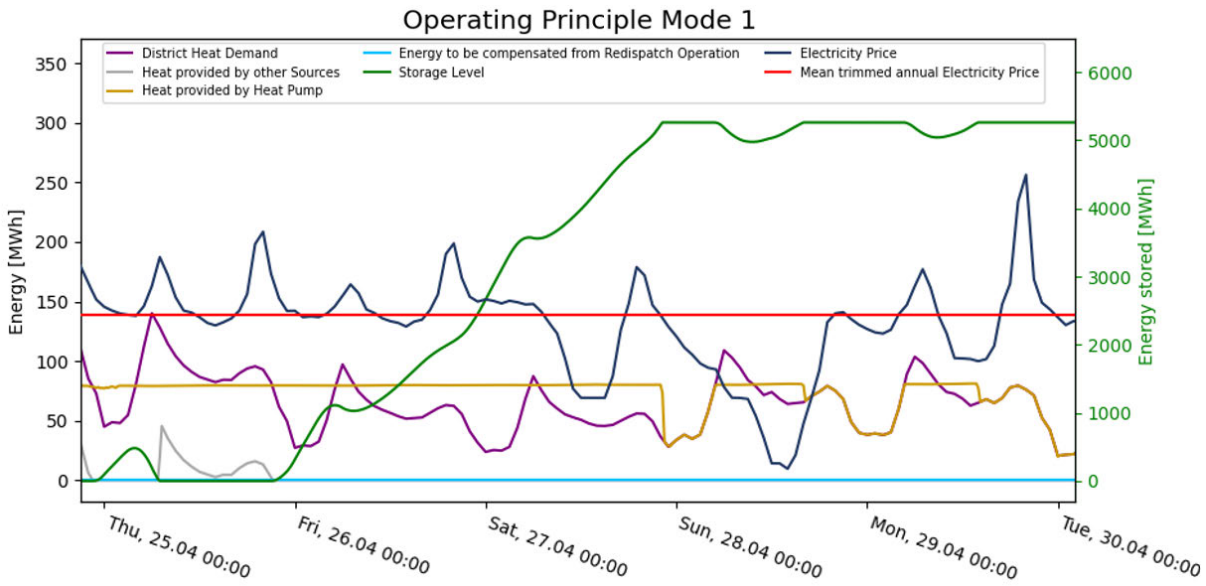

Figure 27: HP's operating Principle Mode 1 (own illustration)

The HP continuously produces the maximum output, irrespective of the high price peaks during the time period. The thermal output is reduced only when the storage capacities are reached as observed during the days on Sunday 28 and Monday 29 April. Whenever the heat demand is not fully covered by the HPs and the thermal storage, the remaining demand is met by other heat sources as seen on Tuesday 25 April.

4.4.2 Mode 2

In mode 2 two optimization objectives exist. The primary objective is to cover the immediate heat demand, and the secondary objective is to reduce operating costs. Therefore mode 2 adjusts the operation of the HP according to the electricity price only if the immediate heat demand is already covered. This mode therefore prioritizes meeting the immediate district heat demand over economic considerations but deprioritizes the supply of heat for future timesteps by omitting charging the storage when electricity prices are unfavorable. Figure 28 presents the operating concept.

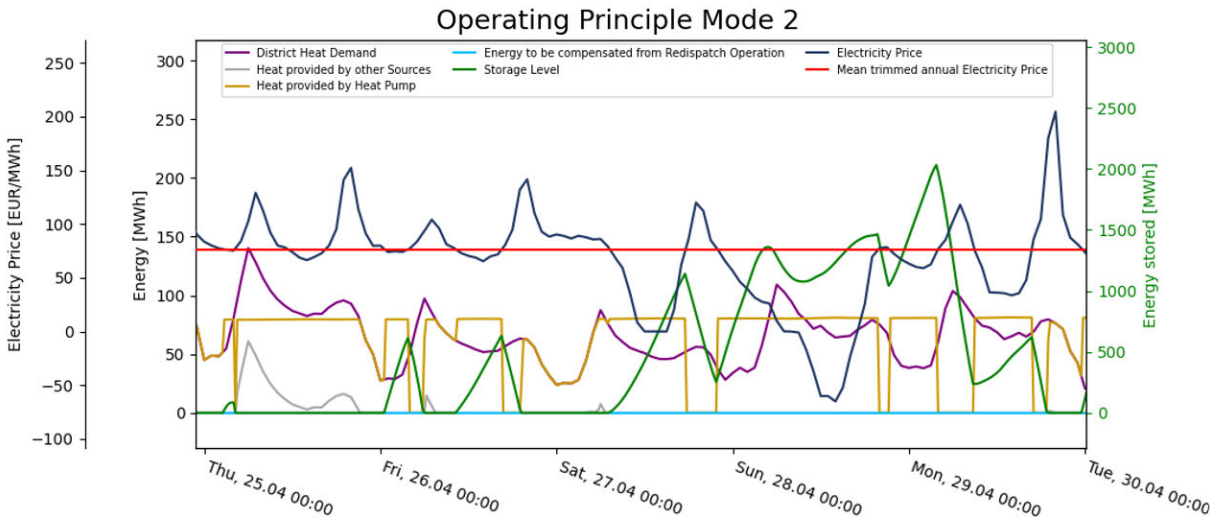

Figure 28: HP's operating principle mode 2 (own illustration)

If the immediate heat demand cannot be fully covered by the storage tank, the heat pump aims to meet the remaining demand despite high electricity prices as seen during the night of 26 to 27 April. If the storage tank already meets the demand, or only partial load operation is required, the heat output is determined based on the electricity price – within the boundaries of sufficient heat coverage. This can be observed multiple times, for instance when the HP reduces its production on the evening of Saturday, 27 April or the morning of Monday, 29 April.

4.4.3 Mode 3

Mode 3 operates solely based on current electricity prices, regardless of whether the district heating demand of the current timestep is covered or not. Figure 29 demonstrates the operating principle.

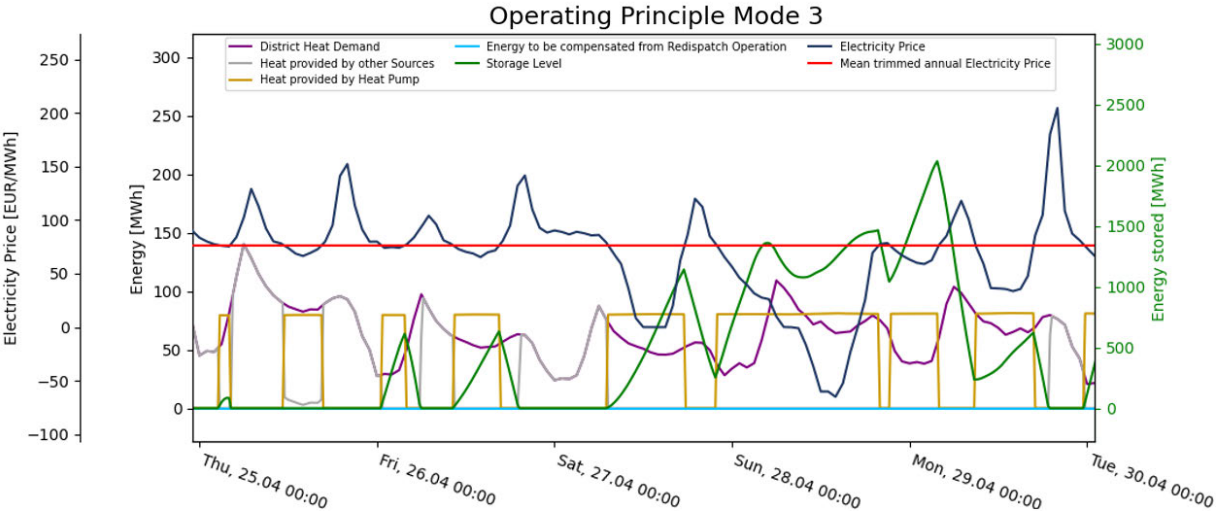

Figure 29: HP's operating principle mode 3 (own illustration)

Whenever the electricity price is below a certain threshold maximum heat output is targeted. Otherwise, heat production is shut down even though the heat demand is not covered by the storage

tank. Thus, other energy source must provide the remaining heat demand as observed for instance during large periods on 25 April and during the night between 26 and 27 April.

4.4.4 Grid-Supportive Operation

In the three basic modes only objectives regarding heat coverage and electricity procurement costs are considered. The aim of contributing to grid-supportive measures imposes an additional requirement on HP operation. Thus, in each of the three modes, the optional setting 'grid_friendly' can be activated. Then the HPs operation additionally takes into account the compensation of energy used for redispatch interventions. The amount of energy relevant for the heat production adjustment, which results from the compensation of redispatch measures for one HP object, is defined as follows:

$$Q_{redispatch,j} = W_{redispatch,total} \cdot \frac{Q_{nominal,j}}{\sum_j^n Q_{nominal,j}} \cdot COP_{real,j,i-1} \cdot \frac{COP_{Carnot,exterior,j,i}}{COP_{Carnot,exterior,j,i-1}} \qquad (28)$$

In the case that multiple HP objects are simulated, the amount of redispatch-related energy to be considered for a single HP object j is scaled by the factor based on the share of the object's heat generation capacity relative to the total heat generation capacity of all HP objects: $\frac{Q_{nominal,j}}{\sum_j^n Q_{nominal,j}}$. When simulating only one representative HP object, this factor is 1. Subsequently, the redispatch-related energy is further scaled using the forecasted COP of the current timestep to convert redispatch-related energy into the amount of thermal energy relevant for heat generation. This is done by the product of COP_{real} of the last timestep $i-1$ and the ratio $COP_{Carnot,exterior}$ from the current timestep i to the last timestep $i-1$. Here, the COP_{real} is tracked in every timestep due to the enthalpy balances of the thermodynamic modelling even if no heat production takes place.

It must be noted that the allocation of redispatch-related energy to individual HP objects using a scaling factor $\frac{Q_{nominal,j}}{\sum_j^n Q_{nominal,j}}$ is only a provisional solution. In the future, a time series representing the redispatch-related energy dedicated to the specific HP object should be stored as an attribute for each individual HP object.

If the 'grid_friendly' option is active, grid-supportive contribution is prioritized over the other optimization objective defined by the selected operating mode. For the process of heat output determination, it is important to understand the implications of a grid-supportive operation in the current model. The assumption is that if the LSHPs adjust their power consumption in response to the power used for redispatch interventions, they could replicate the grid-stabilizing effect of these measures, thereby preventing the need for them. This raises the question of which reference point should serve as the basis for power adjustment. If redispatch intervention occurs during the current operation of the LSHPs, it can be assumed that a power adjustment based on the current operating point of the LSHPs is necessary to avoid grid bottlenecks. Here, it is purposeful to fix the operating point at which the redispatch intervention occurred as threshold value. Otherwise, despite taking the

redispatch measure into account, changing the operating point could result in an undesirable power change due to the internal logic of the operating mode, thus further amplifying the grid bottleneck. This would be the case, for example, if grid congestion which requires power consumption occurs during a low electricity price in mode 3 and in the following timesteps the electricity price rises while the redispatch intervention is still active. In this scenario, despite considering the redispatch-related energy based of the new operating points, a power reduction compared to the previous operating point could take place since the operating point shifted. Nevertheless, a total fixation of the power level without additional flexibility in the desired direction would also be ineffective. This would prevent a win-win situation in which the previous operating objective can further be achieved and additional relief for the power line is provided as illustrated further below in Figure 31. In addition, unnecessary deviations from the planned operation could place a burden on the feed-in and withdrawal balance of the local grid, which in the worst case would require the use of control energy. Therefore, the heat generation level is fixed one-sided starting from the operating point when redispatch intervention occurred. In Figure 30 the working principle of one-sided fixation of the heat generation level to accurately provide contribution to grid-support and cover redispatch-related energy is outlined for the case of redispatch interventions which require further electricity consumption.

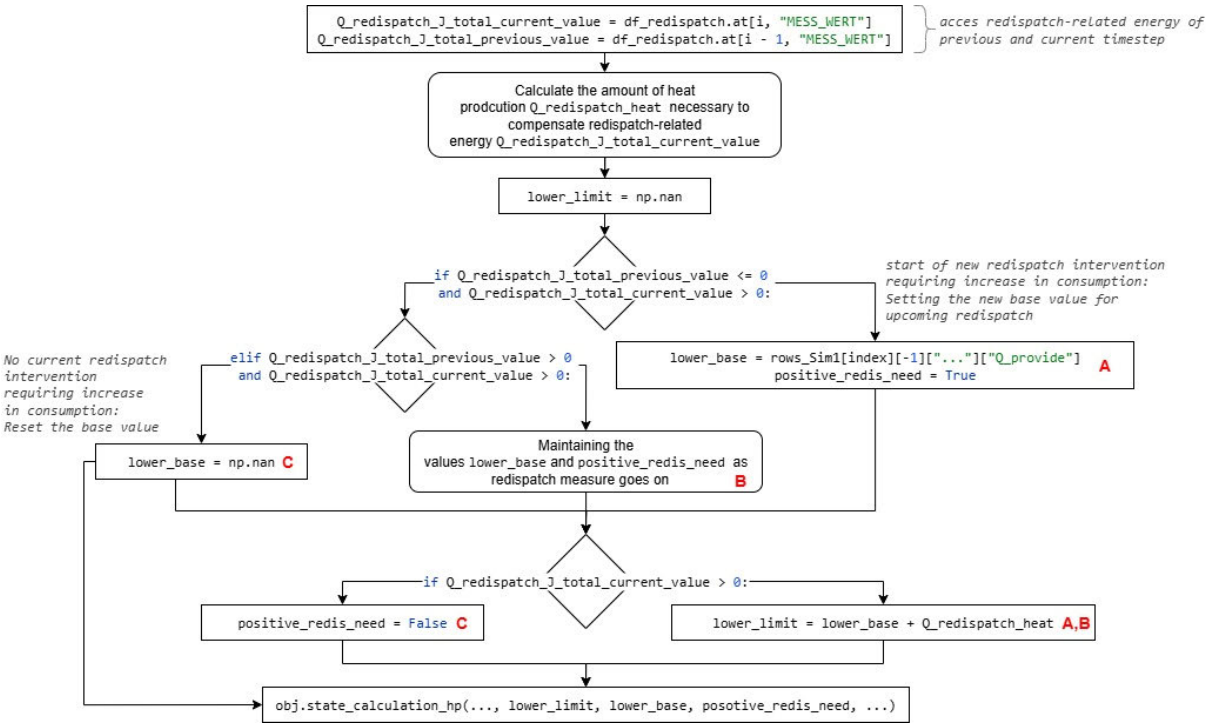

Figure 30: Control strategy to adjust heat generation in response to redispatch interventions (own illustration)

Before a timestep is simulated the requirements towards the heat generation due to redispatch-related energy are checked. Here, first the values of redispatch energy of the previous and current timestep are accessed. Then the amount of energy relevant for the heat production adjustment is calculated as described above. Thereafter, the status of current redispatch measures requiring further heat production is determined. If in the current timestep a new redispatch intervention starts, then the heat

generation level of the last timestep is set as the base level 'lower_base' from which the increase of heat production must take place (case A). From that level the redispatch-related additional heat production is added up for the future timesteps until the end of the redispatch intervention to define the threshold power level 'lower_limit' which the HP shall achieve in the corresponding timesteps (case A, B). If an ongoing redispatch intervention is detected, then the base level 'lower_base' determined at the start of the redispatch intervention is maintained (case B). And if no redispatch intervention in that direction occurs the base level 'lower_base' is reset and the status for the need of redispatch interventions 'positive_redis_need' in that direction is set to 'False'. At the end all variables 'lower_base', 'lower_limit' and 'positive_redis_need' are passed to the function 'state_calculation_hp' where the heat output of the current timestep is determined as described in 4.6. Here, the heat production level 'lower_limit' is set as a soft constraint which can only be violated in case of limitations due to compressor power or storage capacities. The process to consider redispatch interventions which require a decrease in production is analogous to the process described for redispatch interventions leading to production increase. Figure 31 illustrates the results of the control strategy to compensate for redispatch-related energy. Here, the scenario where grid congestion requires the reduction of electricity consumption is depicted for mode 2. The blue line shows the resulting adjustments of heat output needed to compensate for the electrical energy used in redispatch intervention. The redispatch intervention starts at 12:00 on 1 May. Thus, the base level of heat production 'upper_base' (orange) is set to the production level at 11:45. From that base level 'upper_base' the redispatch-related energy of every follow-up timestep is considered until the redispatch intervention ends. During that time the previous operation objectives can just be fulfilled one-sided. At 17:00, the electricity price goes up and the generation is stopped thus allowing the operating mode to follow its default logic of electricity price-led decisions when the heat demand is covered by the storage tank. Here, a win-win situation is created as there is greater reduction in power line congestion and a cost-optimized operation is achieved. However, later at 19:15, the storage tank is empty, thus raising the need for heat demand coverage. Since the primary objective of resolving the grid bottleneck overrides the secondary goal of heat coverage, the heat generation is limited to the 'upper-limit' at this timestep. Hence, one-sided fixation of the 'upper_limit' supports an optimized operation that prioritizes grid congestion prevention while optionally maintaining the planned operation.

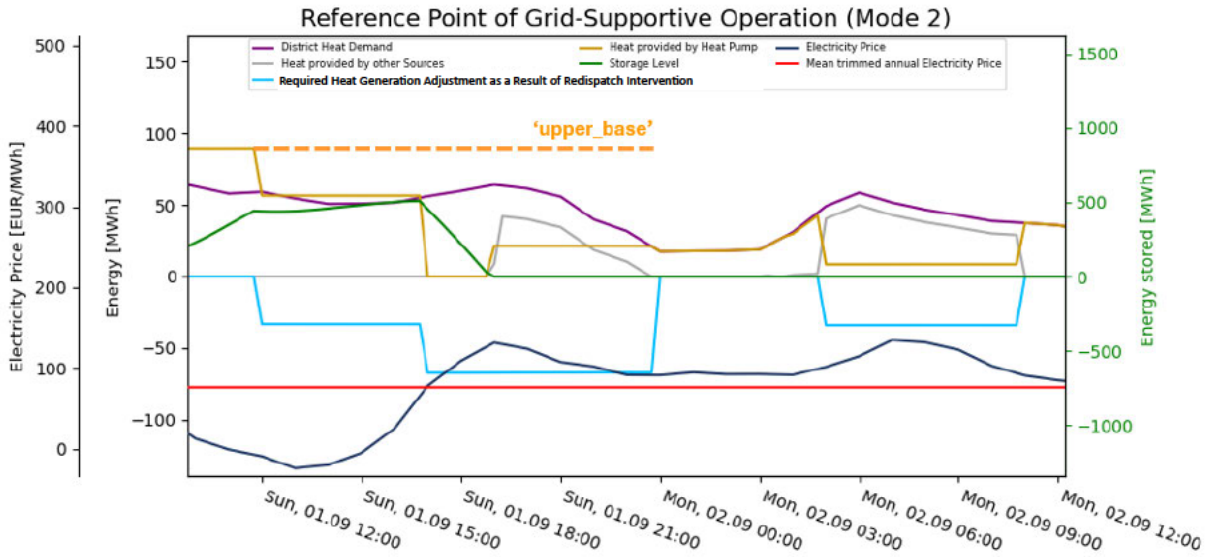

Figure 31: Limiting heat generation in response to redispatch related energy (own illustration)

In contrast to Figure 31, Figure 32 shows the increase in heat production caused by redispatch interventions. Here, a scenario in mode 3 is depicted where the heat generation output is elevated despite high electricity prices. Particularly, the last redispatch intervention starting at 05:00 on 28 November illustrates the working principle. When the redispatch intervention starts, the heat production is at maximum capacity due to low electricity prices. Shortly afterward, the electricity price rises. Without the redispatch intervention the heat production would be shut down, but since production is tied one-sided to the energy level 'lower_base' before the redispatch occurred, it stays at maximum production. This makes sense, as the redispatch intervention started despite the high heat production, meaning that additional electricity consumption would have been required. Only due to compressor power limits the 'lower_base' is very slightly undercut in this scenario.

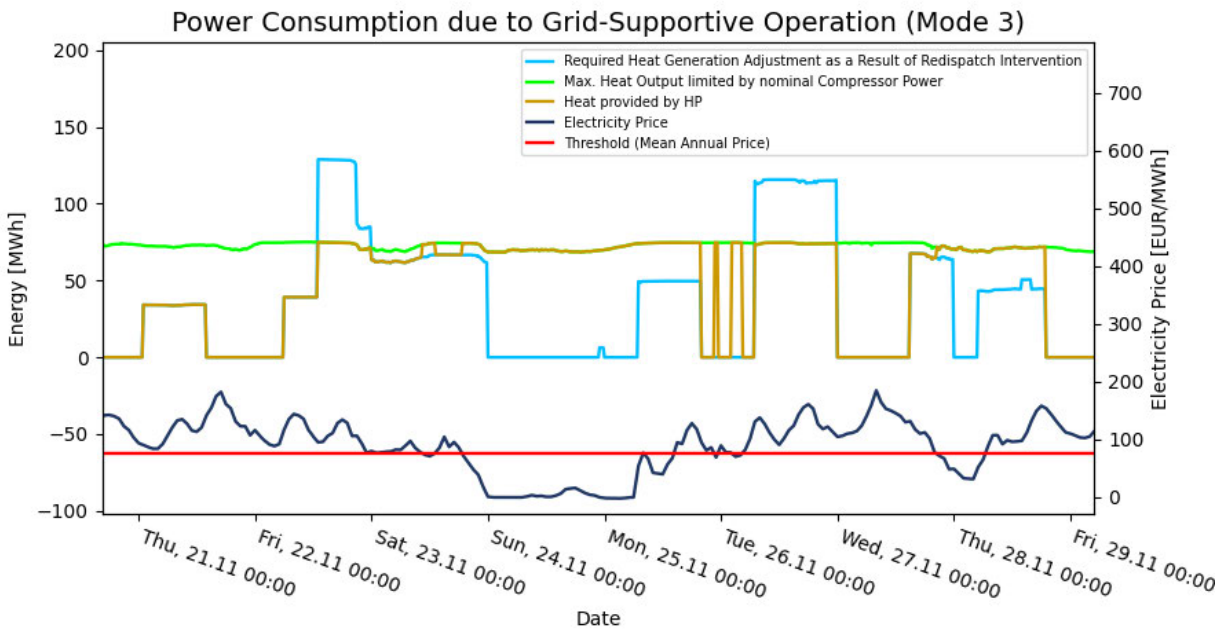

Figure 32: Raising/Maintaining heat generation in response to redispatch-related energy (own illustration)

The concept of one-sided fixation by adding up the required heat generation adjustments to the previously defined heat production level 'upper-base' or 'lower-base' is also used to track the contribution to grid-supportive behavior as explained when analyzing the simulation results in chapter 5.2.2.

The selection of three operating modes (1, 2, 3) in combination with the optional grid-supportive feature results in a total of six different control strategies: the basic modes 1b, 2b, 3b and the grid-friendly modes 1g, 2g, 3g.

4.5 Technical System Control

This chapter describes a control strategy to manage switching commands in response to changing operating conditions in HP operation. The aim is to comply to technical constraints and allow system-friendly operation.

The selection of the mode is decisive for the technical operation of the HP. Based on the information from 'Hamburger Energiewerke', a partial load behavior down to 50 % should ideally be achievable, but the modules should certainly not be switched on and off more than four times a day. According to these constraints, an algorithm was developed for operating mode 3, as mode 3 is regarded as the standard operating mode for the LSHPs [20]. Furthermore, mode 3 is the mode that requires the most switching operations, as an electricity price-led operation necessitates switching on and off all modules of the HP. To adapt the heat output to the required optimization objectives over a certain period without violating the technical constraints, the number of possible switching operations is calculated before each timestep. The simplified process is presented in Figure 33.

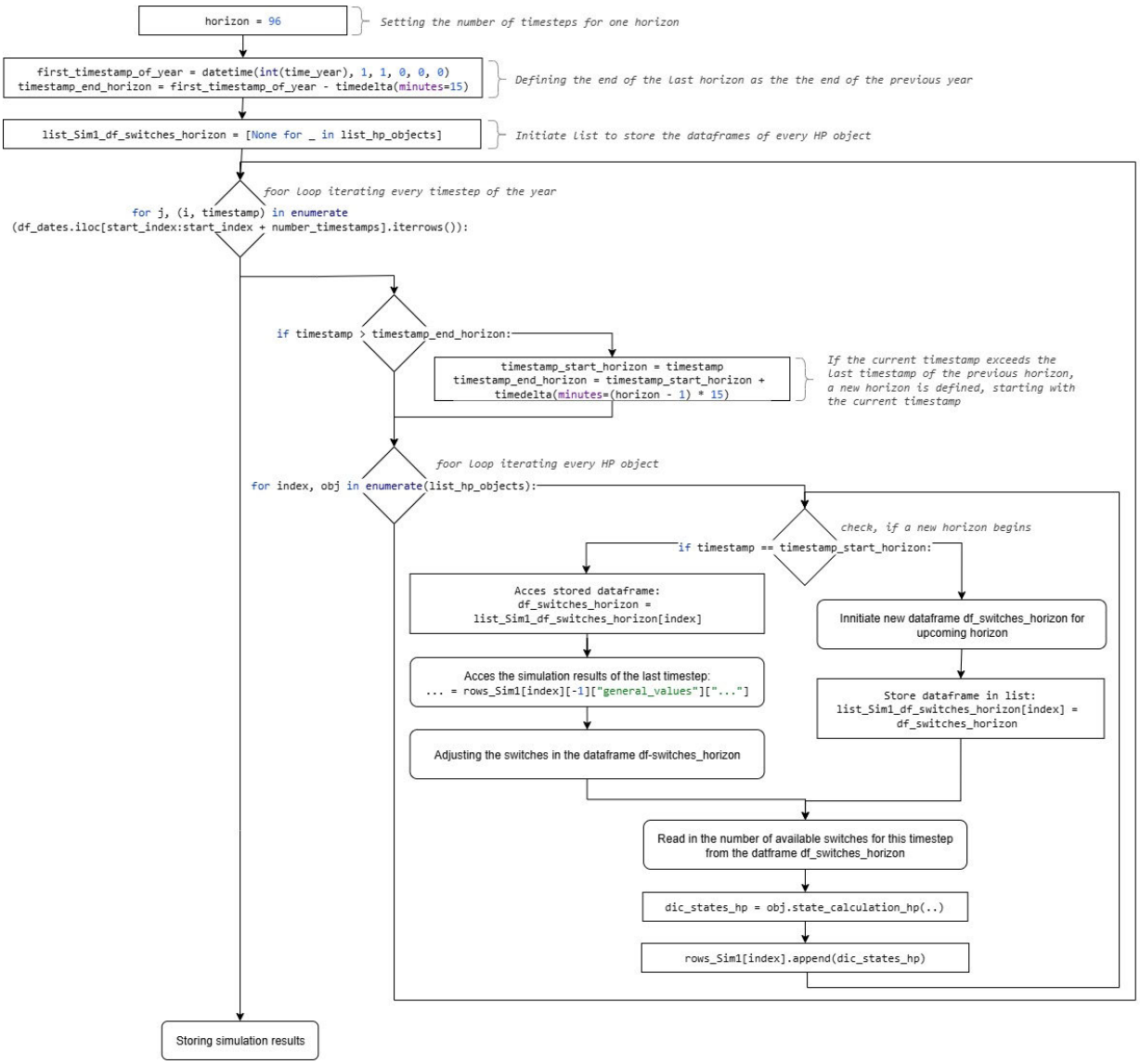

Figure 33: Process of switching allocation for technical operation of the HP (own illustration)

At the beginning, the time horizon for each optimization interval is defined based on the number of 15-minute timesteps. The end of the last time horizon is initially set to a fictitious point in time before the first timestep of the simulation. A list named 'list_Sim1_df_switches_horizon' is then initialized to store the data frames 'df_switches_horizon', each of which contains the switching allocation for the corresponding HP object for a specific time interval. During the simulation loop, it is checked at each timestep whether the current timestep still lies within the currently active time horizon. If this is not the case, a new time horizon is defined, starting from the current timestep. Within the simulation of each HP object, it is checked whether a new time horizon begins or not. If so, a new data frame 'df_switches_horizon' is created, containing the initial distribution of switching operations for the upcoming time horizon. This data frame is then stored in the list 'list_Sim1_df_switches_horizon' for the corresponding HP object. If, on the other hand, the current timestep still lies within the active time horizon, the corresponding data frame 'df_switches_horizon' and the simulation results from the previous timestep are accessed. Based on the results of the previous timestep, the switching allocation

in the data frame is adjusted in case the number of switches used deviates from the number previously assigned to that timestep due to under- or overutilization. Before calling the function 'state_calculation_hp', the number of available switches for the current timestep is read from the data frame. After simulating the timestep, the results are stored as described in chapter 4.2.

A violation of the maximum permitted number of switching operations is only possible in exceptional cases – namely, during emergency shutdowns due to too low source temperatures or if the thermal storage reaches full capacity, or if the compensation of redispatch measures within the whole time horizon necessitates more switching events than initially allowed in the time horizon. The structure of the data frame 'df_switches_horizon', which is responsible for the allocation of switching operations, consists of four columns: 'MESS_DATUM', 'MESS_WERT', 'Prio' and 'Sum_Price_Deviation'. The column 'MESS_DATUM' contains the full date of the current timestep, while the column 'MESS_WERT' indicates the number of switching operations assigned to that timestep. The data frame also has the original indices that the rows with the same timestamp have in the original data frame 'df_dates', which is iterated for each timestep as described in chapter 4.2. The initial assignment of possible switching operations at the beginning of each time horizon is carried out according to a ranking, whereby all future input data within the time horizon are considered. The order of priority for the initial allocation of available switching operations within a time horizon is depicted in Figure 34.

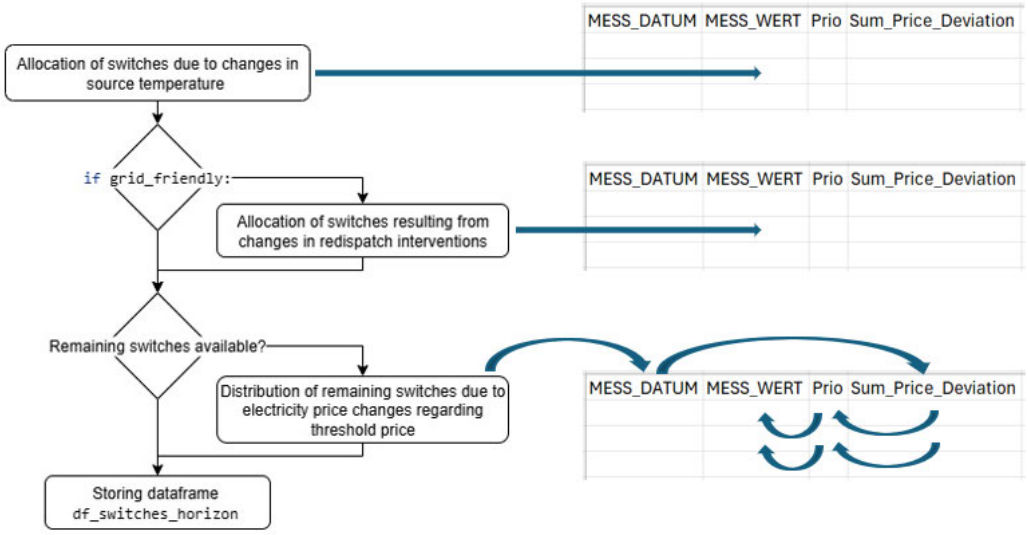

Figure 34: Process of allocation of switching operations (own illustration)

Switching operations are first assigned to those timesteps in which power adjustments are necessary due to the source temperature crossing the threshold value of 5 °C. In this case, the number of assigned switching operations initially corresponds to the number of modules that are not wastewater modules. Subsequently, if the 'grid-friendly' option is activated, switching operations are also assigned to those timesteps in which a change in redispatch-related energy occurs compared to the previous timestep. The number of available switches for a timestep with a change in redispatch-related energy is calculated by:

$$a = \frac{\left|Q_{redispatch,j,i} - Q_{redispatch,j,i-1}\right|}{Q_{module,\min\ \_load} \cdot \frac{COP_{Carnot,exterior,min}}{\overline{COP}_{Carnot,exterior}}} \quad (29)$$

To determine the switching operations, the change in redispatch-related heat energy is divided by the minimum amount of energy that a module could generate under the most unfavorable operating conditions of the year at minimum partial load. This ensures that even under the most unfavorable circumstances, the correct number of modules can be activated or deactivated to balance the redispatch measures. Of course, the number of switching operations that can occur within a single timestep is inherently constrained by the total number of available modules. Up to this point in the initial switching allocation process, exceeding the maximum number of switching operations within the considered time horizon is permitted. The technical limits regarding switching frequency are therefore treated as soft constraints. This means that temporary overutilization beyond the nominal technical limits is permitted for operational changes due to low source temperatures, storage capacity limits and to compensate for grid bottlenecks. In the next step, the switching assignments are determined for the timesteps that require switching due to electricity price changes compared to the previous timestep and the threshold price. At the beginning of the simulation, the user sets the electricity price threshold at which the operation of LSHPs is assumed to be favorable in relation to the trimmed average electricity price for the year on the day-ahead market. Here, a value of 0.8 means that the LSHPs will only operate when the electricity price is less than 80 % of the average annual electricity price. In the event of a threshold crossing of the electricity price compared to the previous timestep, the index of the respective timestep is stored in a list called ‘threshold_crossings’. In addition, the first timestep of a time horizon is always added to begin as the first element to the list. For every timestep where a threshold crossing appears – checked by the list ‘threshold_crossings’ – all electricity prices, which occur in between this timestep and the next timestep with a threshold crossing assigned, are considered. For every timestep in this interval, starting with the timestep where the first threshold crossing takes place, the positive difference to the threshold price is calculated and the cumulative sum of absolute deviations from all electricity prices until the timestep with the next threshold crossing is calculated. If the cumulative sum of absolute deviations is particularly large between two threshold crossings, the first timestep in that interval is ranked as high priority. This reflects the high importance of initiating switching operations at this timestep to adjust the operating strategy in anticipation of a prolonged or significant deviation from the threshold price. Figure 35 shows the allocation of priorities due to electricity price changes on 10 September 2024.

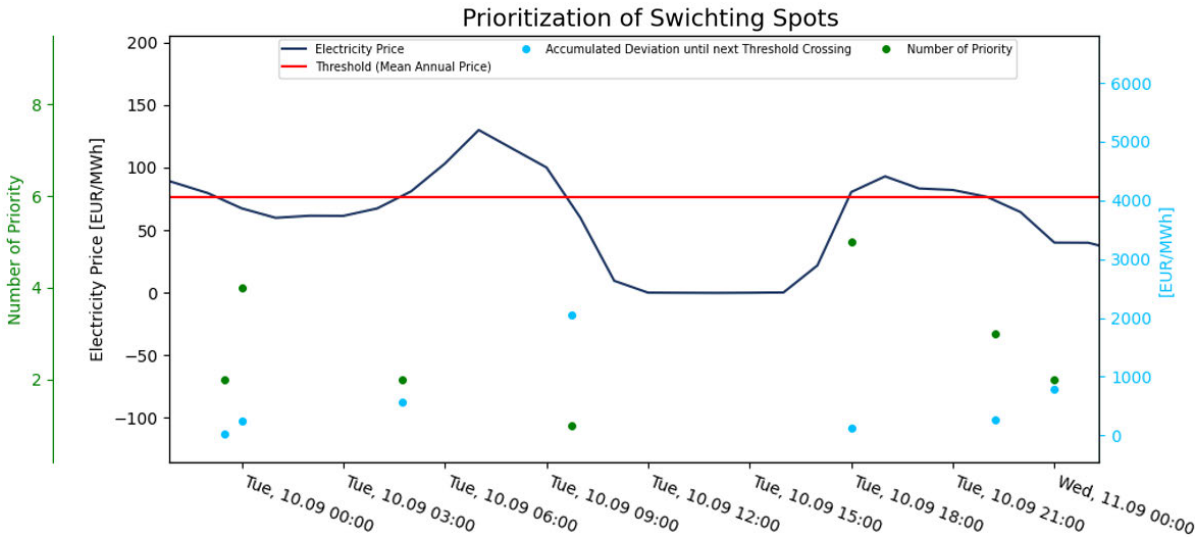

Figure 35: Priority assignment for switching operations across timesteps (own illustration)

Here, the time horizon spans from 00:00 to 23:45 of the current day, before a new horizon for switching assignment begins. The timestep at 09:15 is assigned the lowest priority number, which corresponds to the highest priority, as the cumulative positive deviation of the electricity price from the threshold – up to the next threshold crossing – is the highest. In contrast, the timestep at 18:00 possesses the smallest cumulative deviation, and thus receives the highest priority number, i.e., the lowest switching priority. The timestep at the beginning of the day is also included in the ranking, even if no threshold crossing occurs at that point. This is done to correct an incorrect prioritization of the last threshold crossing from the previous day if necessary. The timestep containing the last threshold crossing within a given time horizon cannot be reliably prioritized, as the algorithm only considers the cumulative sum of absolute deviations in electricity prices up to the end of the current horizon. How the electricity price will evolve beyond the horizon is estimated solely based on the electricity price at the last timestep of the current horizon. If the price of the last timestep shows the maximum deviation from the threshold price among all prices between the last threshold crossing and the end of the horizon, the associated cumulative sum of absolute deviations is multiplied by a factor of 2.5. Otherwise, it is multiplied by a factor of 1.5. This adjustment aims to estimate how much the cumulative sum of absolute deviations would increase if calculated until the next threshold crossing outside of the current time horizon. The values for the cumulative deviation and the priority numbers are added to the data frame ‘df_switches_horizon’ in the rows of the corresponding timesteps. Based on the priority numbers, the remaining switching operations that can be distributed within the current time horizon are then assigned to the timesteps, starting with the one that has the lowest priority number. Assigning switching operations to the first timestep of a time horizon – even if no switching is required at that point – is unproblematic, as the allocation is adjusted after each simulated timestep. If the number of executed switching operations does not match the previously assigned amount for that specific timestep, the distribution for future time steps in the current horizon is updated accordingly by accessing the data frame ‘df_switches_horizon’. Unused switching operations — if switches can still be

distributed within the current time horizon — are always reassigned to future timesteps with the lowest priority numbers, provided those timesteps have not yet reached their maximum allowable number of switches. Conversely, if too many switching operations have been used, the excess switches are removed starting from those future timesteps with the highest priority numbers, i.e., the lowest actual priority. Figure 36 and Figure 37 illustrate the shifting of switching operations from the original distribution, using the 25 November 2024 under the assumption of two switch-on and switch-off operations per module and day as an example.

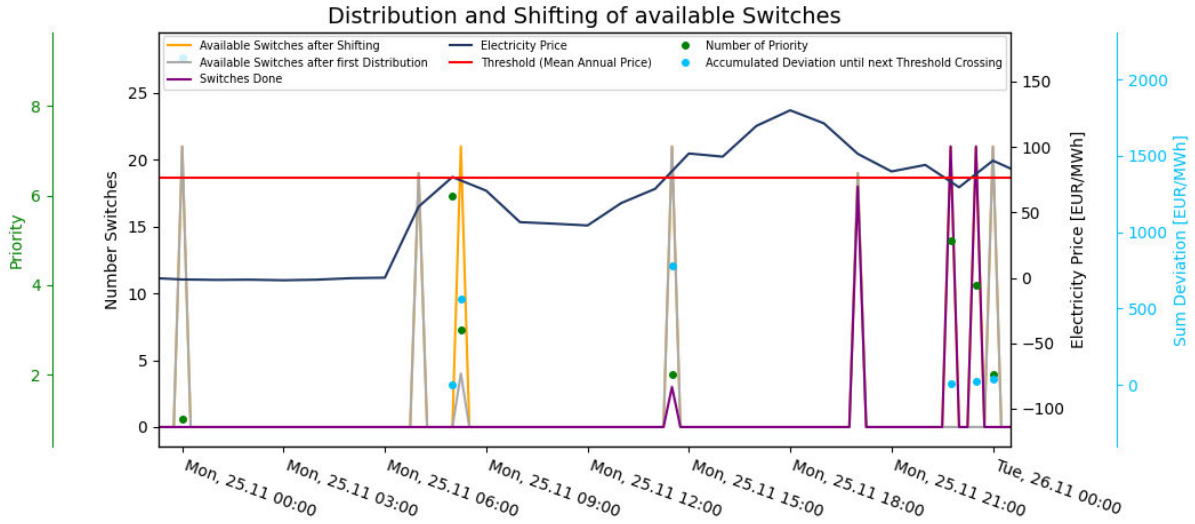

Figure 36: Shifting of available switching operations (own illustration)

The grey line shows the available switches after the first distribution done, the orange line shows the additional switches which are available at a timestep due to shifting and the purple line shows the actual switches done. The switches, which do not have a priority number and a cumulative sum of absolute deviations assigned, are switches due to redispatch interventions. Since the timesteps at the earlier time of the day at 00:00, at 07:00 and at 08:15 have switches available which are not used, the switches get shifted to later timesteps first at 08:15 then to 23:30 and to 22:45 which previously had no switches assigned due to their lower priority. Furthermore, one timestep at 08:00 is left out due to its low priority even though a threshold crossing takes place at this timestep. Thus, unnecessary switching of the modules is prevented. In Figure 37 it is shown how the shifting of distributed switches over the day occurred.

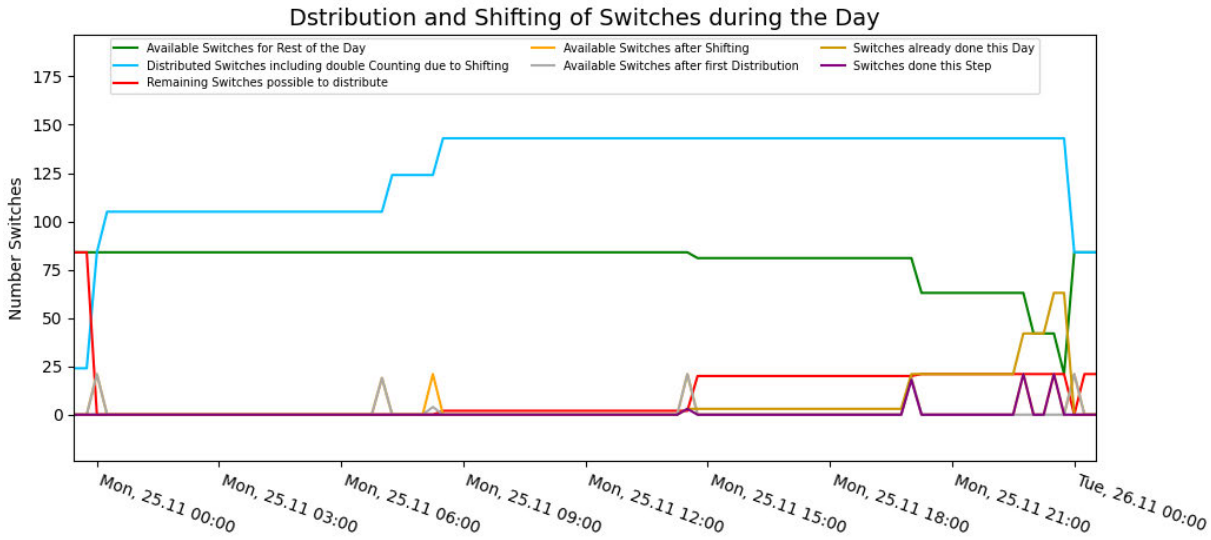

Figure 37: Regulation of Switching behaviour during time horizon (own illustration)

Here the red line shows the remaining switches which are possible to distribute based on the difference between maximal number of switches to distribute during one horizon and the switches which are already assigned. At the beginning all available switches of the horizon are assigned. After the switches at 00:00 and at 07:00 are not used, still no further switches are shown as remaining to distribute since the unused switches got assigned again to the timesteps later that day. Only when the switches at the timestep at 08:15 are not used either, some of the switches remain undistributed since they cannot be allocated to further timesteps. The actual available switches for the rest of the day (green line) are reduced as soon as switches are done (purple line). The blue line counts all switches which have been distributed by the algorithm, even including double counting due to shifting.

By assigning the available switching operations precisely to the timesteps where they are needed, the operating behavior of the LSHP becomes extremely responsive. In addition, no power gradient is assumed to limit the change in partial load behavior. As a result, the LSHP can ramp up or down completely within a single 15-minute timestep. This meets the requirements for future LSHPs for the provision of minute reserve [13]. The realization of rapid load changes and start-up and shut-down operations is therefore a desired system characteristic. However, if the maximum number of allowed switching operations per day and module is set too high and frequent changes in the electricity price occur during one time horizon, the model may still produce switching actions that react to minor electricity price changes. These actions would not make sense in real-world operations considering the technical stress to which the LSHP are exposed. Figure 38 and Figure 39 compare the responsive operation of the LSHP under the assumption of a maximum of four and a maximum of two start-up and shutdown operations per day and per module, using 21 May 2024 as an example.

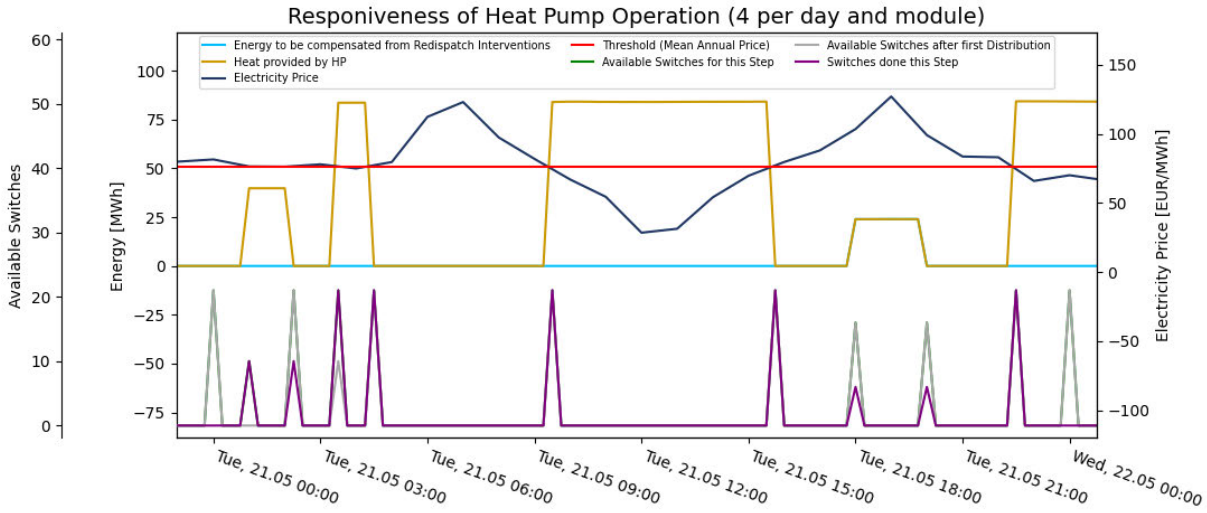

Figure 38: Responsiveness of HP operation under low technical constraints (own illustration)

With the option of 4 start-up and shutdown operations per day and per module, several switching events occur in short succession early in the day, even though the electricity price fluctuates only slightly around the threshold price. In a real-world operation, such switching actions would likely not be carried out. Under the constraint of allowing only 2 start-up and shutdown operations per day and per module, the threshold crossings of the electricity price which occur early in the day are not acted upon due to their lower assigned priority, as shown in Figure 39. Therefore, no switching is executed during these short intervals. Nevertheless, the switching actions required for relevant operational periods and redispatch compensation later in the day are still executed. For 21 May, this outcome reflects a behaviour consistent with real-world operation.

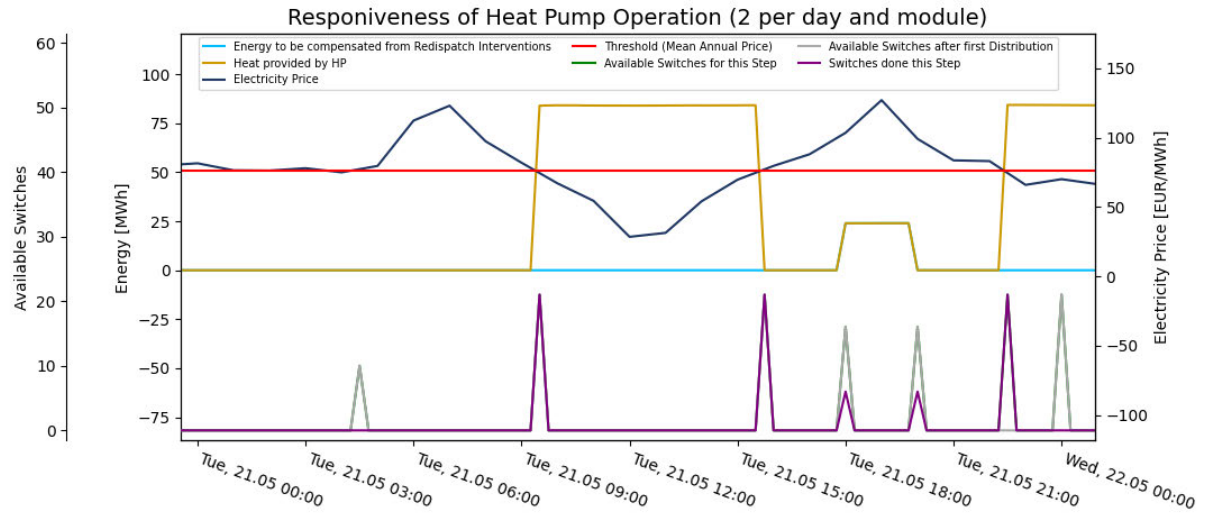

Figure 39: Responsiveness of HP operation under moderate technical constraints (own illustration)

In order to map the most realistic behavior possible over an entire year and to enable sufficient electricity-led adjustments in days where a lot of redispatch-related energy changes occur, the

constraint for switch-on and switch-off operations per day and module is set to three as the default setting. This means that in total 126 module operations per day are possible.

4.5.1 Potential System Improvements

In the current model, the use of switching operations is governed solely by a priority-based allocation within a given maximum switching limit. However, an individual assessment of whether a switching operation makes sense for this timestep is not yet performed. To further prevent unnecessary switching, the implementation of minimum run times and minimum stop times, or even better an individual decision-making process based on the cumulative sum of absolute deviations for the interval between two threshold crossings, is necessary. Furthermore, a switching assignment for regulating switching operations, as it is done for Mode 3, is not implementable analogously for Mode 2. Since Mode 2 prioritizes the coverage of heat demand over the optimization of operating costs, switching operations for heat-led operation must be considered in every timestep. A direct assignment of switching operations to the timesteps at the beginning of a time horizon is therefore not feasible, as the development of storage level, heat demand, and necessary heat production cannot be readily foreseen for future timesteps. However, the correct switching allocation would be possible through an individual assessment of the changes in heat quantities and electricity price before each individual timestep. A proposal for the control logic according to which this switching assignment could take place is illustrated in Figure 40.

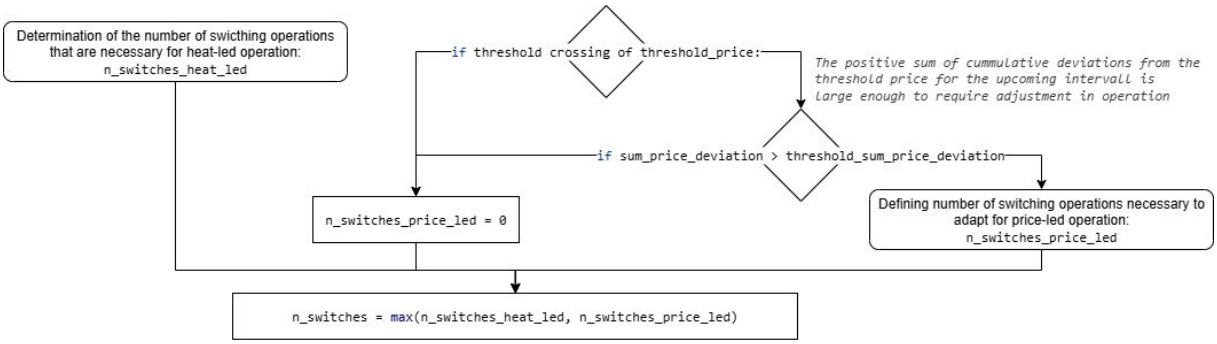

Figure 40: Proposal for improvement of technical control strategy (own illustration)

Here the switches which are necessary for heat-led operation and the switches required for price-led operation are defined independently. The number of switches for price-led operations is specified due to two process steps. In the first step it is checked if a change in electricity price compared to the last step results in a crossing of the threshold price. If not, no switching operations for an electricity price-led operation are needed. Otherwise, in a second step the cumulative sum of absolute deviations for the upcoming interval between the current threshold crossing and the next one is considered. If the cumulative sum of absolute deviations is large enough the assignment of price-led switching operations is worth it. This decision is made based on a comparison with a threshold value for the cumulative sum of absolute deviations. At the end the higher number of switches – calculated for a heat-led and electricity-led operation respectively – is selected. The selection of pre-filtered numbers of switches

does not impact whether a heat-led operation or an electricity led operation is performed. For example, the number “n_switches_price_led” can be selected due to an increase of the electricity price, but the over-prioritization of heat demand coverage leads to an increase in heat production according to the logic of mode 2 as described in chapter 4.4.2. Thus, it is ensured that for an operation of maximum heat coverage always enough switches are available, while for an electricity-led operation only operations which are worth it can be performed. To establish such an algorithm, an individual decision-making process is necessary before each timestep. The constraint of the maximum startup and shutdown operations per day and module could be implicitly controlled by specifying the threshold value for the cumulative sum of absolute deviations between two threshold crossings. The constraint would thus become a soft constraint regarding electricity price-led operations instead of a hard constraint as it is in the current model. Since an individual decision-making process before each timestep enables more flexible operation in several operating modes and better reflects a real-world operation, it turns out that the constraint of maximum switching operations per day and module is ultimately not the best choice to optimize for. Instead, an operating decision is required before every individual timestep. For price optimized operations with a constant threshold price the cumulative sum of absolute price deviations from the threshold price during the interval between two timesteps where threshold crossings occur is considered the best indicator for an electricity price-led operating decision. However, for more complex operating strategies considering further adaptation of the threshold price as a function of the storage level, as they are executed in chapter 5.3, the individual decision-making process before each timestep becomes more complex.

The restructuring of the algorithm in the described way is not yet implemented in the current model but is a highly recommended step for future model improvement.

For operation in mode 2, there is currently no limit to the number of available switching operations. However, it shows that under current operating conditions not many switching operations are needed in mode 2. Even when assuming no partial-load behavior and a threshold price equal to the annual average day-ahead market price, it shows that only in 5 days of the year in 2024 the constraint of more than three on and off switching operations per day and module takes place due to the mainly heat-driven operation. Nevertheless, under different operating conditions a control strategy for mode 2 might be necessary. In Mode 1, switching operations are assigned independently of the described algorithm and are set to the maximum number of switches for each timestep. This approach is justified by the fact that in mode 1 switching only occurs in response to threshold crossings of the source temperature, storage capacity limits, and optionally to compensate for redispatch interventions. When the storage reaches its capacity limit, switching actions are distributed evenly across the day, involving only individual modules. Consequently, the number of switching operations consistently remains well below the daily maximum.

4.6 Model-Based Heat Output Calculation

The following chapter outlines how the algorithm determines the heat output of the HP for each timestep, depending on the selected operating mode. Defining the heat output is the first of two main steps for modelling the HP performance, followed by the calculation of the electrical input power.

The calculation of the heat output consists of the following sub-steps, as shown in Figure 41.

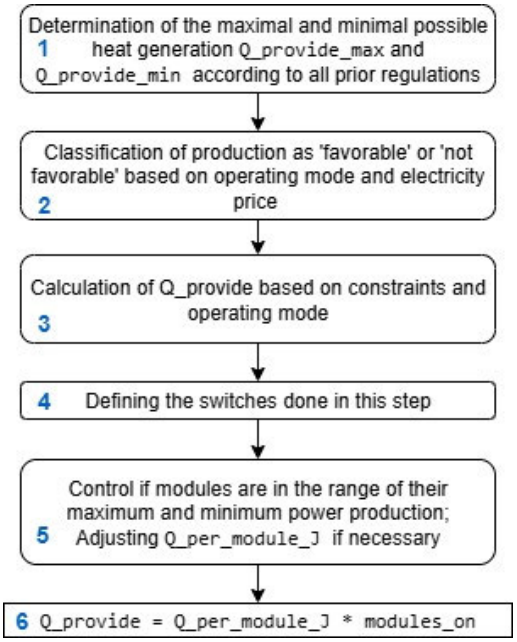

Figure 41: Process steps to determine heat output generation (own illustration)

In the first step, it is defined how much thermal energy the HP can produce maximally and minimally, taking into account all prior operational constraints. These constraints include the technical limitations, and the requirements imposed on the operation for compensating redispatch measures if the 'grid_friendly' option is activated. Here, the values of maximum and minimum thermal output power are increasingly restricted by various requirements until all requirements are met. Figure 42 illustrates the limitational factors of the minimum and maximum thermal output power.[9]

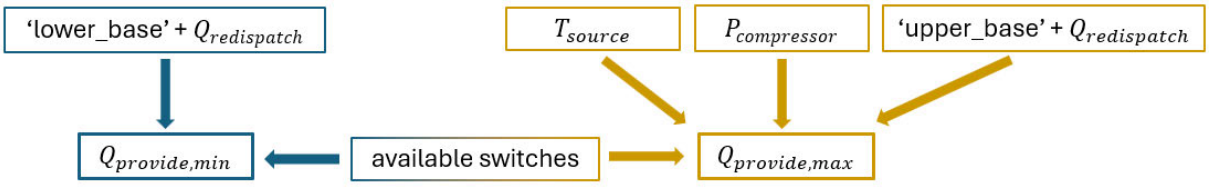

Figure 42: Constraints for minimum and maximum heat output (own illustration)

Here, the number of available switches restricts $Q_{provide,min}$ as well as $Q_{provide,max}$. For $Q_{provide,min}$ it is assumed that all available switches would be used to shut down operating modules of the last

[9] The value for $Q_{redispatch}$ can be positive or negative. That's why it is always summed up to the 'lower-base' or 'upper_base' value as explained in chapter 4.4.4.

timestep and the remaining active modules would be reduced to minimum part-load behavior. In contrast for $Q_{provide,max}$ it is assumed that all available switches are used to switch modules on, and the modules would run at nominal power limited by the compressor. In both cases, $Q_{provide,min}$ and $Q_{provide,max}$, the strongest restriction is the one which defines the value that is used in subsequent steps of the algorithm. As described in chapter 4.5 for compensating redispatch measures there are always enough switching operations assigned to the corresponding timestep. Therefore, the limitations of available switches cannot override the requirements of grid-supportive contribution if 'grid-friendly' is enabled.

In the second step of the process for heat output determination it is defined whether the heat production is considered favorable or not. The decision process is depicted in Figure 43.

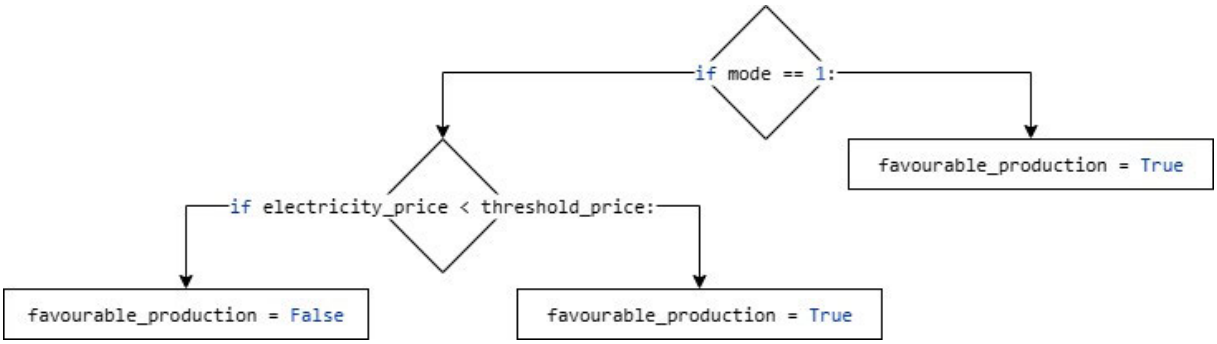

Figure 43: Assessment process of heat generation favourability (own illustration)

In mode 1, heat production is always considered favorable, while in modes 2 and 3 it is only viewed as favorable if the electricity price is below the specified threshold price. At this point, it should be noted that an economic evaluation which exclusively considers the electricity procurement costs per unit of heat generated would also need to take into account the anticipated COP for the current time step, as the electricity procurement costs change proportionally to the COP. However, since a high share of LSHPs in district heating supply is predicted in the future [11], the system boundaries must be considered more broadly here. A unit of heat generated during cold seasons, when heat is most urgently needed, will likely be 'more valuable' to district heating operators than a unit of heat generated during warmer seasons. Without precise knowledge of the valuation of a generated heat unit in Hamburg's district heating network depending on the supply situation, the inclusion of the COP in the economic assessment remains speculative. Therefore, within the limits of operating source temperatures, the COP is not considered as a factor in cost-optimized operation.

In step 3 the desired heat output is determined according to the process logic illustrated in Figure 44. Here, the minimum and maximum values for heat production $Q_{provide,min}$ and $Q_{provide,max}$, which were determined in Step 1, are used.

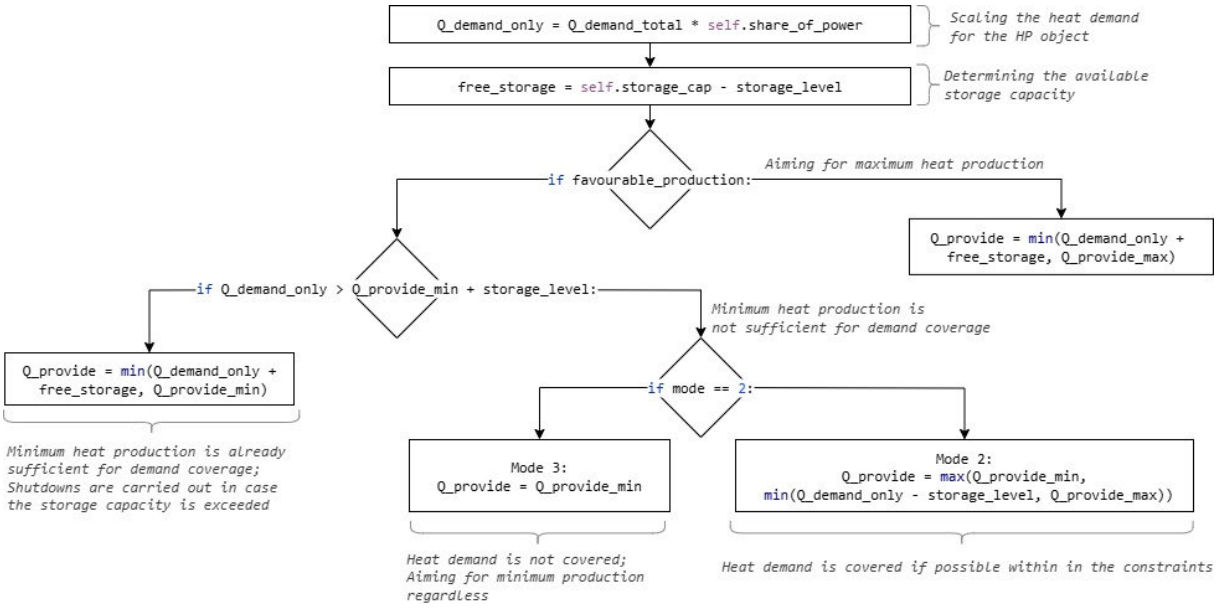

Figure 44: Specification of desired heat output (own illustration)

First the heat demand which shall be covered by the specific HP object in this timestep is specified due to the total heat demand and the share of heat generation capacity of the HP object j in regard to the heat capacity generation of all existing HP objects n. This ratio is stored as an attribute of the HP object. It applies:

$$Q_{demand,j} = Q_{demand,total} \cdot \frac{Q_{nominal,j}}{\sum_j^n Q_{nominal,j}} \qquad (30)$$

Subsequently, the free storage capacity that exists for the specific heat pump object is determined. If heat production is deemed favorable, the goal is to maximize production within the limits of the storage capacity. On the other hand, if heat production is considered unfavorable, then it is checked whether the minimum heat production, in addition to the heat stored in the storage, is already sufficient to cover the heat demand. If that is the case, then the minimum heat production is targeted. If even the minimum heat production – determined previously by the constraints – exceeds the storage capacities, then the heat production is further limited to the boundaries of the maximum storage capacity. However, if the heat demand is not covered by the minimum production and the heat in the storage, a case distinction is made between Mode 2 and Mode 3. In Mode 3, for a production classified as unfavorable, it is always aimed at the minimum heat output. In Mode 2, on the other hand, the coverage of the heat demand is targeted within the limits of 'Q_provide_min' and 'Q_provide_max'.

In step 4 of the heat output determination process illustrated in Figure 41, it is checked how many switching operations are necessary to achieve the desired heat output. After the switching operations have been carried out, step 5 checks whether the required power per module is certainly within the range of their constraints due to compressor power and part-load behavior. If this is not the case – as it can occur, for example, in operating modes without or with only limited part-load capability, then the power of the modules is adjusted to the limits of possible module power. At the end, the final heat

output is calculated based on the number of modules in operation and the power per module. Process steps 4 to 6 are shown in Figure 45.

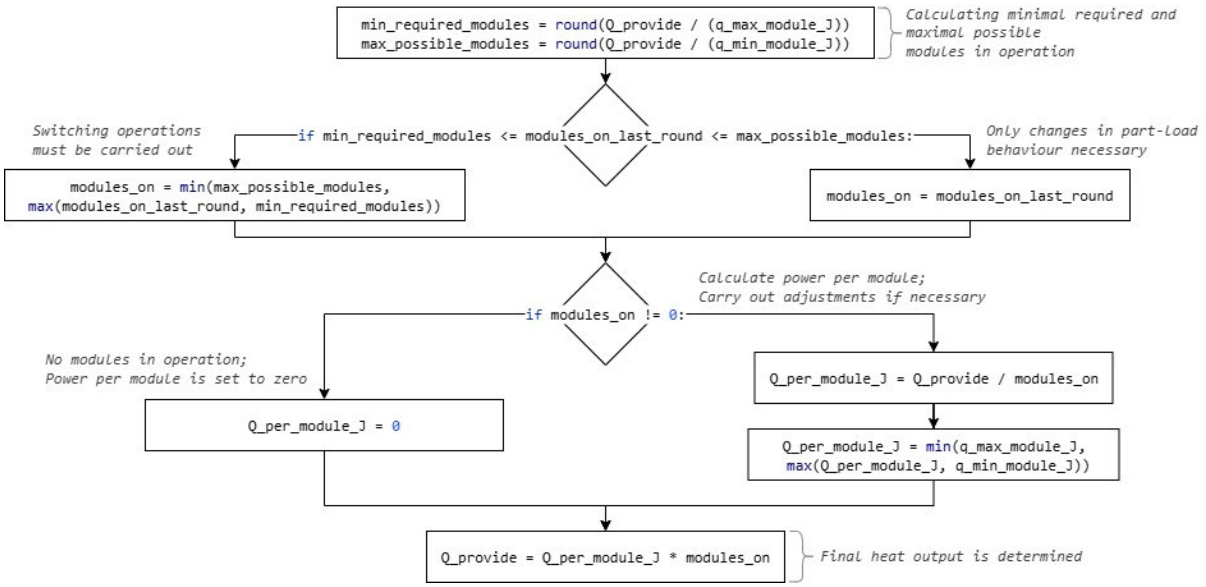

Figure 45: Final determination of heat output (own illustration)

Based on the minimum and maximum heat output per operating module, the minimum required and maximum possible number of modules in operation are defined. If the number of modules that were in operation in the previous time step is within the range of the minimum required and maximum possible modules, then the desired heat output can be achieved by adjusting the part-load behavior. Otherwise, switching operations need to be performed to align with the limits of minimum required and maximum possible modules. In the next step, the heat output per module is set based on the number of operating modules, and if it exceeds the power constraints, it is adjusted to comply with them. As the heat output cannot always be exactly to the desired level, especially if low part-load capabilities are assumed, there may be slight deviations between the desired heat output and the final heat output set. Finally, the heat output is determined based on the heat output per module and the number of operating modules assuming equal power regulation for every module.

After the specification of the heat output provided from the HP object, the remaining energy balance of the HP object is calculated for the current timestep according to the flowchart shown in Figure 46.

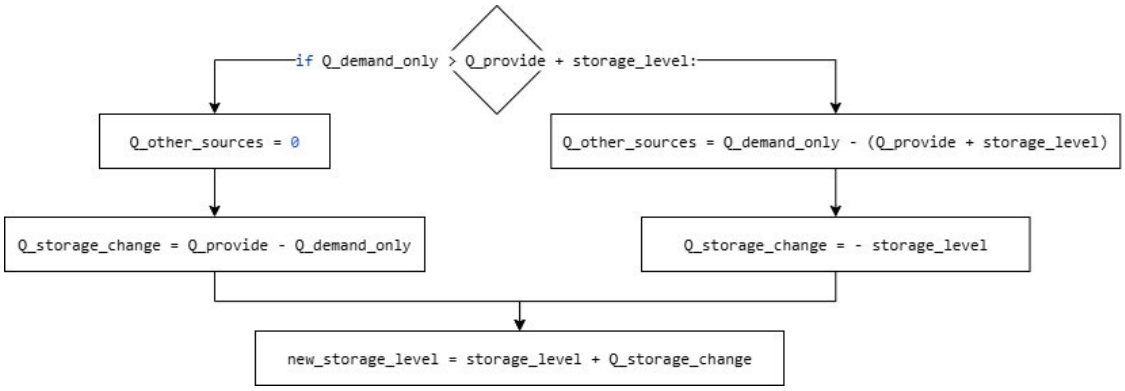

Figure 46: Energy balance of the heat pump unit (own illustration)

If the heat demand is not fully covered by the heat provided from the HP object and the storage tank, the additional heat is delivered by other heat sources, and the heat storage is discharged. Conversely, if the heat provided of the HP and the storage tank are already sufficient to cover the heat demand, no heat from other heat sources must be supplied. In this case the change in the storage level is specified by the difference between the heat provided by the HP and the heat demand. Subsequently, the storage level is updated, and a new storage level is set. When considering the energy balance, it must be recognized that all quantities affecting the energy balance – including the energy for compensating redispatch measures, the storage capacity, the storage level, the heat demand, the heat produced by the HP, and the heat supply by other sources – are always related and scaled to the individual HP object. Thus, in the modelling process each HP object has its own separate energy balance. For the storage capacity, only the capacity available at the specific site of the HP stored as an attribute for the HP object is considered, and not the storage capacity present in the entire district heating network. The heat provided by other energy sources is also calculated individually for each HP object and is a result of the specific heat balance of the HP object. Consequently, the overall balance of all HP objects yields the heat balance in the district heating network. In the simulation of multiple HP objects to date, it is not taken into account that free storage capacity at one site could be used by excess heat production at another site. In contrast, the simplification of the LSHPs to a representative HP object, as described in chapter 4.3.2, implies that thermal storage is not only available locally at each site, but that the district heating network is sufficiently flexible to allow surplus heat injected at one location to supply a storage unit at another.

4.7 Thermodynamic Modelling of Key Parameters

In the subsequent section the thermodynamic modelling process is described. Here, the technical assumptions are presented and several modelling aspects regarding the HP cycle are highlighted. This includes the enthalpy balance of two consecutive cycles, the compliance with process constraints such as the avoidance of liquid drops in the compressor and the right assessment of the supply temperature. Furthermore, the process simplifications are outlined, and the resulting deviations from real-world operation are assessed. The thermodynamic modelling to determine the electrical input power

constitutes the second main and final step in modelling the HP performance for a single timestep in the simulation.

When modelling the thermodynamic cycle of a HP, exactly enough parameters must be given to clearly define the system. If too few input parameters are specified, the system is underdetermined, but if too many parameters are specified, it is overdetermined. In Table 2 the specified input parameters are displayed.

Table 2: Parameter specification for HP modelling

Input Parameter	Description	Type
$Q_{provide}$	The heat which shall be provided by the HP	Measured value / calculated quantity
$\eta_{comp,default}$	Default value for efficiency of the compressor	Technical assumption
T_{source}	The source temperature, i.e. the water temperature of the Elbe	Measured value
T_{dh}	Temperature of the district heating grid	Measured value / calculated quantity
$\Delta T_{source\_vap\_o}$	Temperature difference between the source temperature and the temperature of the refrigerant at the outlet of the evaporator, i.e. temperature gradient at the outlet of the heat exchanger on the evaporator side. This value depends on the profile of the heat exchanger and highly on the mass flow of the water as source medium. With a high mass flow rate, the cooling of the water can be kept low and thus the temperature gradient between water and refrigerant can be reduced. Assumption: 3 °C	Technical assumption
ΔT_{aim_dh}	Temperature difference between the heat flow weighed mean temperature and the temperature of the heating grid: $\bar{T}_{flow\_h} = T_{aim} = T_{dh} + \Delta T_{aim\_dh}$ Assumption: 3 °C	Technical assumption
$T_{overheat} = \Delta T_{1s,1''}$	Temperature difference between superheated steam at the inlet of the compressor and the refrigerant in the evaporator at its saturation point $x_g = 1$ Assumption: 5 °C (typical range 3 to 5 °C)	Technical assumption

$\Delta T_{\min\_cooling\_vapor} = \Delta T_{\min,2s,2''}$	Minimum temperature difference between the superheated vapor at the outlet of the compressor and the condensation temperature. This is a one-sided constraint. Depending on the refrigerant, the value can be much higher, as described below. Assumption: 5 °C	Technical assumption
$\Delta T_{undercool} = \Delta T_{3',3u}$	Temperature difference between the refrigerant at its boiling point $x_g = 0$ in the condenser and the liquid refrigerant entering the expansion valve Assumption: 5 °C	Technical assumption

Other technical parameters such as pressure reduction in the pipes are neglected in this model for reasons of simplification. Therefore, the specified parameters in Table 2 are already sufficient for modelling the HP cycle. The calculation logic for determining the thermodynamic states is illustrated in Figure 47, using a HP cycle with deliberately exaggerated values for improved visualization. The calculations are based on the principle that a single-phase system in equilibrium is completely determined by two independent state variables [52, 100]. Here, it must be considered that in the wet-vapor region the pressure and the temperature are not independent variables as they are coupled by the mass fraction of saturated vapor x_g.

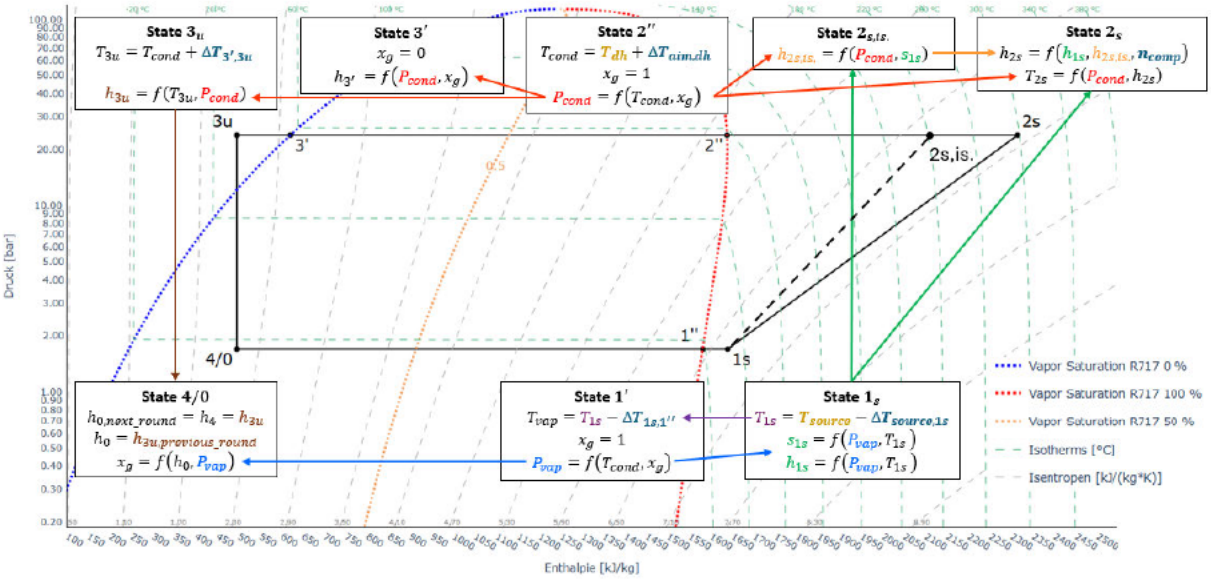

Figure 47: Calculation of thermodynamic states in the HP cycle (own illustration)

The technical assumptions are marked in technical blue and the measured values are marked in gold. To enable a tracking of the calculation path starting at state 1_s the arrows visualizing the interdependencies are color-coded according to the corresponding variables. First, the temperatures and the pressure level in the evaporator are determined. The temperature of the refrigerant at the

inlet of the compressor T_{1s} results from the source temperature T_{source} and the temperature gradient existing at the outlet of the heat exchanger $\Delta T_{source\_vap\_o}$. It applies:

$$T_{1s} = T_{source} - \Delta T_{source\_vap\_o} \tag{31}$$

The evaporation temperature of the refrigerant is then calculated by:

$$T_{vap} = T_{1s} - \Delta T_{1s,1''} \tag{32}$$

Due to the mass fraction of saturated vapor $x_g = 1$ the state $1''$ is completely determined and the pressure in the evaporator P_{vap} is defined as well [101]. Assuming the processes in the evaporator as isobaric $P_{vap} = const.$, the state 1_s is determined as T_{1s} is also known and for states outside of the wet-vapor region the combination of pressure and temperature is sufficient for determination. As the HP cycle of the current round must connect directly to the HP cycle of the previous round, the level of specific enthalpy at the expansion valve of the previous cycle is used as the specific enthalpy at the inlet of the evaporator for the current cycle $h_{3u,previous} = h_{4,previous} = h_{0,current}$. Therefore, the state 0 is defined as well by $h_{4,previous}$ and P_{vap} thus completing the determination of the states in the evaporator. Since the specific enthalpy at the expansion valve can vary slightly from round to round according to different source and heating grid temperatures, the energy balance of one simulated cycle is not completely equalized due to the offset of the previous round. Nevertheless, the energy balance of a series of modelled cycles is equalized since the offsets in specific enthalpy of successive rounds equalize. Figure 48 shows, as an example, the HP cycle with the largest offset in specific enthalpy between two successive timesteps during the year.

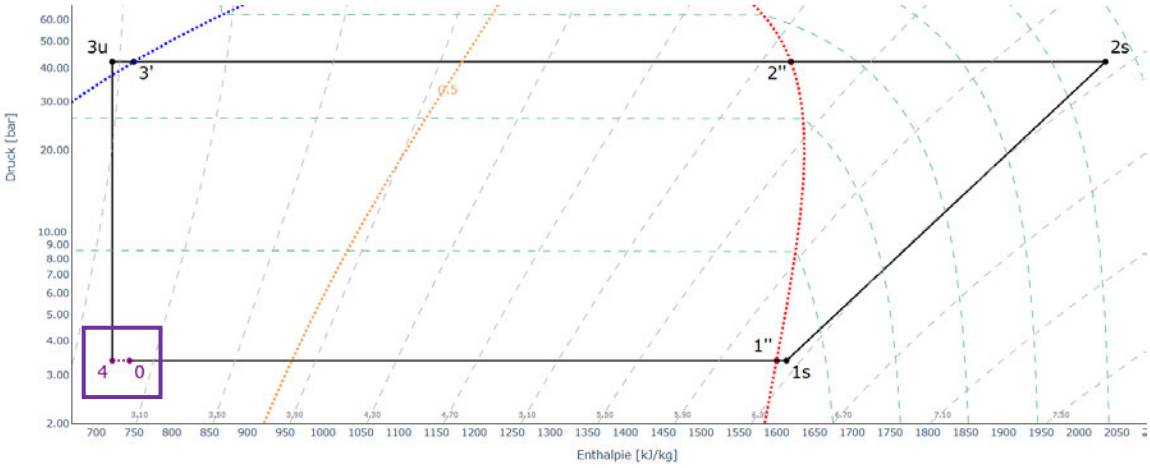

Figure 48: Offset in specific enthalpy between two consecutive HP cycles (own illustration)

As displayed, the enthalpy level at the outlet of the expansion valve of the previous cycle, i.e. the enthalpy level at the inlet of the evaporator of the current cycle – indicated by point 0 – is slightly higher than the enthalpy level at the expansion valve of the current cycle – indicated by point 4. In that case

the specific input energy of the current cycle $q_{source} + w_{el}$ is slightly smaller than the specific output energy $q_{provide}$, thus increasing the COP of the cycle. Since the final state of the previous round is always passed on to the next round $4_{previous} = 0_{current}$, a realistic ongoing process is modelled in which the overall energy balance of the series of ongoing cycles is balanced. Even if the COP of individual cycles differ very slightly compared to a separate, closed cycle, they correspond to the COPs of successive cycles as they occur. In the very first round h_0 is determined at the end of the cycle after defining the states at the condenser by using the specific enthalpy at the expansion valve $h_{3u} = h_4 = h_0$ of the current cycle.

After defining the states at the evaporator side, the states at the condenser side, 2_s, $2''$, $3'$, and 3_u are calculated in an iterative process, which aims to maintain the heat flow weighed mean temperature $\bar{T}_{flow\_h}$ at the right level:

$$\bar{T}_{flow\_h} = T_{aim} = T_{dh} + \Delta T_{aim\_dh} \tag{33}$$

Since ΔT_{aim_dh} is fixed to 3 °C this means the average temperature at which a transfer of energy takes place shall be 3° C above the heating grid temperature. Fixing the heat flow weighed mean temperature is essential, as for some refrigerants, such as R717, the temperature at the compressor outlet differs greatly from the condensation temperature as seen further below in Figure 50. A fixation of T_{cond} or T_{2s} instead of $\bar{T}_{flow\_h}$ is not useful since it would make it more difficult to compare the performance of different refrigerants according to the definition of the Lorentz quality factor $\eta_{quality,Lorenz}$ as described in chapter 3.3. The fixation of $\bar{T}_{flow\_h}$ ensures that simulations with different refrigerants and the same settings for the heating grid temperature provide heat at the same temperature level, thus having a fair comparison of the COP [64]. At the beginning of the iterative process T_{cond} is set as an initial guess:

$$T_{cond} = T_{aim} = T_{dh} + \Delta T_{aim\_dh} \tag{34}$$

The pressure level P_{cond} is derived from T_{cond} and $x_g = 1$ at the state 2_s and assuming isobaric processes the enthalpy at the outlet of the compressor can be calculated using the default value of compressor efficiency. Since the state 1_s is known the specific enthalpy for an isentropic compression $h_{2s,isentropic}$ can be calculated assuming $s_{1s} = s_{2s}$ [50, 52]. According to the explanations in chapter 3.1 the specific enthalpy h_{2s} is defined by:

$$h_{2s} = h_{2s,first\_try} = \frac{h_{2s,isentropic} - h_{1s}}{\eta_{default}} + h_{1s} \tag{35}$$

Here, a further case distinction must be made depending on the refrigerant and the default value for the compressor efficiency $\eta_{default}$. The state $2_{s,first\_try}$ which is determined due to P_{cond} and h_{2s} must be checked as valid. Depending on the shape of the wet-vapor curve of the refrigerant it can happen that the state $2_{s,first\_try}$ does not respect the safety boundaries or is even placed inside the wet-vapor region. The validation can be done by checking if:

$$T_{2s,first\_try} - \Delta T_{\min,2s,2''} \geq T_{2''} \tag{36}$$

If this condition is fulfilled, then the first determination of $2_{s,first\_try} = 2_s$ is valid. Otherwise $2_{s,first\_try}$ is too close to the wet-vapor region or even placed inside and thus must be shifted to a higher level of specific enthalpy. The shift takes place by determining T_{2s} according to the minimal temperature difference between 2_s and $2''$:

$$T_{2s} = T_{2''} + \Delta T_{\min,2s,2''} \tag{37}$$

The new specific enthalpy h_{2s} is calculated due to P_{cond} and the new temperature T_{2s}. Consequently, the compressor efficiency is adapted to [50, 52]:

$$\eta_{new} = \frac{w_{el,isentrop}}{w_{el,real}} = \frac{h_{2s,isentrop} - h_{1s}}{h_{2s} - h_{1s}} \tag{38}$$

If a shift takes place, then the new compressor efficiency exceeds the default value $\eta_{new} > \eta_{default}$. This means the compressor must provide more energy to keep the refrigerant in a state of superheated vapor by aiming for a higher temperature. Thus, the procedure results in a generation of entropy. Hence, it is assumed that the shift done in the simulation corresponds to real-world processes in HP compressors. In Figure 49 the shift is illustrated in the p-h diagram for the refrigerant R245fa.[10]

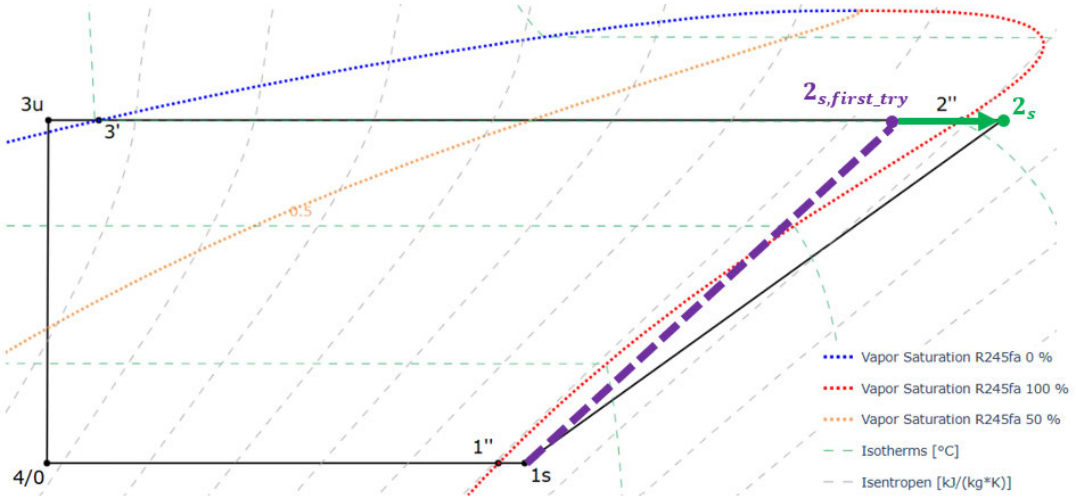

Figure 49: Shift of state at the compressor outlet to comply to operational constraints (own illustration)

For refrigerants where the wet-vapor region has a more vertical shape, such as R717, there is no need for an extra shift since even at an isentropic compression the temperature at the outlet of the compressor exceeds the condensation temperature clearly, thus ensuring a state of superheated vapor during the whole compression process as seen in Figure 50. After determining the state 2_s the states $2''$and $3'$ can be defined using $P_{cond} = const.$ and $x_g = 1$ or $x_g = 0$ respectively. Assuming an isobaric

[10] The refrigerant R245fa is not considered in the scope of this work, but the effect applies as well for R1234ze(E), R290 and R1234yf which are considered as refrigerants for the LSHPs.

process the state 3_u is determined as well using P_{cond} and the temperature T_{3u}, which is calculated by:

$$T_{3u} = T_{3'} - \Delta T_{3',3u} \tag{39}$$

Now all specific enthalpy values of the states at the condenser are defined and the heat flow weighed mean temperature is calculated by:

$$\bar{T}_{flow\_h} = \frac{\Delta h_{2s,2''} \cdot \bar{T}_{2s,2''} + \Delta h_{2'',3'} \cdot T_{cond} + \Delta h_{3',3u} \cdot \bar{T}_{3',3u}}{\Delta h_{2s,3u}}$$
$$\approx \frac{\sum_{i=1}^{n} \left(\left(h_{i,upper} - h_{i,lower}\right) \cdot \left(\frac{T_{i,upper} + T_{i,lower}}{2}\right)\right) + (h_{2''} - h_{3'}) \cdot T_{cond} + (h_{3'} - h_{3u}) \cdot \left(\frac{T_{3'} + T_{3u}}{2}\right)}{h_{2s} - h_{3u}} \tag{40}$$

To make a more precise approximation of $\bar{T}_{flow\_h}$ the enthalpy section $\Delta h_{2s,2''}$ is split by an adjustable variable into smaller sections divided by $h_{i,upper}$ and $h_{i,lower}$ respectively. Here, the mean temperatures of the sub-sections are calculated through the limit values $T_{i,upper}$ and $T_{i,lower}$ as illustrated in Figure 50 for the refrigerant R717.

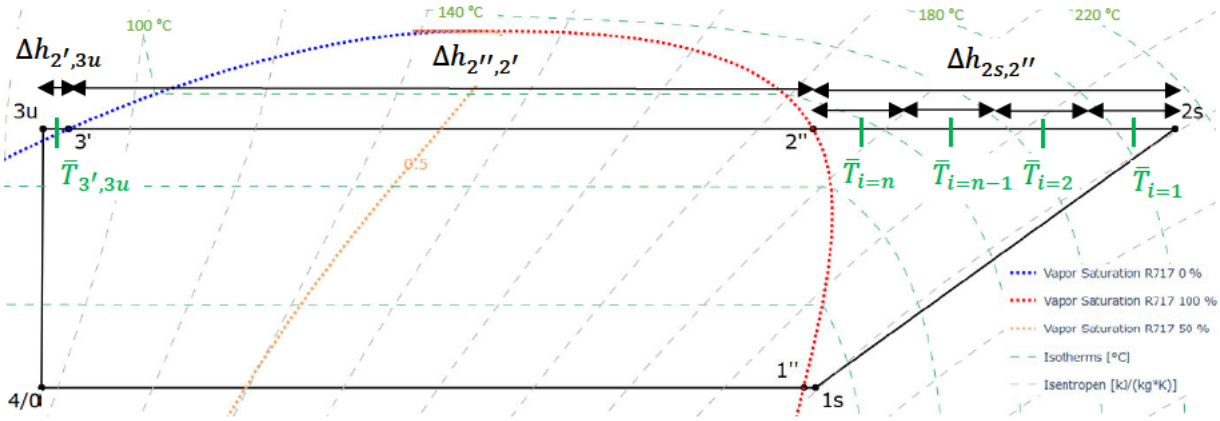

Figure 50: Calculation of heat flow weighed mean temperature (own illustration)

This subdivision in the area of superheated vapor is crucial, since here the temperature change is not proportional to the change in specific enthalpy, especially not at a pressure level close to the critical point. This is shown by the decreasing distance in enthalpy between the isotherms on the right side of the wet-vapor region. If no further subdivision were made the calculation of $\bar{T}_{2s,2''} \approx \frac{T_{2s}+T_{2''}}{2}$ would be overestimated, as most of the enthalpy exchange takes place at lower temperatures. This would lead to an overestimated $\bar{T}_{flow\_h}$ and thus simulate a heat exchange at a higher temperature level than it actually takes place. In the liquid phase, at the left side of the wet-vapor region, no subdivision is necessary even at higher sections of subcooling since here the temperature change is almost proportional to the change in enthalpy due to the small Joule-Thomson-coefficient for liquids. This is reflected in the p-h diagram, where isenthalpic and isothermal lines run nearly parallel in the liquid

region. After calculating $\bar{T}_{flow\_h}$, it is compared with the targeted temperature T_{aim}. If the difference $\Delta T = \bar{T}_{flow\_h} - T_{aim}$ is smaller than a preset tolerance or the maximum number of iterations has been reached the calculated states at the condenser side 2_s, $2''$, $3'$, 3_u are verified. Otherwise, the condensation temperature T_{cond} is readjusted using a feedback loop based on $\Delta T = \bar{T}_{flow\_h} - T_{aim}$ and a damping factor $f_{damping}$. It applies:

$$T_{cond,new} = T_{cond} - \Delta T \cdot f_{damping} \tag{41}$$

After the readjustment of $T_{cond} \rightarrow T_{cond,new}$, the calculation of the states in the condenser and the resulting heat flow weighed mean temperature $\bar{T}_{flow\_h}$ is repeated. If no adjustment of the heat flow weighed mean temperature is intended, the number of maximum iterations can be set to 1, which prevents an adjustment of the condensation temperature, as the loop is interrupted before. This can be purposeful for evaluating special modelling conditions with a fixed condensation temperature.

After defining all states of the cycle, the mass flow, the energy quantities and other parameters such as the COP and the electricity costs are calculated [52]. For one timestep it applies [52]:

$$m_{ref} = \frac{Q_{provide}}{h_{2s} - h_{3u}} \tag{42}$$

$$Q_{source} = m_{ref} \cdot \left(h_{1s} - h_{4/0}\right) \tag{43}$$

$$W_{el,comp} = m_{ref} \cdot (h_{2s} - h_{1s}) \tag{44}$$

$$W_{el,with\_aux} = W_{el,comp} + aux_{percent} \cdot W_{el,comp} \tag{45}$$

$$EUR = W_{el,comp} \cdot price_{electr.} \tag{46}$$

$$EUR_{with\_aux} = W_{el,with\_aux} \cdot price_{electr.} \tag{47}$$

Additional to the electrical input for compressor power $W_{el,comp}$ the model allows the consideration of auxiliary energy as a percentage of the electrical input for compressor power $aux_{percent}$.

Figure 51 summarizes the entire process of calculating the thermodynamic variables that determine the electrical input power in a simplified flowchart.

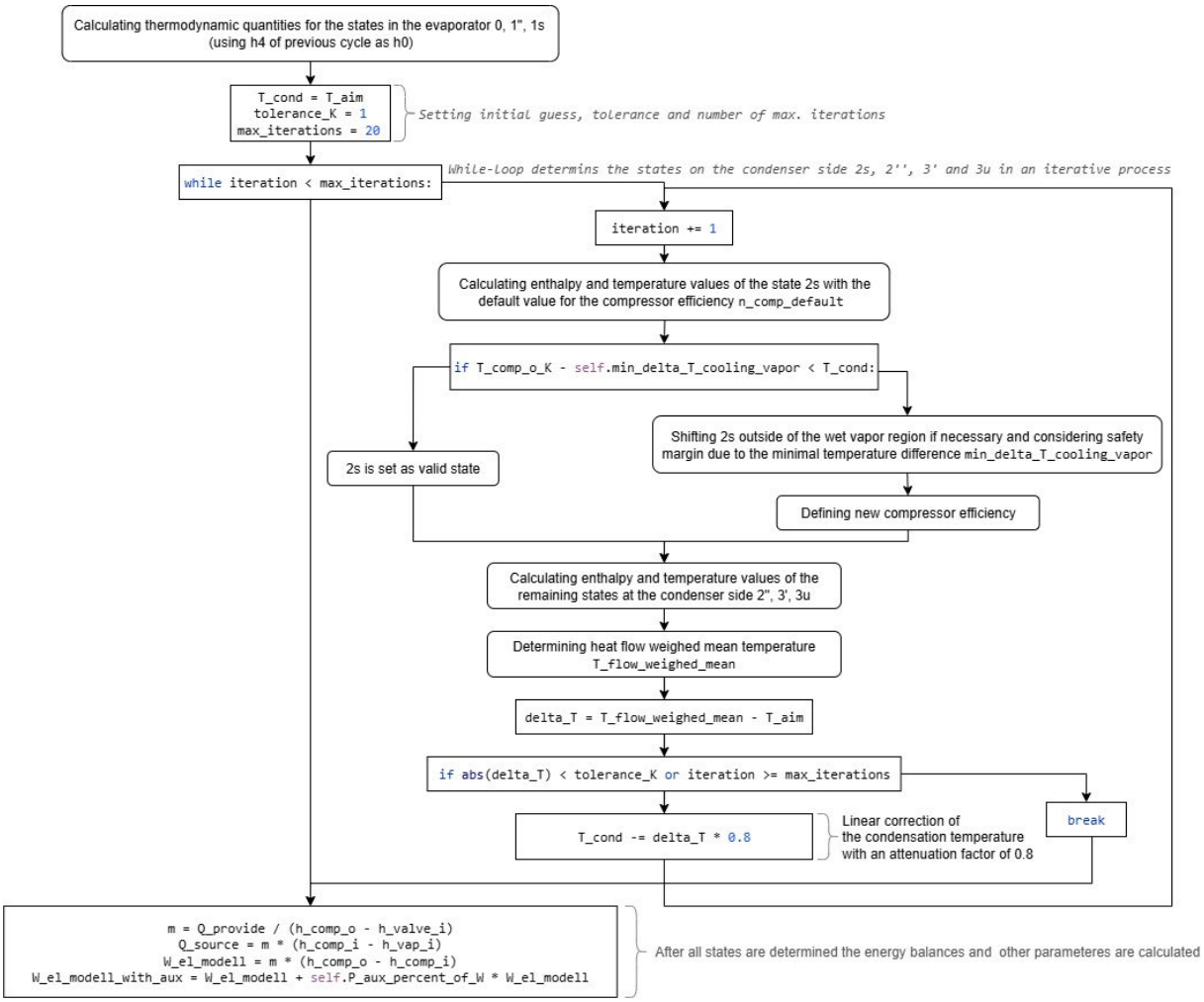

Figure 51: Process of thermodynamic modelling (own illustration)

4.7.1 Simplification of the Control Circuit

In this chapter it is described which simplifications the current modelling approach implies regarding the control circuit and the plant design of the HP system. Here, particular focus is placed on the causal relationships between the refrigerant mass flow rate $\dot{m}_{ref}$ and the heat exchange processes.

The fixation of the mass flow $\dot{m}_{ref}$, i.e. the transferred refrigerant mass in one timestep m_{ref}, due to the heat output produced $Q_{provide}$ in this timestep is thermodynamically correct but a simplification in terms of control technology which does not correspond to the real HP control circuit. As described in 3.2 the mass flow $\dot{m}_{ref}$ is adjusted by the expansion valve to ensure that the temperature difference $\Delta T_{1s,1''}$ is maintained so that no drops of liquid enter the compressor [47, 55]. Assuming the attributes of the heat exchanger as constant the temperature differences $\Delta T_{1s,1''}$ and $\Delta T_{3',3_u}$ cannot be assumed as fixed values but are dependent from the mass flow rate $\dot{m}_{ref}$ set [58]. To consider the changes in $\Delta T_{1s,1''}$ and $\Delta T_{3',3_u}$ due to changes in $\dot{m}_{ref}$ instead of defining the states 2_s, $2''$, $3'$, 3_u in an iterative process aiming for the smallest $\Delta T = \bar{T}_{flow\_h} - T_{aim}$ the states h_{1s}, 2_s, $2''$, $3'$, 3_u would need to be defined in an iterative process optimizing the heat flow weighed mean temperature $\bar{T}_{flow\_h}$ as well as

the heat output provided $\Delta Q = Q_{provide} - Q_{provide,aim}$ inside of the boundaries of $\Delta T_{overheat,min} \leq \Delta T_{overheat} \leq \Delta T_{overheat,max}$ and $\Delta T_{undercool,min} \leq \Delta T_{undercool} \leq \Delta T_{undercool,max}$. This results in a multivariate optimization problem that would need to be solved either through nested, iterative feedback loops or simultaneous solution methods such as minimization of the sum of squared errors. In a feedback control loop optimizing towards $min(\Delta Q = Q_{provide} - Q_{provide,aim})$ and $min(\Delta T = \bar{T}_{flow\_h} - T_{aim})$ while considering the changes in $\Delta T_{1s,1''}$ and $\Delta T_{3',3_u}$ which occur due to a change in $\dot{m}_{ref}$ the changes in specific enthalpy due to the changes in $\Delta T_{1s,1''}$ and $\Delta T_{3',3_u}$ would need to be taken into account as well. This would lead to an adjustment of electrical input power W_{el} and compressor efficiency η to keep $Q_{provide}$ and $\bar{T}_{flow\_h}$ at the desired level, thus replicating the control behaviour of a HP more accurately. However, the implementation of such a feedback loop would be much more complex and it would be necessary to exactly know the correlation between a change in mass flow rate $\dot{m}_{ref}$ and the temperature changes in $\Delta T_{1s,1''}$ and $\Delta T_{3',3_u}$ in regard to a fixed state at the inlet of the respective heat exchanger. In Figure 52 the processes in the condenser during a reduction of $\dot{m}_{ref}$ are shown in an exaggerated manner to illustrate the effect.

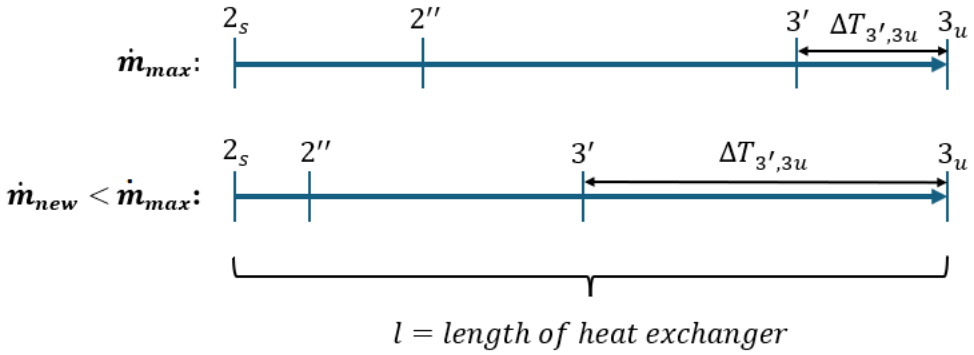

Figure 52: Temperature profile changes in the condenser as result of change in mass flow rate (own illustration)

If the mass of the refrigerant flows more slowly through the heat exchanger and the mass flow of the heating grid stays constant then a refrigerant mass unit transfers more heat per area of heat exchanger, since the timespan in which it the heat transfer takes place is longer. Therefore, the condensation starts and finishes after having passed a smaller spatial fraction of the heat exchanger. Thus, a larger spatial fraction remains in which the liquid refrigerant is cooled down. The result is that $\Delta T_{3',3_u}$ is increased as well as the enthalpy difference $\Delta h_{2s,3u}$. In the context of this work, an attempt was made to approximate the correlation between a change in mass flow rate $\dot{m}_{ref}$ and the consequences for $\Delta T_{1s,1''}$ and $\Delta T_{3',3_u}$ using the usual formulas for heat exchange and assuming a turbulent flow and a change in heat transfer coefficients with $\alpha \sim \dot{m}^{0.8}$ according to the Dittus-Boelter equation. Unfortunately, no physically consistent and robust correlation could be established. Here, a more detailed analysis would be required, including assumptions on additional parameters of the heat exchangers as well as the mass flow rates of the heat source and the district heating medium. Since detailed analysis of the heat exchanger profiles are beyond the scope of this work, the model assumes

fixed values for the temperature differences $\Delta T_{1s,1''}$ and $\Delta T_{3',3_u}$. Accordingly, a simplification is applied which assumes that the heat exchangers at each timestep are dimensioned in a way that $\Delta T_{1s,1''}$ and $\Delta T_{3',3_u}$ are exactly maintained. Although this does not reflect actual operational conditions, it is considered acceptable within the intended accuracy of this study.

4.7.2 Single-Stage vs. Multiple-Stage Heat Pump

The subsequent chapter compares the single-stage and two-stage heat pump cycle and evaluates to what extent the thermodynamic model developed thus far serves as an approximation for multi-stage heat pump systems.

In single-stage HPs, only one compression cycle is carried out using a single refrigerant. In contrast, multi-stage HPs divide the compression process into multiple stages, either within a single refrigerant circuit that includes intercooling [102], or, as in cascade systems, by using two separate circuits. In cascade systems, the condensation heat of the first circuit serves as the heat source for the second. Although single-stage systems are less complex, multi-stage configurations can offer several advantages, especially under demanding operating conditions. Particularly in applications with high temperature lifts, a multi-stage configuration can be useful to reduce compressor outlet temperatures and ensure a more material-friendly operation. For example, as shown in Figure 53, when using a single-stage heat pump with R717, providing heat for grid temperatures at 100 °C during periods with low source temperatures would require compressor outlet temperatures T_{2s} above 220 °C. Such high temperatures create substantial challenges regarding design and material selection of the compressor [103]. In addition, some lubricating oils begin to cork at excessively high temperatures, which requires the use of special alternative oils. Therefore, depending on the refrigerant considered, a multi-stage HP with at least two stages – possibly using two different refrigerants – could be more effective for the LSHPs in Hamburg [47, 104]. To account for the effects of different HP designs, the process characteristics of single-stage and two-stage HPs must be considered. The component diagram of a two-stage HP with intercooling by a flash-tank is shown in Figure 53 and the thermodynamic cycle is compared with the one of a single-stage HP in a p-h diagram.

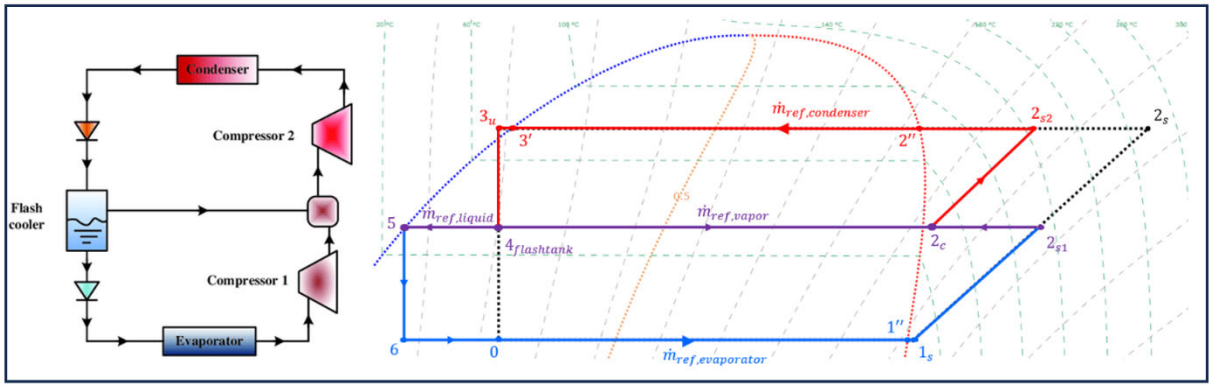

Figure 53: Multiple stage HP with intercooling vs. single-stage HP [102] (own illustration)

The refrigerant cycle of the two-stage HP is represented by the blue, purple, and red connecting lines, while the corresponding single-stage refrigerant cycle is displayed through the additional black dashed lines. In the two-stage HPs with intercooling, the refrigerant exiting the condenser is throttled by the upper-stage expansion valve, forming a liquid–vapor mixture at intermediate pressure, which is then directed into the flash tank. In the flash tank, the refrigerant mixture is separated into a liquid and a vapor phase [102, 105, 106]. The vapor phase is mixed with the superheated vapor from state 2_{s1} for intercooling purposes, while the liquid refrigerant is further throttled by the lower-stage expansion valve, forming a low-pressure, low-temperature liquid–vapor mixture that enters the evaporator [102]. By introducing the colder refrigerant vapor, the superheated vapor from the first compression stage is cooled down before a second compression takes place [102]. As a result, the discharge temperature after two compressions is reduced compared to the discharge temperature of the single-stage cycle while achieving the same pressure level. Although the specific enthalpy balances of single-stage and two-stage HPs are similar, they still differ in several aspects. As the pressure gradient of the isentropic lines in the p-h diagram usually decreases with increasing temperature, the sum of specific enthalpy balances for the compression processes of the two-stage HP is lower than the specific enthalpy difference of the one-stage compression $\Delta h_{2s1,1s} + \Delta h_{2s2,2c} < \Delta h_{2s,1c}$ – in case equal compressor efficiencies are assumed. This reduces the electrical power required for the two-stage HP. Nevertheless, the enthalpy balance at the condenser for the two-stage HP is also lower than for the single-stage HP $\Delta h_{2s2,3u} < \Delta h_{2s,3u}$, which leads to a reduction of heat output. On the other hand, it must be taken into account that the mass flow at the condenser is higher with the two-stage HP than with the single-stage HP, thus increasing the heat output. A part of the mass flow in the flash tank, the vapor-saturated part $x_g = 1$, is kept at intermediate pressure level and is fed directly to the superheated vapour of the first compression stage $x_g = 1$, hence increasing the mass flow in the condenser and lowering it in the evaporator [102]. Consequently, different mass flows occur in the cycle of the two-stage HP, while in the cycle of the single-stage HP one uniform mass flow exists. In the current model the simulation of a further compression stage would be possible to add without structural problems. However, the precise balancing of the mass flows and the modeling of the flash tank component require further assumptions and investigations that go beyond the scope of this work. Due to the similarity in enthalpy balances between the single-stage and two-stage HP cycles, the modeling of a single-stage process is considered a valid approximation for two-stage designs within the scope of this work – as it has also been applied in previous studies [107]. In addition, other simulation software such as heatpumps.streamlit developed by the ‘Zentrum für Nachhaltige Energiesysteme’ (ZNES) also show that the efficiency of a single-stage and a two-stage heat pump cycles with the same refrigerant are similar [108]. However, the results obtained from this approximation, such as in the simulation of the HP system using R717 as refrigerant, have to be taken with some uncertainty [107]. In general, it must be clearly stated that the HP model developed in this work is not suitable for reliably representing more complex configurations such as cascade systems using two different refrigerants.

4.8 Alternative Mode

This section presents an alternative modelling approach which omits detailed thermodynamic calculations to allow the modelling of various HP designs and enable a time-efficient computation.

In certain cases, modelling the thermodynamic processes in detail can be disadvantageous. If the HP to be modelled is too complex, a single-stage cycle as implemented in the current model no longer provides a robust approximation. In such cases, it is more appropriate to represent the HP characteristics based on literature values. Therefore, an additional alternative mode was developed. In the alternative mode, the HP performance over the course of a year is scaled by the annual average quality factor $\bar{\eta}_{quality,exterior}$ analogously to the explanations in chapter 3.3:

$$\bar{\eta}_{quality,exterior} = \frac{\overline{COP}_{real}}{\overline{COP}_{Carnot,exterior}} \approx \frac{APF}{\overline{COP}_{Carnot,exterior}} \quad (48)$$

During modelling in alternative mode, in each timestep i the $COP_{Carnot,exterior,i}$ is determined based on the time series of the heat source temperatures and temperatures of the district heating grid. Using the specified quality factor $\bar{\eta}_{quality,exterior}$ and the $COP_{Carnot,exterior,i}$, the corresponding $COP_{real,i}$ is then derived for each timestep i:

$$COP_{real,i} = COP_{exterior,Carnot,i} \cdot \bar{\eta}_{quality,exterior} \quad (49)$$

All technical assumptions, such as the temperature gradients in the heat exchangers, the compressor efficiency, selected refrigerants, auxiliary power and the general design structure of the HP, are represented by the quality factor $\bar{\eta}_{quality,exterior}$. As a result, the model is capable of simulating any type of HP for which the annual quality factor $\bar{\eta}_{quality,exterior}$ can be approximated. In the alternative mode the model-based heat output calculation as described in chapter 4.6 is performed as regular to determine $Q_{provide}$. Thus, after the $COP_{real,i}$ is defined for the corresponding timestep i all other relevant quantities such as the electrical input power, the heat extracted from the heat source, and the electricity costs can be calculated as well. However, when using the alternate mode based on literature values, it is important to check if the source and sink temperatures specified in the literature correspond to the values used in the simulation. A different scale or level of the temperature lift can affect the quality factor $\bar{\eta}_{quality,exterior}$ depending on the refrigerant used. If the temperature lift on which the literature values are based varies strongly in level or scale compared to the temperature lift applied in the individual timesteps, the quality factor calculated based on literature values might not be an optimal approximation to apply in the simulation. Furthermore, the assumption of a constant quality factor over the year $\bar{\eta}_{quality,exterior}$ is an approximation as the temperature conditions change for the individual timesteps. Thus, the ratio of the $COP_{real,i}$ to the $COP_{exterior,Carnot}$ is not always constant for every timestep i throughout the year. In Figure 54 the quality factors over a year based on thermodynamic modelling are illustrated for various refrigerants assuming the temperature conditions under standard operation.

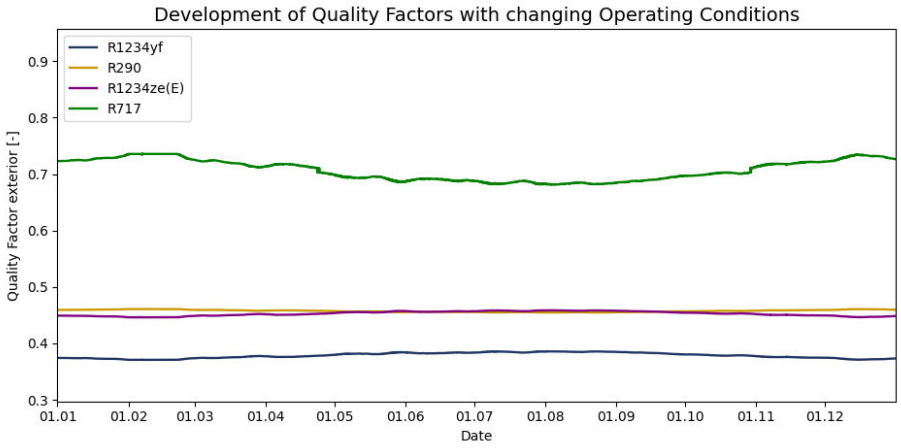

Figure 54: Development of quality factor due to changing operating conditions

For R290 the quality factor is almost constant during the year and for R1234ze(E) and R1234yf it slightly increases with increasing source temperatures. Nevertheless, for R717 a decrease in the quality factor during increasing source temperatures and lower temperature lifts is shown. Solely based on the current thermodynamic model the HP cycle of R717 comes closer to the Carnot cycle during colder seasons than during warmer seasons. That means modelling with a constant quality factor assesses the timesteps at colder seasons with lower COPs and the timesteps at warmer seasons with higher COPs compared to the thermodynamic modelling. At this point, the limitation of the thermodynamic model must be highlighted. The model does not account for variations in compressor efficiency or auxiliary energy losses that may occur under changing operating conditions within the timesteps throughout the year. This is further discussed in chapter 5.1. In reality, it is questionable whether a higher quality factor can actually be achieved at higher temperature lifts, as losses in real-world operation tend to increase with higher temperature lifts and operating levels. Considering the deviations in the quality factor of R717, the maximum deviation of the minimum or maximum quality factor from the annual average quality factor is 4.13 %. To check the effect on the simulation results the average annual quality factor $\bar{\eta}_{quality,exterior}$ resulted from thermodynamic modelling – which is tracked every timestep due to enthalpy balances – is applied and used for the simulation in alternative mode. The results show that throughout the comparison of every operating mode in every category such as the heat generation $Q_{provide}$, the electricity procurement costs, the total costs, the COP and further parameters there is no deviation higher than 1.5 % as the overestimation of the COP in warmer seasons equalizes the understimation of the COP in colder seasons. Only in one category, higher deviations occur. This is the case when it is tracked how redispatch-related heat energy has been provided in response to redispatch intervention. The tracking process is further detailed in chapter 5.2.2. However, it is pointed out here that the cause of deviations is that the redispatch-related energy which shall be taken into account for the heat production decision is scaled in every timestep i according to the COP of the last timestep $i-1$. Therefore, the amount of redispatch-related heat energy in one timestep can differ more widely in alternative mode compared to thermodynamic modelling. Nevertheless, it can be stated that apart from the deviations in redispatch-related energy in individual timesteps the alternative mode aligns

with the thermodynamic model. A key advantage of the alternative mode is the optimized simulation speed. Excluding the time for loading and storing of data before and after the simulation, the modelling of individual timesteps over one year based on thermodynamic calculation takes between 27 and 12 minutes, depending on the selected refrigerant. In contrast, the simulation in alternative mode for a one-year period requires approx. 1 minute. The alternate mode thus enables the simulation of several HP units within a larger power grid model without the simulation time becoming the bottleneck factor.

5 Variation of Parameters and Scenario Optimization

The following section presents and discusses the simulation results. In the first step, the thermodynamic model is used to determine the final HP design and to outline the impact of varying system parameters. Thereafter, the refined HP design is used to carry out simulations for each operating mode. The simulation results are discussed with a particular focus on heat generation, operating costs and contribution to grid support. Subsequently, operation mode 3 is enforced by varying the threshold price, and the corresponding simulation results are analysed.

5.1 Performance-Based Comparison and Refrigerant Selection

The subsequent chapter investigates the performance of different HP designs under variating operating conditions. Here, the performance of different refrigerants for distinct sink temperatures is evaluated. Furthermore, the impact of decreasing compressor efficiencies for various sink temperatures is analyzed and the effect of increasing auxiliary electricity consumption is examined. In the end, a final HP design is specified for the subsequent simulations, as defining the boundary conditions is essential for comparing individual system parameters [109].

As a restructuring of the district heating network resulting in a temperature drop is being discussed extensively [40, 110], the simulation under different temperature levels is carried out and the behavior of different refrigerants is analyzed. Apart from the temperature level assumed in the standard configuration, 90 – 100 °C, scenarios with lower heat supply temperatures are considered. Here constant heat supply temperatures are selected since a constant operating temperature is deemed more system friendly. The analyzation of refrigerants in chapter 3.4 has prefiltered the refrigerants R717, R290, R1234ze(E) and R1234yf for subcritical operation as well as R744 for transcritical operation. Refrigerants, which due to their high boiling point are only an option for the second stage of a multiple-stage HP, are not take into account in the analysis. Figure 55 shows the performance development of the subcritical refrigerants for variating temperature levels of the heating grid assuming a constant compressor efficiency of 0.8 and no electricity consumption due to auxiliary units.

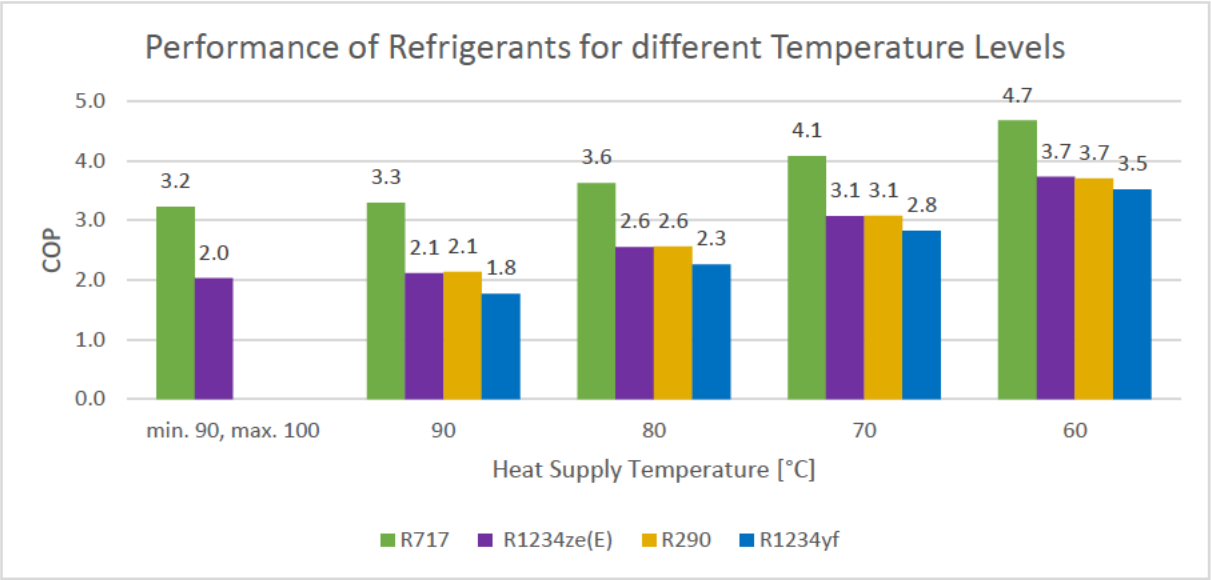

Figure 55: Performance of refrigerants for different temperature levels (own illustration)

The results are visualized for the COP that would result on average from a year-round operation in mode 1. The average COP which are determined only for the timesteps when HP operation takes place in Mode 3 are slightly lower (1 to 2 %). On the other hand, the COP which are determined only when HP operation takes place at a temperature level above 5 °C are slightly higher (3 to 4 %). R717 is outperforming the other refrigerants at every temperature level, whereby the relative difference decreases with lower temperature levels. For a temperature level between 90 and 100 °C supply temperature R1234ze(E) only reaches 62.8 % of the performance of R717. In contrast, at a temperature level of 60 °C supply temperature R1234ze(E) reaches 79.8 % of the performance of R717. The performance of R1234ze(E) and R290 is almost equal at every temperature level and the performance of R1234yf is slightly below. It must be considered that the results are based on the purely thermodynamic modeling of a single-stage HP cycle. As discussed in chapter 4.7.2, to use the refrigerant R717 at supply temperatures of 90 to 100 °C, a two-stage HP design would be necessary at least. For R1234ze(E), a series configuration would be the practicable concept. In the literature LSHPs using R1234ze(E) with up to 95 °C and 3 MW_{th} are documented [72]. Smaller systems even reach 100 °C supply temperature [111]. Nevertheless, it is questionable if systems only using R1234ze(E) as refrigerants would be technical and economically feasible for the LSHPs planned in Hamburg. For R717 market available products with up to 11 MW_{th} and supply temperatures of 90 °C are listed in comparative literature [72]. Furthermore, it is stated, that the operation up to 110 °C supply temperature and 76 bar is possible for R717 LSHPs with special designed compressors [13, 47, 72]. Therefore, it is assumed that the use of R7171 as a refrigerant in the LSHPs planned in Hamburg is technically possible, even though higher investment costs and safety requirements are necessary [47, 112]. As this study does not analyze feasibility on the basis of investment costs in more detail, the use of R717 in the LSHPs in Hamburg is anticipated solely on a performance-based view and therefore applied for modelling and evaluating further scenarios. Nevertheless, it must be clearly stated that other HP designs such as cascade HPs with two different refrigerants or a transcritical operation with

CO_2 as refrigerant are also a likely option [113]. With the current model a transcritical HP design cannot be approximated. Compared to a transcritical cycle with CO_2 the thermodynamic modelling of an R717 HP cycle would result in unrealistically high efficiency values [112]. Nevertheless, as no literature values are known for large CO_2 river-source HPs of this dimension, even the modelling in alternate mode is omitted here. Regarding cascade designs, if R717 is used in the first stage, it is plausible that a simplified R717 cycle may approximate the efficiency behavior of the full system to a certain extent.

For medium-high temperature lifts of 75 °C the compressor efficiency of HPs is assumed to be 0.8 in comparative literature [78]. However, it must be considered that for larger temperature lifts, compressor efficiency tends to decrease [114]. Thus, the assumption of a constant compressor efficiency of 0.8 across all temperature levels is a simplification. Figure 56 indicates the development of the COP with distinct compressor efficiencies for different grid temperature levels assuming no electricity consumption by auxiliary units.

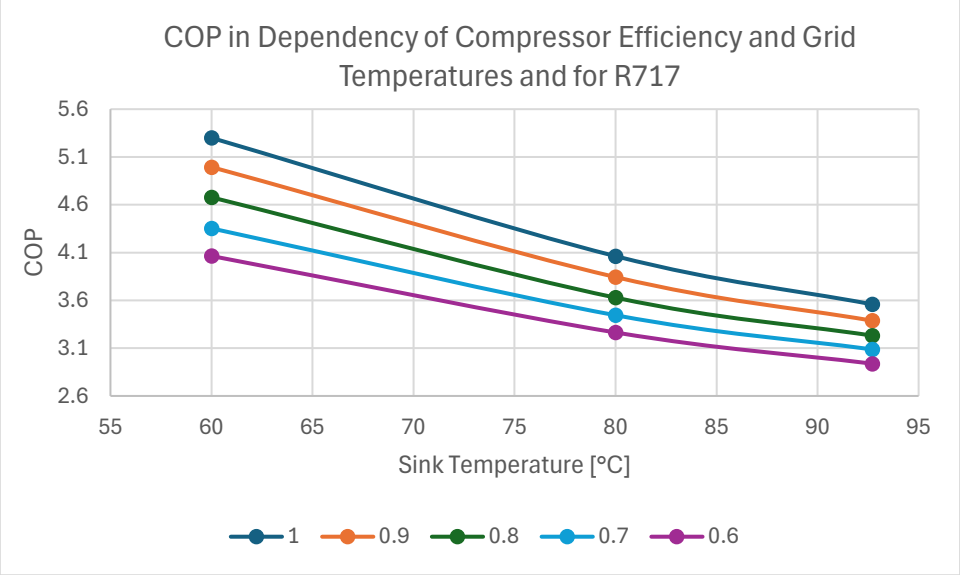

Figure 56: COP Dependency of Compressor Efficiency and Grid Temperatures (own illustration)

As expected, the COP declines with higher grid temperatures and lower compressor efficiencies. At lower supply temperature levels, the decrease of compressor efficiency has a higher impact on HP performance. With higher temperature levels the impact of poor compressor efficiency declines. This corresponds to results from comparative literature [107]. When considering the effect of the compressor efficiency on the overall performance in the current model, it must be considered that the thermodynamic simulation assumes the HP as a hermetic system. As a result, the entropy generation in the compressor due to poor efficiency leads to a higher compressor outlet temperature. This in turn allows to reduce the pressure in the condenser while maintaining the heat flow weighed mean temperature. Thus, the loss effect of poor compressor efficiency can be thermodynamically somewhat mitigated. In case that lower compressor efficiencies would cause heat losses to the environment the COP dependency on the compressor efficiency would be much higher than in the thermodynamic modeling. Due to the large temperature lift when aiming for supply temperatures of 90 to 100 °C a

compressor efficiency of 0.7 is selected as default setting. An adjustment of the compressor efficiency due to changing operating conditions during the individual timesteps is not yet carried out in the current model but recommended for further model improvement.

The previous results did show the COP without the use of auxiliary power. However, in real-world operation auxiliary power is necessary. Figure 57 shows the development of the COP for a compressor efficiency of 0.7 and heating grid temperatures from 90 to 100 °C is shown in mode 3 for increasing auxiliary power.

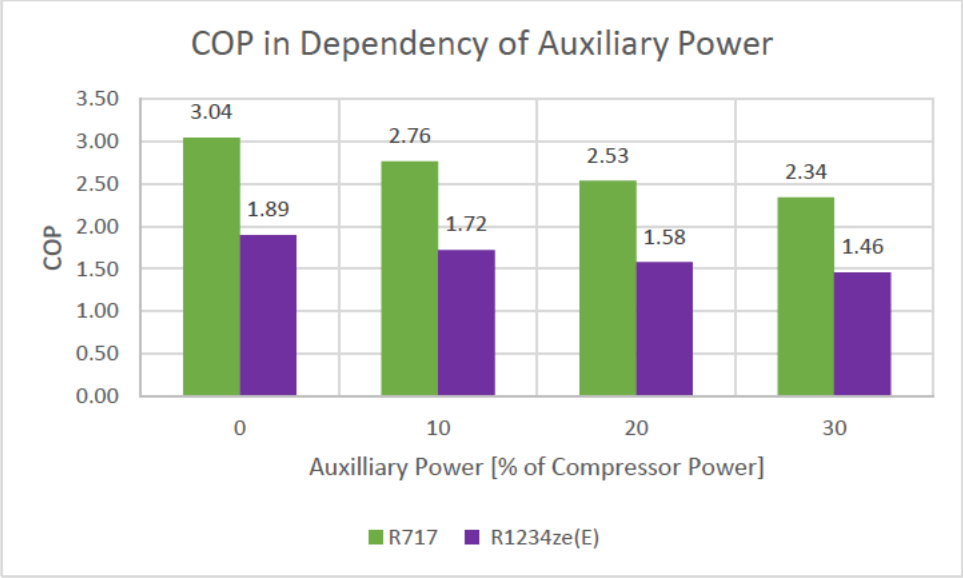

Figure 57: COP in Dependency of Auxiliary Power (own illustration)

The increase of electricity consumption due to auxiliary power up to 30 % of the compressor power during the timesteps when the HP is running in mode 3 leads to a maximum decrease of 23.1 % compared to an operation without auxiliary consumption. Due to the fact that a HP design with the specified dimensions and temperature lift using R717 is complex and technically challenging, it is assumed that the proportion of auxiliary energy required to support the operation is correspondingly higher. Thus, an auxiliary power consumption of 20 % of the compressor power is assumed. Here, a slightly higher estimation of auxiliary energy is also intended to compensate for other idealized assumptions, such as neglecting pressure losses in the pipes and treating the HP as a hermetic system without external heat losses. Nevertheless, it must be noted that a constant factor for all timesteps during the year is a simplification as auxiliary energy demand varies with operating conditions.

Table 3 displays the most essential operational parameters of the final HP design. If not explicitly stated otherwise, further simulations are carried out using these parameters.[11]

11

Table 3: Essential system parameters in final HP design

Parameter	Value
Refrigerant	R717
Temperature of district heating grid	90 – 100 °C
Compressor efficiency η_{comp}	0.7
Auxiliary power consumption	20 % of compressor power consumption
Time horizon (relevant for mode 3)	1 day (96 timesteps)
Part-load behavior	0.5
Switching operations (relevant for mode 3)	3 times on and off per module and day

5.2 Comparison of Operating Modes

This chapter presents the simulation results for the different operating modes described in chapter 4.4. To better contextualize the results, the annual energy profiles of the three standard operating modes 1b, 2b and 3b are illustrated. The results are analysed and discussed.

At the beginning of this chapter, it has to be pointed out that during the simulation an error was made, which was only noted retrospectively. As explained in chapter 4.4.4 the amount of heat, which shall be considered in the heat production as a result of redispatch intervention, is scaled based on the COP of the last timestep. In the simulations, the COPs of the last timesteps – excluding auxiliary power – were unintentionally applied for scaling the redispatch-related heat. This is not correct as the auxiliary power consumption must be considered to scale the effect of heat production on the power line correctly. The result is that slightly too high COPs were used to calculate the amount of redispatch related heat necessary to provide the desired change in the power line. Thus, the total amounts for provision or reduction of redispatch related heat considered in the heat production decision are estimated 20 % too high. Running the simulations 3b and 3g under correct conditions and comparing the simulation results with those of the previous simulation results from 3b and 3g shows that all simulation results except the one which exclusively measure redispatch related heat energy does not deviate more than 2 %. Therefore, the simulation results presented in the following chapter can be deemed reliable. To avoid irritation, it shall be clearly pointed out that only the COP for scaling the redispatch-related heat was not correctly applied, in all other aspects of modelling the auxiliary power was correctly considered. As the amounts of redispatch-related heat are important to evaluate the contribution to grid support, chapter 5.2.2 discusses the implications of the deviation for the results regarding grid-supportive behavior.

Figure 58 shows the district heat demand and generation for mode 1b in 2024 in daily resolution. Here, the left y-axis indicates the total amount of energy accumulated over one day, while the right y-axis shows the average storage level throughout the day.

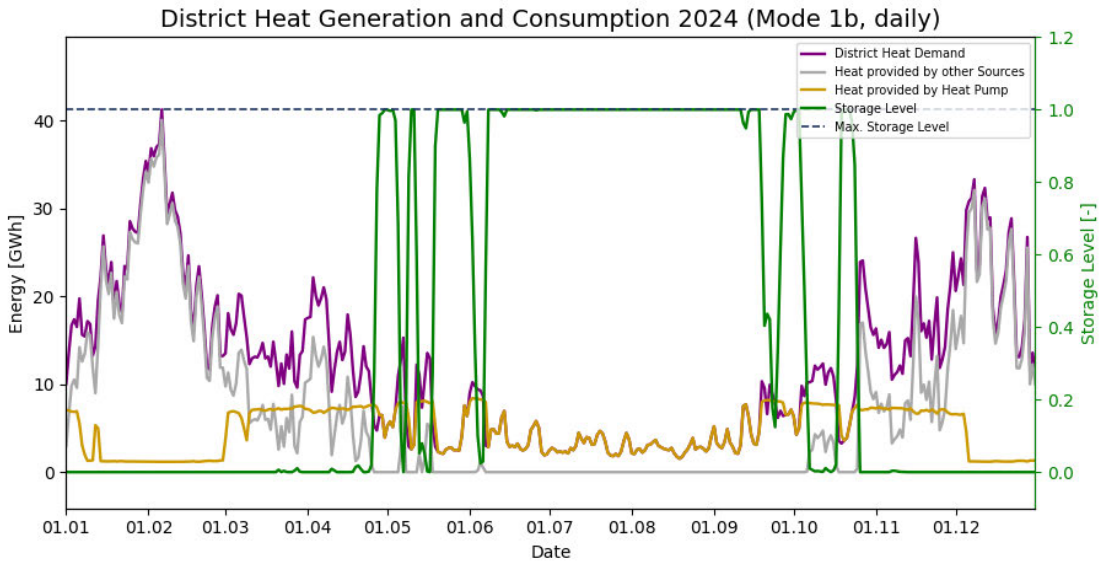

Figure 58: Demand and consumption profile 2024 for mode 1b in daily resolution (own illustration)

In the colder seasons at the beginning and end of the year, the heat demand significantly exceeds the heat generated by the LSHPs. Nevertheless, in warmer seasons from May to October the LSHPs are able to fully cover the heat demand, and the storage capacity limit is reached during large periods of the year, thus preventing the LSHPs from further production.

In Figure 59 the district heat demand and generation for mode 2b in 2024 in daily resolution is illustrated.

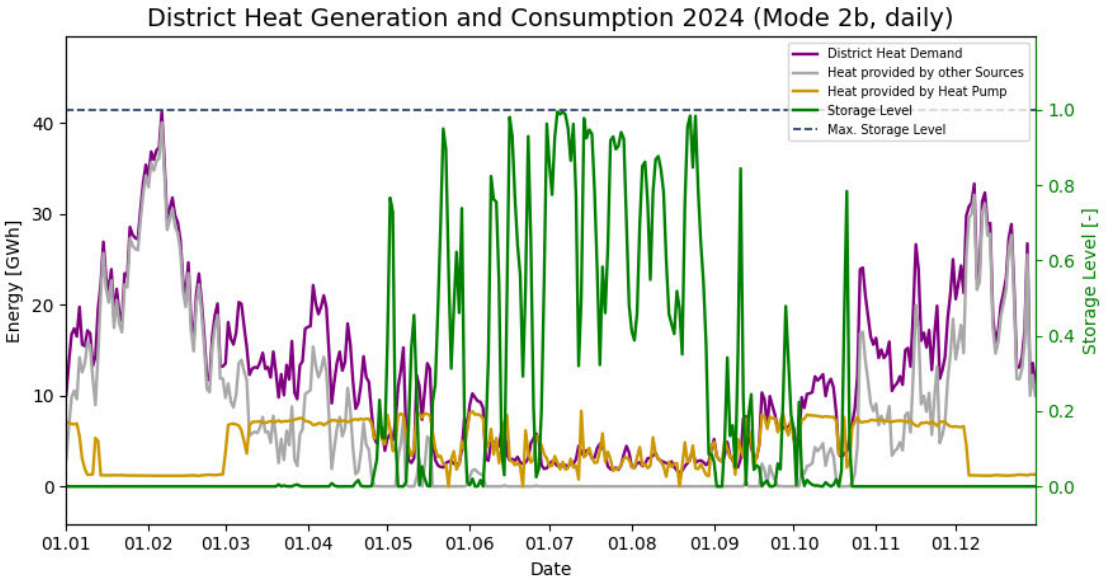

Figure 59: Demand and consumption profile 2024 for mode 2b in daily resolution (own illustration)

During the cold seasons the production profile of the LSHPs is equal to the one of mode 1 since mode 2 primarily aims for heat demand heat demand coverage as well. In the warmer seasons the storage level fluctuates as the LSHP operation is mostly electricity-price driven.

Figure 60 displays the district heat demand and generation for mode 3b in 2024 in daily resolution.

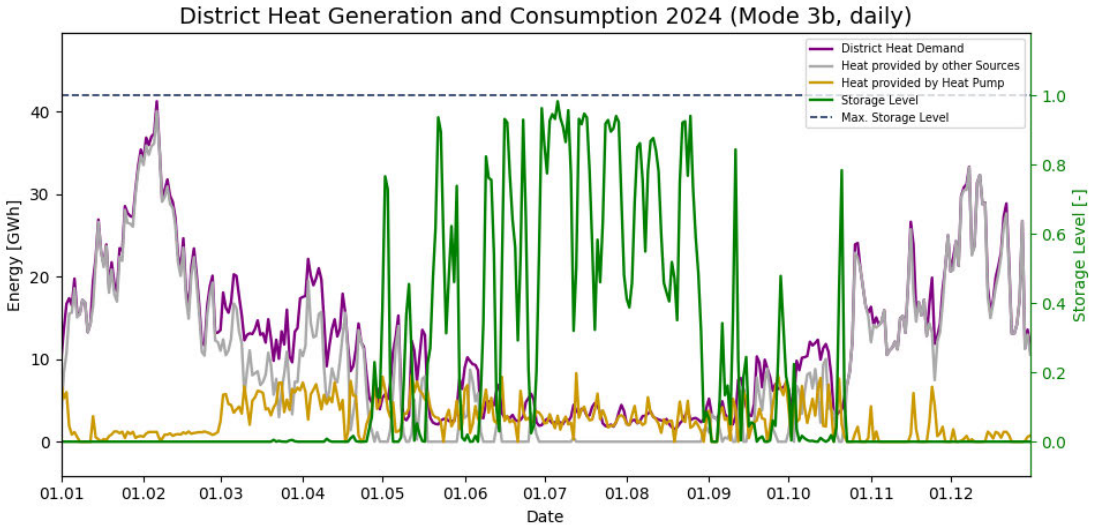

Figure 60: Demand and consumption profile 2024 for mode 3b in daily resolution (own illustration)

Here, the heat output fluctuates during the whole year due to the electricity price-led operation. It is observed that the profile of the storage level in mode 2b and 3b is almost the same. Thus, during warmer seasons an electricity price-led operation based on the annual average day-ahead market price is already sufficient to cover the district heat demand completely in 2024. Even though the graph of the storage profile for daily average storage levels never fully reaches the maximum level, it can be observed that the storage capacity indeed limits heat production in mode 3b when viewing the profile in 15-minute resolution. The profile showing the amount of energy and the storage level for every individual 15-minute timestep is presented in Figure 61. For better assessment the trimmed monthly average electricity price is shown as well.

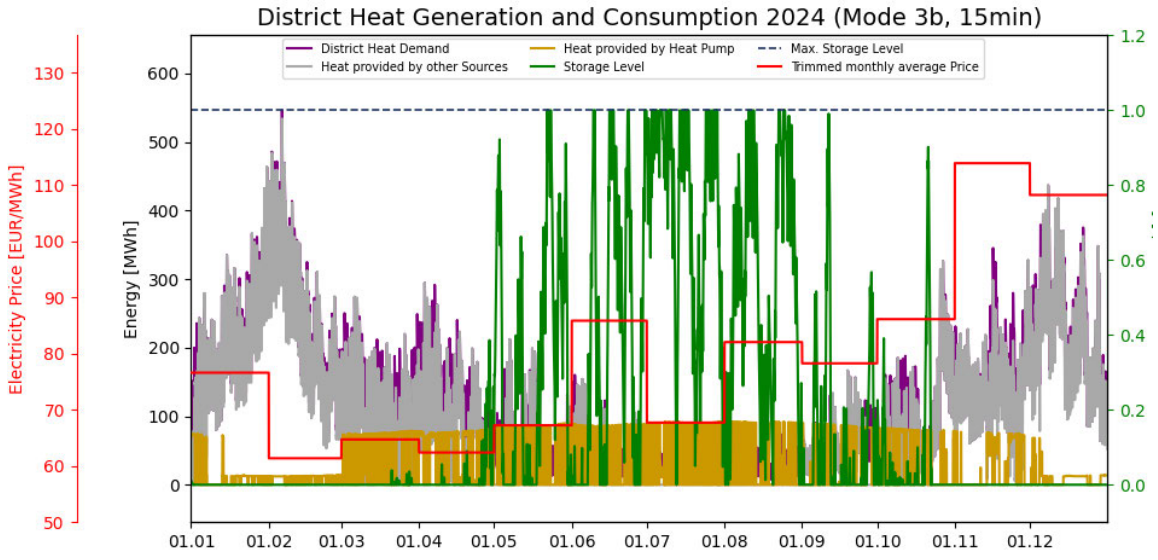

Figure 61: Demand and consumption profile 2024 for mode 3b in 15-minute resolution (own illustration)

It is observed that during several periods heat production is cut due to limited storage capacity, thus preventing the LSHPs from exploiting low electricity prices. Therefore, in chapter 5.3 an adaptation of the electricity threshold price is examined.

5.2.1 System Utilization vs. Operating Costs

In the following chapter the simulation results regarding heat generation, system utilization und operating costs are analyzed.

The various control strategies lead to a difference in system utilization. The heat generation quantity produced during modeling of the LSHPs in 2024 and the associated full-load hours are illustrated in Figure 62.

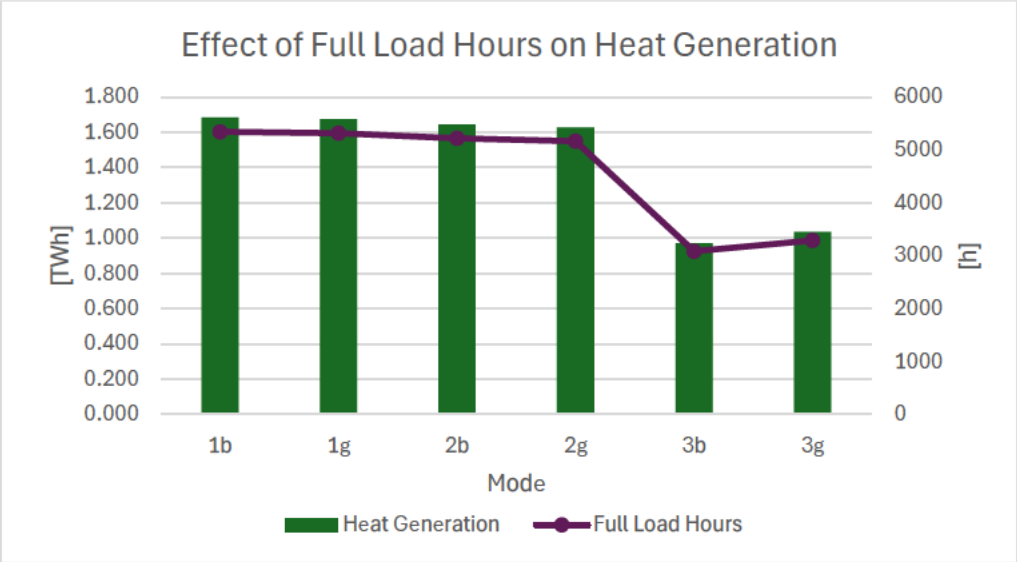

Figure 62: Effect of full load hours on heat generation (own illustration)

Mode 1b achieves a heat generation of 1.683 TWh, covering 38.2 % of the district heating demand. In Mode 2b, there is a slight decrease in heat generation (1.644 TWh) with a coverage of 37.4 % of district heat demand, and in Mode 3b, with a generation of 0.971 TWh, only 22.1 % of the demand is covered. In operating modes 2 and 3, the LSHPs each exhibit operation with over 5,000 full-load hours, while in mode 1b the LSHPs are active for only 3,083 full-load hours and in Mode 1g for 3,285. Thus, the number of full-load hours in mode 1 and 2 highly exceeds the number of full-load hours anticipated in future scenarios for 2045. In the future scenarios for 2045, an over dimensioning of the generation capacity of LSHPs is assumed to enable the most flexible operation possible, resulting in 1,300 to 2,400 full-load hours per year [13, 115]. Hence, even in mode 1 the number of full-load hours would be increased compared to the predicted number in future scenarios for 2045. Therefore, in chapter 5.3 the reduction of full-load hours due to the decrease of the threshold electricity price is discussed.

The variations in system utilization and operating times are reflected in the operation costs. Figure 63 shows the absolute annual operating costs and the resulting average specific electricity procurement costs as well as the average specific heat generation costs.

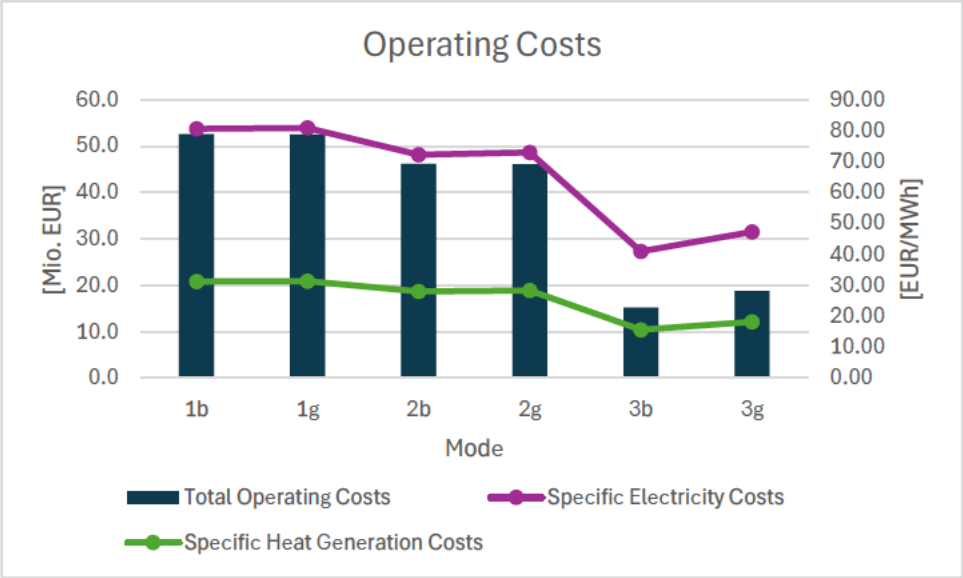

Figure 63: Operating cost for different control strategies (own illustration)

Due to the price-led operation in mode 3 and the partial price-led operation in mode 2, the specific electricity costs and specific heat generation costs are declining compared to mode 1. While in mode 1b the electricity is purchased for an average of 80.6 $\frac{EUR}{MWh}$, in mode 2b an average electricity purchase of 72.3 $\frac{EUR}{MWh}$ is reached and in mode 1b an average electricity purchase price of 41.0 $\frac{EUR}{MWh}$ is achieved. Thus, the total operational costs decrease disproportionately to the full-load hours operated. With a reduction of 2.8 % in full-load hours due to switching from mode 1b to mode 2b, there is already a reduction of 10.3 % in electricity procurement costs and 12.3 % in total operational costs. Comparing mode 1b to mode 3b, a reduction in full-load hours of 42.3 % results in a reduction of 49.2 % in electricity procurement costs and 71.1 % in total operating costs. Thus, the reduction in heat demand coverage is less significant than the improvement in electricity procurement cost optimization. Consequently, mode 1 maximizes heat demand coverage with less regard to electricity costs, while mode 3 attains a more favorable trade-off by optimizing operating costs and still meeting heat demand to a reasonable extent.

While both the heat production and electricity costs in modes 1b and 1g as well as in mode 2b and 2g are at a similar level respectively, the heat production mode 3g is 6.5 % higher and the operating costs are 23.6 % higher than those in mode 3b. The extent to which the higher operating costs and the amount of heat provided have affected grid serviceability is examined in the following chapter 5.2.2.

5.2.2 Impact of Grid-Supportive Operation

The following section investigates to what extent the different operating modes would have contributed to grid support in the year 2024. Here, a tracking parameter based on the explanations of grid-supportive operation in chapter 4.4.4 is introduced and the results are analyzed.

As pointed out in the beginning of chapter 5.2, the redispatch-related heat energy was scaled too high. A comparison of the results of mode 3b and 3g with the results of the correct simulation for the corresponding modes shows that the values of redispatch-related heat energy presented in this chapter have to be taken with an uncertainty of up to 12 %. A more detailed assessment of individual important values presented is made further below within this chapter.

To track the contribution to grid support the adjustment in heat energy which would lead to an 'actual compensation' is considered. Here, the concept of one-sided fixation of the heat production level as described in chapter 4.4.4 is important. It was outlined that during redispatch intervention the energy which the LSHPs shall provide is determined based on the heat production level the LSHPs had before the redispatch intervention occurred. These reference points were referred to as 'upper-base' or 'lower_base'. The heat production level of the following timesteps were defined by the base value and the redispatch-related energy – which can also be negative – added up to the base value 'upper-base' or 'lower_base'. When evaluating the grid supportive distribution during a redispatch intervention the difference between the heat production level and the base value is considered. If the difference is towards the right direction it is counted as grid-supportive energy which would compensate for redispatch related energy. In other words, the heat for 'actual compensation' is the heat generation adjustment which could lead to direct replacement of redispatch intervention by conventional power plants when the LSHP is located at the same grid node in the electricity grid. Thus, it can be measured if the behavior during the redispatch intervention would actually compensate for the power used by traditional power plants. Here, for every timestep at maximum the redispatch-related energy can be credited. Figure 64 illustrates the heat quantities which have been actively considered in adjustment of HP operation and therefore did lead to actual compensation for redispatch-related energy in 2024.

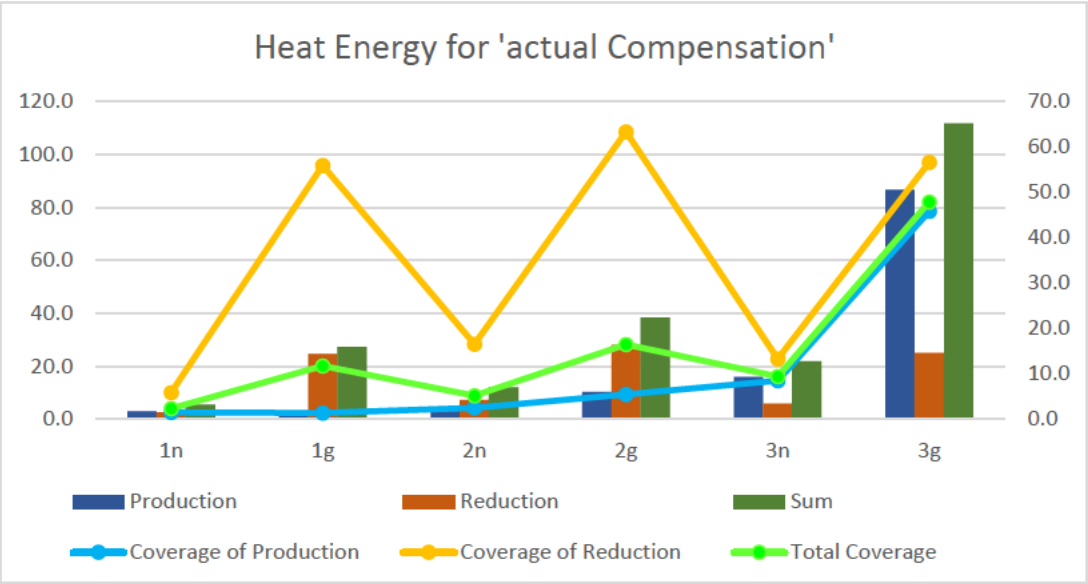

Figure 64: Heat energy provided to replace redispatch intervention of conventional power plants (own illustration)

The bars represent the amount of heat that was considered due to a change in production and did actually lead to compensation for redispatch-related energy. Here, production means that the heat generation was increased, reduction means that the heat generation was decreased, and the sum considers the adjustments in both directions. The lines show the covered percentage compared to the total amount of heat adjustment that would've been necessary in the corresponding category to compensate for all redispatch-related energy throughout the year. Here it shall be pointed out that the overscale effect due to too high COP estimation as explained above mitigates to a certain extent when considering the relative values (lines), which are given in relation to the total amount of redispatch-related heat in this year. Therefore, particularly the sum value of the covered percentage can be regarded with higher accuracy. The percentage of provided heat generation adjustments to achieve actual compensation in the modes 1g, 2g and 3g is significantly higher than in the corresponding modes 1b, 2b and 3b. In mode 1g 12.7 % of all necessary heat adjustments were carried out, in mode 2g 16.4 % and in mode 3g 47.8 % were performed. It becomes evident that all modes 1g, 2g and 3g cover almost the same amount of heat energy accounted for production reduction, but the necessary adjustments due to heat generation increase are rarely carried out by mode 1g (1.4 %) and mode 2g (10.3 %) while in mode 3g 45.8 % of the adjustments due to heat generation are executed. This is plausible, since when operating in mode 1g or mode 2g the LSHPs are already operating at a point of maximum heat production during large periods of the year. Consequently, if a redispatch intervention calls for a rise in output, the LSHPs cannot respond with additional heat production. As 81.0 % of the redispatch-related energy in 2024 required the LSHPs to increase their electricity consumption, the amount of heat energy that actually contributed to the compensation of redispatch interventions is accordingly much lower in mode 1g and mode 2g compared to mode 3g. This remains the case even if the LSHPs in mode 1 and 2 were already operating at their maximum grid-supportive capacity when the redispatch interventions occurred. Even though the tracking parameter of 'actual Compensation'

does not provide a full picture of whether the LSHPs have been operated grid supportive as it only considers the operation adjustment referred to the operating point prior to the redispatch intervention, the results show that in a price-led operation mode 3g the LSHPs are much more flexible to react to commands regarding redispatch interventions. A recalculation of the heat quantities tracked into the actual compensated electrical power is not yet implemented in the model. However, a manual back-calculation based on the thermal energy used for actual compensation measures and the annual average COP shows that in mode 3g, 44.1 GWh_{el} of redispatch energy could ideally be compensated, which would otherwise have been provided by conventional power plants in 2024. In mode 1b it would have been 8.6 GWh_{el}. Considering the total operating costs of mode 1b and mode 1g, this results in costs of 101,840 EUR per GWh_{el} of redispatch energy compensated. As mentioned before, an error was made scaling the redispatch-related heat energy of every timestep with the COP without considering auxiliary consumption. Therefore, the simulation was repeated only for the modes 3b and 3g considering the auxiliary consumption correctly. When applying a manual back-calculation based on the average annual COP, it shows that here in mode 3g only 39.0 GWh_{el} and in mode 3b only 7.5 GWh_{el} of redispatch energy could ideally be compensated. Considering the total operating costs of mode 1b and mode 1g in these simulations, it results in costs of 104,008 840 EUR per GWh_{el} of redispatch energy compensated. As most of the redispatch-related energy required an increase in production, the benefit of the associated heat generation is not accounted for in this figure. In addition, this figure must be considered with some uncertainty since the back-calculation based on the average annual COP does not take into account when the redispatch interventions occurred. Since the amount of heat adjustment due to redispatch interventions is scaled based on the COP of the previous timestep, the resulted heat energy presented here might not correspond exactly to the average annual COP of the year.

5.3 Variation in Threshold Price

The following chapter investigates the development of heat generation, system utilization, and operating costs under varying threshold prices in operating mode 3b. Since mode 3 represents the targeted operating strategy and an initial analysis in chapter 5.2.1 has shown that it provides the best trade-off between district heat demand coverage and operating costs, this mode is the focus of the subsequent analysis. For the generation of the simulation results presented in this chapter, the alternative mode was applied for reasons of time optimization.

Based on future scenarios for 2045, the threshold price would have to be reduced below the average annual electricity purchase price in order to reflect operations as forecasted for 2045 [13, 115]. However, it cannot be ruled out that LSHPs in Hamburg will be expected to cover a larger share of district heating demand at the beginning of the transformation process. Therefore, the development of the operating profile is analyzed for both decreasing and increasing threshold prices. Here, the threshold price is changend in gradations due to a multiplicator applied on the trimmed annual average

day ahead market price of 2024. The results are presented in Figure 65 and Figure 66. Figure 65 shows the specific electricity procurement cost and the specific heat generation costs (left y-axis) as well as the district heat demand coverage and system utilization (right y-axis).

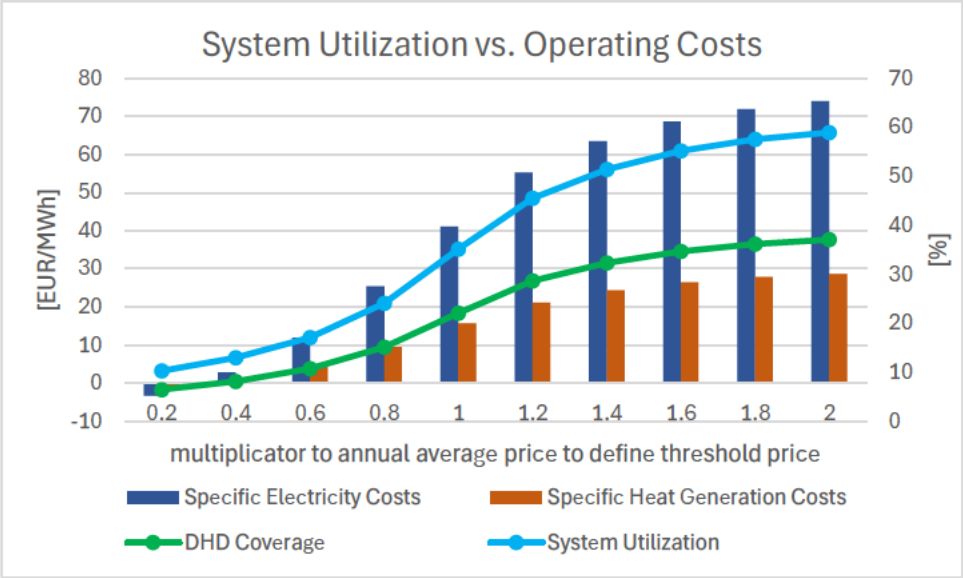

Figure 65: System utilization vs. operating costs for variating threshold price (own illustration)

With operation restricted to periods when the electricity price falls below 20 % of the annual average, negative operating costs – i.e., profits during heat production due to low electricity procurement prices – can be achieved. Here, an operation of 901 full-load hours takes place. As the multiplication factor for the threshold price increases, both system utilization and operating costs rise. Up to a factor of 1, this increase is not linear but rather exhibits an accelerating slope. Once the threshold surpasses the annual average electricity price, the slope begins to decrease. At a multiplication factor of 2 the operation almost reaches the district heat demand coverage (37.1 %) of the one in mode 1 (38.2 %) presented in chapter 5.2.1, while having with 73.0 $\frac{EUR}{MWh}$ 9.45 % lower electricity procurement costs compared to mode 1 $\left(80.6\ \frac{EUR}{MWh}\right)$. This, once again, emphasizes the benefits of mode 3. When considering the future scenarios for 2045 the simulations with a multiplicator of 0.4 to 0.8 correspond approximately to the anticipated system utilization as the number of full load hours in that range varies from 1138 to 2114. Figure 66 shows the heat generation vs. the total operating costs in that area.

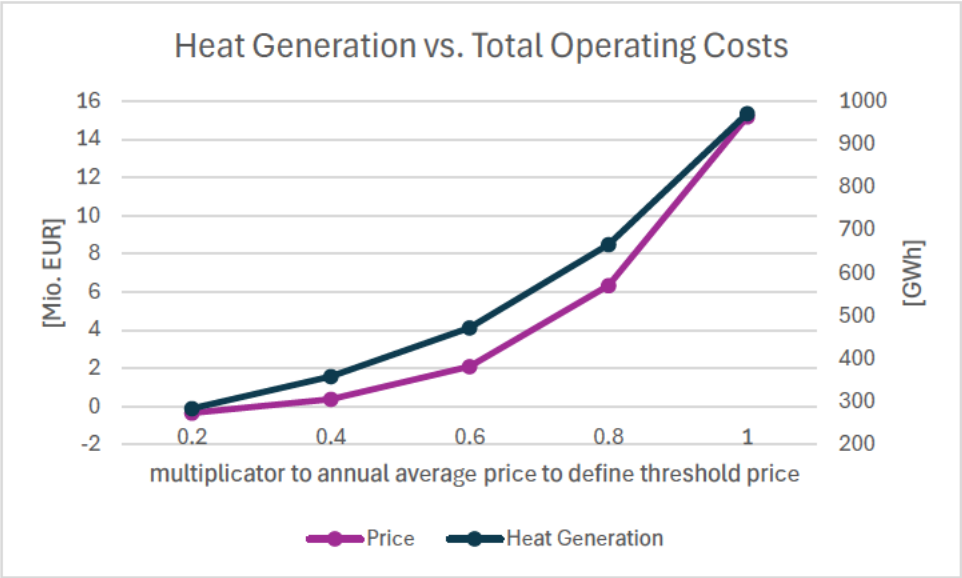

Figure 66: Heat generation vs. total operating costs for variating threshold prices (own illustration)

It is observed that the heat production and the total operating costs rise simultaneously, while even at very low total operating costs for the multiplicators 0.2 and 0.4 heat production takes place to a certain extent, covering 6.5 % and 8.2 % of the district heat demand. However, without further economic considerations regarding investment costs and the requirements for district heat demand coverage, the determination of an optimal operating point remains ambiguous. Moreover, it suggests that the operating point of an economically optimized operation should be specified more flexibly throughout the year rather than by a threshold price fixed at the beginning of the year. For instance, it shows that even at multiplicator of 0.4 for tiny periods of the year the heat generation is restricted due to limited storage capacity, as illustrated in Figure 67.

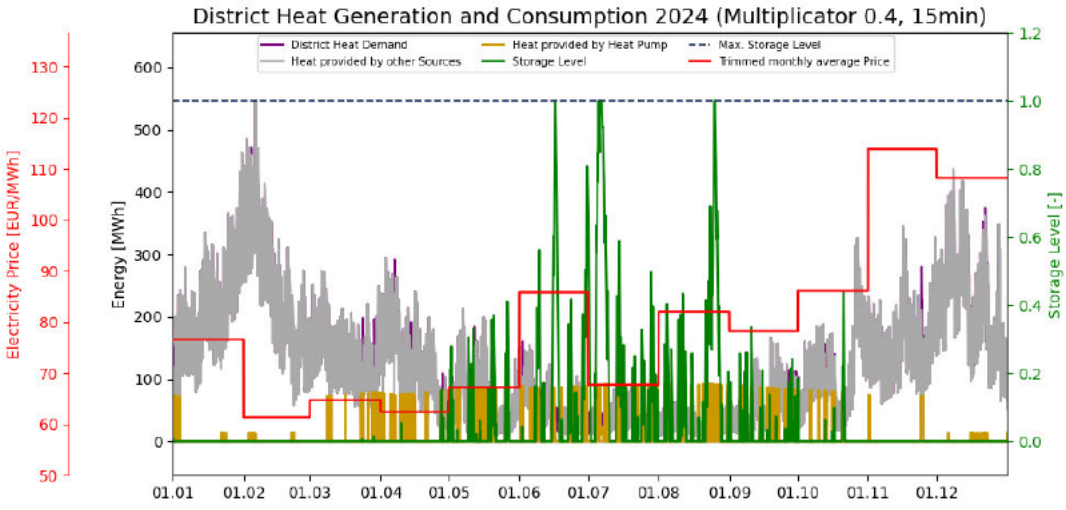

Figure 67: Heat generation profile for threshold price with multiplicator 0.4 (own illustration)

Therefore, it becomes evident that with higher multiplicators the exploitation of low electricity prices with a fixed threshold price can lead to loss situations when a relatively high electricity – but still

considered favourable – is used to charge the storage and subsequent drop in the electricity price cannot be utilized for further heat production due to limited storage capacity. Therefore, a feedback loop has been implemented regulating the threshold price as a result of the current storage level s. It applies:

$$price_{threshold} = price_{initial,threshold} \cdot \left(1 - \left(f_{damping} \cdot s\right)\right) \quad (50)$$

Thus, the threshold price gets lowered when the storage level rises allowing capacity for exploiting upcoming price drops. Here, the challenge is to finetune the damping factor. Furthermore, the question arises as to how often the feedback shall be applied. If applied to often it could lead to undesired switching behaviour during constant electricity price levels because threshold price fluctuates. If applied to rarely the feedback effect would not be effective and overcompensation could occur. The simulation has been carried out for different damping factors and storage sizes – since storage capacity is expected to increase in the future [13, 116] – while applying a feedback every four hours. At this point, it should be noted that a flexible adjustment of the threshold price requires a concept regarding module switching operations that differs from the one presented in chapter 4.5. As already emphasized in chapter 4.5 assigning switching operations at the beginning of a time horizon limits the operational flexibility too strongly. Therefore, an individual decision-making process regarding switching operation must be performed before every single timestep. This assumption holds true when adapting the threshold price as a result of the storage level. Here, the feedback loop must be executed in short time intervals. However, allocating switching operations over very short time horizons is not useful, since the maximum number of allowable switches per period would limit the system's ability to react to significant changes. Accordingly, the control strategy for switching allocation was suspended in the simulations with a variable threshold price. Unfortunately, the results could not be sufficiently analysed and presented within the scope of this work and therefore omitted here.

6 Evaluation

In the subsequent chapter, the simulation results are evaluated and put into context.

Regarding the HP design it is shown that R717 performs best in thermodynamic modelling among all refrigerants and is therefore favored from a performance-based view. Furthermore, it is shown that in the thermodynamic model the effect of poor compressor efficiency on overall performance can be mitigated to a certain extent by increasing the compressor outlet temperature – especially at high supply temperatures. On the other hand, a percentage increase in auxiliary power use affects the overall efficiency more significantly.

A comparison of the operating strategies in terms of district heat coverage and operating costs indicates that a price-led operation offers a better compromise between both criteria than a fully heat-led approach. Even with small cuts in heat generation as they take place when switching from mode 1b to mode 2b (2.28 %), a significant decrease in total operation costs is achieved (12.3 %). A similar outcome is produced when switching from mode 1b to mode 3b with a threshold price multiplicator of 2. Here a reduction in heat generation of 3.1 % percent and a drop in total operating costs of 11.2 % is the result. Therefore, a completely electricity market-independent operation is not recommended, even with a low penetration of LSHPs in the district heating grid. It is observed that during colder seasons mode 2 practically converts to mode 1 as the fluctuations in heat demand are not strong enough to allow price-led operation. Given this and the fact that a fixed electricity price threshold may cause inefficient operation by missing out on lower prices due to limited storage capacity, a more flexible operational approach appears necessary. This could be enabled by continuous adjustment of the threshold price. Here, a control strategy including an individual decision-making process regarding switching operations prior to each individual timestep is necessary.

As expected, constant lowering of a fixed threshold price leads to a decrease in electricity costs and heat generation. Therefore, when a higher penetration of renewable energy sources in the heating and electricity grids allows the reduction of required full-load hours for LSHPs, a significant drop in operating costs can be achieved. However, in this regard, the optimal compromise highly depends on additional factors such as investment costs and the surrounding infrastructure including minimum requirements for heat generation or grid-friendly operation. Regarding the contribution to grid support, it is observed that in 2024 a price-led operation in mode 3 would've enabled a much more flexible HP response to avoid grid congestion than heat-led or partial heat-led operations due to mode 1 or 2. This is caused by the fact, that in mode 1 and 2 during large periods of the year no further increase of electricity consumption in response to a grid congestion is possible compared to the prior operation point when the redispatch intervention occurred. However, in the accurate simulations of mode 3 – considering the auxiliary energy correctly when scaling the redispatch-related heat energy – due to an increase in total operation costs of 21.7 % the amount of redispatch-related heat that would've ideally led to direct relief for the power line increased from 19.3 GWh_{th} to 100.8 GWh_{th}, thus

covering 51.86 % of all redispatch-measures executed in 2024. That means with perfect position on the grid node of the electricity grid more than half of the energy provided by conventional power plants for redispatch intervention in Hamburg in 2024 could have been avoided due to adjustment in LSHP operation. However, it is very important to point out that the simplified modelling approach with one representative HP object and one aggregated data time series for redispatch interventions is a simplification that does not take into account the local position of each individual LSHP. As outlined in chapter 4.1.6 local position in the power grid is key when it comes to compensate for grid bottlenecks. Therefore, the figures regarding contribution to grid support should be interpreted with caution, since it is not guaranteed that a redispatch intervention covered by the full available power of one representative HP object could have been covered by the individual HP object on the site where the redispatch-related energy is needed. Nevertheless, the figures presented indicate the future potential of LSHPs to help alleviate grid congestion in Hamburg.

7 Conclusion and Outlook

In the following chapter, the outcome of this study is summarized and an outlook is provided.

In this study, the operation of the LSHPs planned in Hamburg was simulated throughout a year and the impact on the energy infrastructure with particular focus on the power grid was analyzed. In this process, the interdependencies between LSHP operation and the heating and electricity sector were outlined. Important aspects regarding HP plant design and the compatibility of refrigerants to the specific operating conditions in Hamburg's district heating grid were examined. The input data time series with a 15-minute resolution for modelling the HP operation over the course of one year were generated and the system characteristics were determined. Thereafter, a simulation framework in Python was constructed and the HP model including thermodynamic modelling as well as an alternative mode were created. Different operating modes as well as a control strategy for switching operation regarding technical management were developed and integrated into the simulation framework. A final HP design was determined due to performance-based aspects and the aim of operational realism. The simulation using the final HP design was run and the simulation results of different operating modes were compared regarding operating costs, heat demand coverage and contribution to grid support. The results were discussed, evaluated and put into context regarding future LSHP operation in Hamburg.

When considering the number and type of input parameters and system characteristics of the HP model, it becomes evident that the results generated in the scope of this work just cover a share of future scenarios regarding LSHP operation in Hamburg. A number of scenarios have been omitted to simulate and evaluate. This includes the increase in system and storage size, the assumption of less ability for part-load behavior and stricter technical constraints, the application of data input for different years, a fine-tuned operating mode with more flexible operation regarding economical and heat-sided signals and others. However, the current simulation framework enables flexible access to operating parameters and allows the variation of single parameters so that further future scenarios can be readily simulated. Due to the clear separation of heat output determination and thermodynamic modelling algorithms for new operating modes or finetuning of existing ones is possible without engaging in the thermodynamic calculations. Furthermore, the allocation of attributes to specific HP objects facilitates the integration of the HP model inside larger power flow analysis. This makes the developed model a powerful tool for future analysis of HP operation in power grids.

8 References

[1] IPCC, Core Writing Team, Lee, H. and Romero, J. et al., „Climate Change 2023: Synthesis Report," 2023. [Online]. Available: https://www.ipcc.ch/report/ar6/syr/downloads/report/IPCC_AR6_SYR_FullVolume.pdf. [Zugriff am 9 July 2025].

[2] N. Ghantous, „"We are walking when we should be sprinting" – IPCC," 21 March 2023. [Online]. Available: https://www.energymonitor.ai/international-treaties/ipcc-synthesis-report-we-are-walking-when-we-should-be-sprinting/. [Zugriff am 9 July 2025].

[3] P. e. a. Dießelberg, „Aktuelle Ausgabe: 369 Conflicts Globally," 2023. [Online]. Available: https://hiik.de/wp-content/uploads/2024/12/coba23_v3.pdf. [Zugriff am 9 July 2025].

[4] S. Richter, „Ressourcenkonflikte," 17 May 2018. [Online]. Available: https://www.bpb.de/themen/kriege-konflikte/dossier-kriege-konflikte/76755/ressourcenkonflikte/#footnote-target-3. [Zugriff am 9 July 2025].

[5] European Commission, „REPowerEU: Kommission will Abhängigkeit von fossilen Brennstoffen aus Russland schnell verringern," European Commission, 18 May 2022. [Online]. Available: https://germany.representation.ec.europa.eu/news/repowereu-kommission-will-abhangigkeit-von-fossilen-brennstoffen-aus-russland-schnell-verringern-2022-05-18_de. [Zugriff am 9 July 2025].

[6] European Comission, „REPowerEU: Ein Plan zur raschen Verringerung der Abhängigkeit von fossilen Brennstoffen aus Russland und zur Beschleunigung des ökologischen Wandels*," 18 May 2022. [Online]. Available: https://ec.europa.eu/commission/presscorner/api/files/document/print/de/ip_22_3131/IP_22_3131_DE.pdf. [Zugriff am 9 July 2025].

[7] European Union, „COMMUNICATION FROM THE COMMISSION TO THE EUROPEAN PARLIAMENT, THE EUROPEAN COUNCIL, THE COUNCIL, THE EUROPEAN ECONOMIC AND SOCIAL COMMITTEE AND THE COMMITTEE OF THE REGIONS REPowerEU Plan," 2022 May 2022. [Online]. Available: https://eur-lex.europa.eu/legal-content/EN/TXT/?uri=COM%3A2022%3A230%3AFIN&qid=1653033742483. [Zugriff am 9 July 2025].

[8] Umweltbundesamt (UBA), „Erneuerbare Energien in Zahlen," 18 June 2025. [Online]. Available: https://www.umweltbundesamt.de/sites/default/files/medien/372/dokumente/erneuerbare-energien-in-deutschland-2024_diagramme.pdf. [Zugriff am 9 July 2025].

[9] Umweltbundesamt (UBA), „Energieverbrauch für fossile und erneuerbare Wärme," 25 April 2025. [Online]. Available: https://www.umweltbundesamt.de/daten/energie/energieverbrauch-fuer-fossile-erneuerbare-waerme. [Zugriff am 9 July 2025].

[10] B. 9. G. F. D. P. (. Sozialdemokratische Partei Deutschlands (SPD), „Koalitionsvertrag 2021–2025 zwischen der SPD, BÜNDNIS 90/DIE GRÜNEN und FDP," 2021. [Online]. Available: https://www.spd.de/fileadmin/Dokumente/Koalitionsvertrag/Koalitionsvertrag_2021-2025.pdf. [Zugriff am 9 July 2025].

[11] Fraunhofer-Institut für System- und Innovationsforschung (ISI) and Sensfuß, Frank et al. , „Wärmenetze in Deutschland O45 / Heatgrids in Germany O45," Fraunhofer-Institut für System- und Innovationsforschung ISI, 2025. [Online]. Available: https://enertile-explorer.isi.fraunhofer.de:8443/open-view/65117/e8e079d138624d1d44889848da037f7c. [Zugriff am 9 July 2025].

[12] Prognos, Öko-Institut, Wuppertal-Institut, „Klimaneutrales Deutschland 2045," June 2021. [Online]. Available: https://www.agora-energiewende.de/fileadmin/Projekte/2021/2021_04_KNDE45/A-EW_231_KNDE2045_Langfassung_DE_WEB.pdf. [Zugriff am 9 July 2025].

[13] Agora Energiewende, Fraunhofer IEG, „Roll-out von Großwärmepumpen in Deutschland," 1 June 2023. [Online]. Available: https://www.agora-energiewende.de/fileadmin/Projekte/2022/2022-11_DE_Large_Scale_Heatpumps/A-EW_293_Rollout_Grosswaermepumpen_WEB.pdf. [Zugriff am 9 July 2025].

[14] M. Gebauer, „Energiespeicherkonzepte und ihre Nutzungsmöglichkeiten unter Berücksichtigung einer optimalen Sektorenkopplung," 26 June 2023. [Online]. Available: https://publications.rwth-aachen.de/record/963847/files/963847.pdf. [Zugriff am 9 July 2025].

[15] P. M. Z. A. Komarnicki, Sektorenkopplung – Energetisch-nachhaltige Wirtschaft der Zukunft, Magdeburg/Berlin, Germany: Springer, 2020.

[16] S. A. e. a. Umweltbundesamt (UBA), „Sozialverträglicher Klimaschutz – Sozialverträgliche Gestaltung von Klimaschutz und Energiewende in Haushalten mit geringem Einkommen," Umweltbundesamt (UBA), 2017.

[17] H. E. GmbH, „Fernwärmenetz und Übergabestationen," 2025. [Online]. Available: https://unternehmen.hamburger-energiewerke.de/wissen-themen/fernwaerme/fernwaermenetz-uebergabestationen#:~:text=Hamburg%20hat%20eines%20der%20gr%C3%B6%C3%9Ften,zunehmend%20die%20digitale%20Zukunft%20ein.. [Zugriff am 9 July 2025].

[18] Hamburger Energiewerke GmbH, „Hamburg gewinnt aus Abwasser Wärme," 2025. [Online]. Available: https://unternehmen.hamburger-energiewerke.de/presse-media/pressemitteilungen/hamburg-gewinnt-aus-abwasser-waerme. [Zugriff am 9 July 2025].

[19] LEA LandesEnergieAgentur Hessen GmbH, „Projekte," 2025. [Online]. Available: https://grosswaermepumpen-info.de/de/projekte/?sort=-thermal_capacity_kw#project-table. [Zugriff am 10 May 2025].

[20] U. Liebenthal, Interviewee, *Leiter Systemplanung & Innovation, Hamburger Energiewerke GmbH.* [Interview]. 20 September 2024.

[21] Statista GmbH, Pawlik, V., „Verbrauch von Fernwärme in Deutschland in den Jahren 1990 bis 2023," 23 June 2025. [Online]. Available: https://de.statista.com/statistik/daten/studie/166824/umfrage/verbrauch-von-fernwaerme-in-deutschland/. [Zugriff am 26 2 2025].

[22] F. e. a. Fraunhofer-Institut für System- und Innovationsforschung (ISI) and Sensfuß, „Wärmenachfrage in Wärmenetzen O45 /Heat demand in Heat Grids O45," 2025. [Online]. Available: https://enertile-explorer.isi.fraunhofer.de:8443/open-view/65115/25e223527619bf4f379a7f308dae9ddc. [Zugriff am 9 July 2025].

[23] Umweltbundesamt (UBA), „Szenarien zum Endenergieverbrauch in Deutschland 2008 und 2030," 2025. [Online]. Available: https://www.umweltbundesamt.de/bild/szenarien-endenergieverbrauch-in-deutschland-2008. [Zugriff am 9 July 2025].

[24] AGFW | Der Energieeffizienzverband für Wärme, Kälte und KWK e. V., „Preistransparenz-plattform Fernwärme," 2025. [Online]. Available: https://www.waermepreise.info/. [Zugriff am 10 1 2025].

[25] Verbraucherzentrale NRW e.V., Havlat, Oliver, „Fernwärme: Kosten sparen und gleichzeitig das Klima schonen," 2025. [Online]. Available: https://www.verbraucherzentrale.de/wissen/energie/heizen-und-warmwasser/fernwaerme-kosten-sparen-und-gleichzeitig-das-klima-schonen-34038. [Zugriff am 9 July 2025].

[26] Bundesverband der Verbraucherzentralen und Verbraucherverbände – Verbraucherzentrale Bundesverband e.V., „BEZAHLBARKEIT VON FERNWÄRME LANGFRISTIG SICHERN," 4 December

2024. [Online]. Available: https://www.vzbv.de/sites/default/files/2024-12/24-12-04_Stellungnahme_vzbv_AVBFernw%C3%A4rmeV%20_final.pdf. [Zugriff am 9 July 2025].

[27] Verband kommunaler Unternehmen e. V. (VKU), „Oberlandesgericht Hamburg weist Klage der Verbraucherzentrale gegen HanseWerk Natur ab," 5 May 2024. [Online]. Available: https://www.vku.de/themen/recht/artikel/fernwaerme/. [Zugriff am 9 July 2025].

[28] Umweltbundesamt (UBA) , „Preise und Preistransparenz als Akzeptanzfaktor in der Fernwärme," 11 October 2023. [Online]. Available: https://www.umweltbundesamt.de/sites/default/files/medien/11850/publikationen/factsheet_kurzanalyse_fw_preistransparenz_10_2023.pdf. [Zugriff am 9 July 2025].

[29] M. Zapf, Stromspeicher und Power-to-Gas im deutschen Energiesystem, Mönchsberg, Germany: Springer Vieweg, 2022.

[30] P. a. K. M. Konstantin, Praxisbuch Energiewirtschaft, Burgstetten, Germany: Springer-Verlag, 2023.

[31] E. e. a. Popovski, „The role and costs of large-scale heat pumps in decarbonising existing district heating networks – A case study for the city of Herten in Germany," *Energy,* 1 August 2019.

[32] M. e. a. Pehnt, „Dekarbonisierung von Energieinfrastrukturen," August 2023. [Online]. Available: https://www.umweltbundesamt.de/sites/default/files/medien/479/publikationen/cc_08-2023_dekarbonisierung_von_energieinfrastrukturen.pdf. [Zugriff am 14 July 2025].

[33] O. Kozlenko, „Masterarbeit - Optimierungsmodell für die Anlagenauslegung in der Energiezentrale des KEBAP als Grundlage für ein nachhaltiges Wärmeversorgungskonzept im Quartier," 1 January 2022. [Online]. Available: https://reposit.haw-hamburg.de/bitstream/20.500.12738/16714/1/MA_Optimierungsmodell%20f%c3%bcr%20die%20Anlagenauslegung%20in%20der%20Energiezentrale%20des%20KEBAP_geschw%c3%a4rzt.pdf. [Zugriff am 14 July 2025].

[34] D. Schön, „Potentiale und Hemmnisse bei der Einbindung eines intelligenten Energiemarkts in die wärme- und kältetechnische Konzeption," 10 March 2016. [Online]. Available: https://opus.hs-offenburg.de/frontdoor/deliver/index/docId/1286/file/Abschlussarbeit_einseitig.pdf. [Zugriff am 14 July 2025].

[35] 50Hertz Transmission GmbH, „Redispatchmaßnahmen," 2025. [Online]. Available: https://www.netztransparenz.de/de-de/Systemdienstleistungen/Betriebsfuehrung/Redispatch. [Zugriff am 10 April 2025].

[36] naturstrom AG - energiezukunft, „Groß und stabil oder klein und agil," 12 May 2025. [Online]. Available: https://www.energiezukunft.eu/erneuerbare-energien/stromnetze-speicher/gross-und-stabil-oder-klein-und-agil. [Zugriff am 15 July 2025].

[37] Freie und Hansestadt Hamburg, „Neue Hamburger Klimaschutzziele auf der Grundlage von fachlich-wissenschaftlichen Szenarien," 2022. [Online]. Available: https://www.hamburg.de/politik-und-verwaltung/behoerden/bukea/themen/klima/szenarienhamburgerklimaplan-169018#:~:text=Die%20neuen%20Hamburger%20Klimaziele%20wurden,von%2069%20Prozent%20bis%202030). [Zugriff am 9 July 2025].

[38] H. e. a. Falkenberg, „ENTWICKLUNGSSZENARIEN FÜR NEUE KLIMAZIELE - GESAMTERGEBNIS SZENARIO A UND B," 24 October 2022. [Online]. Available: https://www.hamburg.de/resource/blob/169826/d375518d8b3a9b879e9dfb4fb47b2001/d-szenarien-ergebnisab-data.pdf. [Zugriff am 9 July 2025].

[39] M. e. a. Sandrock, „ENTWICKLUNGSSZENARIEN FÜR NEUE KLIMAZIELE SZENARIO B," 27 October 2022. [Online]. Available: https://www.hamburg.de/resource/blob/169824/ce5cfe6fcfda8b841bfb309bb7c42453/d-szenarien-szenariob-data.pdf. [Zugriff am 9 July 2025].

[40] I. e. a. Peters, „https://www.hcu-hamburg.de/fileadmin/documents/Professoren_und_Mitarbeiter/Irene_Peters/Suedvariante_AnmerkungenHCUundHAW_20210607.pdf," Hafen City University and HAW Hamburg, 7 June 2021. [Online]. Available: https://www.hcu-hamburg.de/fileadmin/documents/Professoren_und_Mitarbeiter/Irene_Peters/Suedvariante_AnmerkungenHCUundHAW_20210607.pdf. [Zugriff am 9 July 2025].

[41] Dornier Group GmbH, „Laufzeitverlängerung Heizkraftwerk Wedel," [Online]. Available: https://dornier-group.com/referenz/laufzeitverlaengerung-hkw-wedel/. [Zugriff am 24 July 2025].

[42] Energiebeinetzrat, „Bericht," 18 April 2019. [Online]. Available: https://www.hamburg.de/resource/blob/157844/092f62b2c36e5072aa1c019a3e07d64a/d-top-4-bericht-der-ag-ersatz-des-hkw-wedel-an-den-enb-18-4-2019-data.pdf. [Zugriff am 9 July 2025].

[43] Freie und Hansestadt Hamburg, „Nachhaltigkeit & Primärenergiefaktor," 2025. [Online]. Available: https://waerme.hamburger-energiewerke.de/heizen-mit-fernwaerme/nachhaltigkeit-

primaerenergiefaktor#:~:text=Die%20Neubestimmung%20der%20Anlagen%20der,jetzt%2064g%20CO2%2FkWh.. [Zugriff am 9 July 2025].

[44] F. u. H. Hamburg, „Hamburgs Fernwärme wird klimafreundlich," 2025. [Online]. Available: https://www.hamburg.de/politik-und-verwaltung/behoerden/bukea/themen/klima/klimaschutz-klimaplan/fernwaerme-hamburg-169216. [Zugriff am 9 July 2025].

[45] Freie und Hansestadt Hamburg, „Das Heizkraftwerk Tiefstack," 2025. [Online]. Available: https://www.hamburg.de/politik-und-verwaltung/behoerden/bukea/themen/energie/hamburgs-energienetze/heizkraftwerk-tiefstack-157298. [Zugriff am 9 July 2025].

[46] D. a. F. C. I. v.d. Bor, „Quick selection of industrial heat pump types including the impact of thermodynamic losses," *Energy,* 2013.

[47] C. Arpagaus, Hochtemperatur-Wärmepumpen - Marktübersicht, Stand der Technik und Anwendungspotenziale, Berlin/Offenbach, Germany: VDE Verlag GmbH, 2019.

[48] H. e. a. Herwig, Technische Thermodynamik, Bd. 2nd edition, Wiesbaden, Germany: Springer-Vieweg, 2016.

[49] B. e. a. Weigand, Thermodynamik kompakt, Berlin Heidelberg: Springer-Verlag, 2016.

[50] P. Sumerauer, „Optimierung einer R410A Heizungs-Wärmepumpe," 2012. [Online]. Available: https://repository.tugraz.at/publications/n03w7-5mj33. [Zugriff am 9 March 2025].

[51] P. a. S. M. v. Böckh, Technische Thermodynamik - Ein beispielorientiertes Einführungsbuch, Berlin Heidelberg, Germany: Springer Vieweg, 2015.

[52] J. a. K. J. Lauth, Thermodynamik - Eine Einführung, Bd. 2. Auflage, Berlin/Heidelberg, Germany: Springer-Verlag, 2022.

[53] R. Müller, „Thermodynamik - Vom Tautropfen zum Solarkraftwerk," Walter de Gruyter GmbH, Berlin/Boston, 2014.

[54] J. Bonin, Handbuch Wärmepumpen : Planung und Projektierung, 4th Hrsg., D. D. I. f. N. e.V, Hrsg., Berlin/Wien/Zürich: Beuth Verlag GmbH, 2023.

[55] T. Hackensellner, Wärmepumpen in Haushalt, Gewerbe und Industrie, Kulmbach: VDE Verlag GmbH, 2023.

[56] Z. e. a. Wang, „Creative Commons Attribution 4.0 International," 2025. [Online]. Available: https://www.researchgate.net/figure/Flow-chart-of-compression-heat-pump-heating-system_fig1_351452856. [Zugriff am 9 July 2025].

[57] VDMA, „Energieeffizienz von elektrisch angetriebenen Wärmepumpen - Effizienzkennzahlen und deren Definition," HAW Hamburg, 2014.

[58] H. D. a. S. K. Baehr, Wärme- und Stoffübertragung, 9th Hrsg., Bochum, Germany: Springer Vieweg, 2016.

[59] Technische Universität Darmstadt (TUD), „Physikalisches Grundpraktikum - W10 Wärmepumpe," 1 April 2022. [Online]. Available: https://www.physik.tu-darmstadt.de/media/fachbereich_physik/phys_studium/phys_studium_bachelor/phys_studium_bsc_praktika/phys_studium_bsc_praktika_gp/phys_studium_bsc_praktika_gp_waermelehre/w10/w10.pdf. [Zugriff am 9 July 2025].

[60] Y. A. a. B. M. A. Çengel, THERMODYNAMICS - AN ENGINEERING APPROACH, 8th Hrsg., New York, USA: McGraw-Hill Education, 2015.

[61] Glenwin and Glen Refrigeration, „Electronic Expansion Valve: Types, Advantages & Work Principle," 2023.

[62] M. Zogg, „Wärmepumpen," 7 September 2009. [Online]. Available: https://www.zogg-engineering.ch/Publi/WP_ETH_Zogg.pdf. [Zugriff am 10 July 2025].

[63] J. K. e. a. Jensen, „Heat pump COP, part 2: Generalized COP estimation of heat pump processes," 2018. [Online]. Available: https://backend.orbit.dtu.dk/ws/portalfiles/portal/151965635/MAIN_Final.pdf. [Zugriff am 10 July 2025].

[64] K. E. e. a. Herold, ABSORPTION CHILLERS AND HEAT PUMPS, 2nd Hrsg., NW, USA: Taylor & Francis Group, 2016.

[65] M. a. O. T. Kofler, Wärmepumpen, Bonn: Rheinwerk Verlag/VDE Verlag, 2024.

[66] H.-J. Seifert, Effizienter Betrieb von Wärmepumpenanlagen, Berlin Offenbach, Germany: VDE Verlag GmbH, 2024.

[67] LEA LandesEnergieAgentur Hessen GmbH, „Project List - API Documentation," 2025. [Online]. Available: https://grosswaermepumpen-info.de/de/api/projects/. [Zugriff am 5 May 2025].

[68] LEA LandesEnergieAgentur Hessen GmbH w.f.n. Fraunhofer IEG 2024 based on Arpagaus 2019 , „Selection of refrigerant for large heat pumps,“ [Online]. Available: https://grosswaermepumpen-info.de/en-us/refrigerants/. [Zugriff am 25 July 2025].

[69] Umweltbundesamt (UBA), „Wärmepumpen,“ 2024. [Online]. Available: https://www.umweltbundesamt.de/themen/klima-energie/fluorierte-treibhausgase-fckw/natuerliche-kaeltemittel-in-stationaeren-anlagen/anwendungen/waermepumpen#:~:text=Art.,1. [Zugriff am 10 July 2025].

[70] G. A. Longo, „Boiling of the new low-GWP refrigerants R1234ze(Z) and R1233zd(E) inside a small commercial brazed plate heat exchanger,“ *International Journal of Refrigeration,* 2019.

[71] Ian H. Bell and the CoolProp Team, „Welcome to CoolProp,“ 2025.

[72] F. e. a. Schlosser, „Large-scale heat pumps: Applications, performance, economic feasibility and industrial integration,“ *Renewable and Sustainable Energy Reviews,* 2020.

[73] Deutscher Wetterdienst (DWD), „Open Data Bereich des Climate Data Center,“ 2025. [Online]. Available: https://www.dwd.de/DE/leistungen/cdc/climate-data-center.html;jsessionid=2501AC9399172532EFC5FFFABE8B0B68.live11053?nn=17626. [Zugriff am 11 July 2025].

[74] Deutscher Wetterdienst (DWD), „Index of /climate_environment/CDC/observations_germany/climate/10_minutes/air_temperature/historical/,“ 2025. [Online]. Available: https://opendata.dwd.de/climate_environment/CDC/observations_germany/climate/10_minutes/air_temperature/historical/. [Zugriff am 1 November 2024].

[75] Freie und Hansestadt Hamburg, „Bescheibungen der Messstationen,“ 2025. [Online]. Available: https://www.hamburg.de/politik-und-verwaltung/behoerden/bukea/hu/umweltuntersuchungen/wasseruntersuchungen/wassergutemessnetz/messstationen-des-wgmn. [Zugriff am 1 November 2024].

[76] Blohm, Werner w.f.r. Institut für Hygiene und Umwelt, „2024,“ [Online]. Available: https://www.hamburg.de/politik-und-verwaltung/behoerden/bukea/hu/umweltuntersuchungen/wasseruntersuchungen/wassergutemessnetz/messstationen-des-wgmn.

[77] Deutscher Wetterdienst, „Index of /climate_environment/CDC/observations_germany/climate/10_minutes/air_temperature/historical/,“ 2024. [Online]. Available:

https://opendata.dwd.de/climate_environment/CDC/observations_germany/climate/10_minutes/air_temperature/historical/.

[78] T. e. a. Ommen, „Comparison of COP estimation methods for large-scale heat pumps used in energy planning," *Energy,* 15 August 2020.

[79] Hamburger Energiewerke GmbH, „Technische Anschlussbedingungen [TAB-Stadtnetz]," 2025. [Online]. Available: https://mediafra.admiralcloud.com/customer_624/8f49b77a-f889-4f37-ae99-ebe4f1ef582a?response-content-disposition=inline%3Bfilename*%3DUTF-8%27%27TAB_Stadtnetz.pdf&Expires=1752282479&Key-Pair-Id=K3XAA2YI8CUDC&Signature=dPxjnl2mKD3IbjzulkIZJNBNtw5syQ6UJXcFr. [Zugriff am 12 July 2025].

[80] M. Wilcke, „Diese XXL-Pumpe soll Hamburgs Wärmeversorgung revolutionieren," 7 July 2025. [Online]. Available: https://www.mopo.de/hamburg/diese-xxl-pumpe-soll-hamburgs-waermeversorgung-revolutionieren/. [Zugriff am 15 July 2025].

[81] D. Eller, Integration erneuerbarer Energien mit Power-to-Heat in Deutschland, Wiesbaden: Springer Vieweg, 2015.

[82] BDEW Bundesverband der Energie- und Wasserwirtschaft e.V/VKU Verband kommunaler Unternehmen e. V./GEODE, „BDEW/VKU/GEODELeitfaden," 22 March 2024. [Online]. Available: https://filehub.admiralcloud.com/v5/deliverFile/387dc7f8-098a-41e8-9d1a-3655eeb4a1d9?download=true. [Zugriff am 11 July 2025].

[83] Deutscher Wetterdienst w.f.r. Kai Biermann, *Beschreibung der Gasprognosetemperatur (GPT),* Deutscher Wetterdienst, 2022.

[84] Deutscher Wetterdienst DWD, „Model Output Statistics-MIX (MOSMIX)," 2025. [Online]. Available: https://www.dwd.de/DE/leistungen/met_verfahren_mosmix/met_verfahren_mosmix.html. [Zugriff am 25 12 2024].

[85] D. w. H. E. G. Jahns, Interviewee, *Energiedatenmanagement Betrieb Gasnetz Hamburger Energienetze GmbH.* [Interview]. 13 12 2024.

[86] Forschungsgesellschaft für Energiewirtschaft mbH (FfE), „Weiterentwicklung des Standardlastprofilverfahrens Gas," July 2015. [Online]. Available: https://www.ffe.de/wp-content/uploads/2022/08/Studie_Weiterentwicklung-SLP-Gas_FfE.pdf. [Zugriff am 10 January 2025].

[87] Statistische Amt für Hamburg und Schleswig-Holstein (Statistikamt Nord), „Dokumentenansicht," [Online]. Available: https://www.statistik-nord.de/zahlen-fakten/umwelt-energie/energie/dokumentenansicht/product/3381/energie-und-co2-bilanzen-fuer-hamburg-361?cHash=4201529a752424c94a05eb3c4ae751ea. [Zugriff am 2 May 2025].

[88] M. Hellwig, „Entwicklung und Anwendung parametrisierter Standard-Lastprofile," TU München, München, 2003.

[89] M. a. G. B. Hellwig, „Entwicklung von Lastprofilen für die Gaswirtschaft im Auftrag des Bundesverbandes der deutschen Gas- und Wasserwirtschaft e.V. und des Verbandes kommunaler Unternehmen e.V. - Gewerbe, Handel und Dienstleistung," TU München, München, 2002.

[90] M. a. G. B. Hellwig, „Entwicklung von Lastprofilen für die Gaswirtschaft im Auftrag des Bundesverbandes der deutschen Gas- und Wasserwirtschaft e.V. und des Verbandes kommunaler Unternehmen e.V. - Haushalte," TU München, München, 2002.

[91] BGW and VKU, „Abwicklung von Standardlastprofilen," 2007. [Online]. Available: https://www.eichsfeldwerke.de/fileadmin/user_upload/Praxisinformation_P2007_13.pdf. [Zugriff am 2025 June 25].

[92] Statistisches Amt für Hamburg und Schleswig-Holstein (Statistikamt Nord), „Energiebilanz und CO2-Bilanzen für Hamburg 2023," Dezember 2024. [Online]. Available: https://www.statistik-nord.de/fileadmin/Dokumente/EB_CO2_HH_2023.pdf. [Zugriff am 10 March 2025].

[93] A. Blinn, „Sektorengekoppeltes Energiemodell (UCB -SEnMod)," 24 August 2021. [Online]. Available: https://www.researchgate.net/profile/Alexander-Blinn/publication/359893882_Mathematische_Modellierung_und_Simulation_von_Energieclustern_und_Entwicklung_eines_vollstandigen_Energienutzungsmodells_fur_den_europaischen_Strom-_Warme-_und_Verkehrssektor/links. [Zugriff am 10 February 2025].

[94] M. a. W. J. Berger, „A novel approach for estimating residential space heating demand," *Energy,* 2018.

[95] W. e. a. Heitkoetter, „Regionalised heat demand and power-to-heat capacities in Germany – An open dataset for assessing renewable energy integration," *Applied Energy,* 2020.

[96] S. e. a. Ortner, „Analyse des wirtschaftlichen Potenzials für eine effiziente Wärme- und Kälteversorgung," June 2021. [Online]. Available: https://www.umweltbundesamt.de/sites/default/files/medien/1410/publikationen/2021-08-05_cc_54-2021_effiziente_waerme-kaelteversorgung.pdf. [Zugriff am 10 June 2025].

[97] O. e. a. Ruhnau, „Time series of heat demand and heat pump efficiency for energy system modeling,“ *Scientific Data,* 1 October 2019.

[98] Bundesnatzagentur (BNetzA), „Market - Day-ahead prices,“ 2025. [Online]. Available: https://www.smard.de/page/en/marktdaten/5542?marketDataAttributes=%7B%22resolution%22:%22hour%22,%22from%22:1679094000000,%22to%22:1680299999999,%22moduleIds%22:%5B8004169%5D,%22selectedCategory%22:8,%22activeChart%22:false,%22style%22:%22color%22,%22cate. [Zugriff am 10 June 2025].

[99] Hamburger Energienetze GmbH, „Aktueller Verlauf von Stromerzeugung und Last in Hamburg,“ 2025. [Online]. Available: https://www.energieportal-hamburg.de/. [Zugriff am 13 July 2025].

[100] H. Pitsch, „Thermodynamik I - Einführung und Allgemeine Grundlagen,“ Aachen.

[101] H. a. K. S. Baehr, Thermodynamik - Grundlagen und technische Anwendungen, 15th Hrsg., Berlin/Heidelberg, Germany: Springer Vieweg, 2012.

[102] H. Ambarita, „The optimum intermediate pressure of two-stages vapor compression refrigeration cycle for Air-Conditioning unit,“ *Journal of Physics,* 2018.

[103] C. e. a. Höges, „Decarbonizing Steam Generation with High Temperature Heat Pumps: Refrigerant Selection and Flowsheet Evaluation,“ May 2023. [Online]. Available: https://www.researchgate.net/publication/371314235_Decarbonizing_Steam_Generation_with_High_Temperature_Heat_Pumps_Refrigerant_Selection_and_Flowsheet_Evaluation. [Zugriff am 14 July 2025].

[104] AIT, Austrian Insitute of Technology GmbH, „FME HighEFF - Centre for an Energy Efficient and Competitive Industry for the Future,“ January 2017. [Online]. Available: https://www.sintef.no/globalassets/project/higheff/deliverables-ra3/d3.2_2017.01-feasibility-study-on-high-temperature-heat-pump-to-200-degc.pdf?utm_source=chatgpt.com. [Zugriff am 4 June 2025].

[105] B. e. a. Hu, „Exergy analysis of R1234ze(Z) as high temperature heat pump working fluid with multi-stage compression,“ November 2017.

[106] X. e. a. Jin, „Performance analysis of a two-stage vapor compression heat pump based on intercooling effect,“ *Case Studies in Thermal Engineering ,* 2023.

[107] K. e. a. Filipan, „Influence of Condensing Temperature on Heat Pump Efficiency,“ 16 October 2010. [Online]. Available: https://www.davidpublisher.com/Public/uploads/Contribute/55e42128bbbff.pdf. [Zugriff am 26 July 2025].

[108] M. J. Fritz, „heatpumps," 2025. [Online]. Available: https://heatpumps.streamlit.app/. [Zugriff am 20 June 2025].

[109] V. Venzik, „Dissertation - Experimentelle Untersuchung des Fluideinflusses auf die Thermodynamik der Wärmepumpe: Kohlenwasserstoffe und deren Gemische," 25 October 2019. [Online]. Available: https://duepublico2.uni-due.de/servlets/MCRFileNodeServlet/duepublico_derivate_00070713/Diss_Venzik.pdf. [Zugriff am 14 July 2025].

[110] M. A. F. Blesl, „Transformation und Rolle der Wärmenetze," 2023. [Online]. Available: https://ariadneprojekt.de/media/2023/04/Ariadne-Analyse_Waermenetze_April2023.pdf. [Zugriff am 26 July 2025].

[111] C. e. a. Arpagaus, „Industrial Heat Pumps: Technology readiness, economic conditions, and sustainable refrigerants," 11 July 2023. [Online]. Available: https://www.aceee.org/sites/default/files/pdfs/IHP_Workshops_2023/Cordin_Arpagaus_-_OST.pdf?utm_source=chatgpt.com. [Zugriff am 14 July 2025].

[112] H. a. H. I. C. G. (. Pieper, „COP in Großwärmepumpen in Abhängigkeit von Netztemperaturen, Wärmequellen und Kältemitteln," VDI Wissensforum, 2024.

[113] F. e. a. Bless, „High temperature heat pumps: Market overview, state of the art, research status, refrigerants, and application potentials," *Energy,* June 2018.

[114] T. e. a. El Samad, „A review of compressors for high temperature heat pumps," Bd. Thermal Science and Engineering Progress, 2024.

[115] 50Hertz Transmission GmbH/Amprion GmbH/TenneT TSO GmbH/TransnetBW GmbH, „Szenariorahmen zum Netzentwicklungsplan Strom 2037/2045, Version 2025," 2024. [Online]. Available: https://www.netzentwicklungsplan.de/sites/default/files/2024-07/Szenariorahmenentwurf_NEP2037_2025.pdf. [Zugriff am 14 July 2025].

[116] Bundesministerium für Wirtschaft und Klimaschutz, „Speicher für die Energiewende," [Online]. Available: https://www.bundeswirtschaftsministerium.de/Redaktion/DE/Downloads/S-T/speicher-fuer-die-energiewende.pdf?__blob=publicationFile&v=6. [Zugriff am 10 July 2025].

[117] J. Dohmann, Thermodynamik der Kälteanlagen und Wärmepumpen, Berlin Heidelberg: Springer Vieweg, 2016.

[118] G. a. K. J. Lauth, Thermodynamik - Eine Einführung, Berlin Heidelberg: Springer-Verlag, 2015.

[119] D. Paczona, „Simulation und Vermessung einer R744 - Kompressionskalteanlage/Wärmepumpe fur Kraftfahrzeuge," 7 October 2018. [Online]. Available: https://unipub.uni-graz.at/obvugrhs/content/titleinfo/3290442/full.pdf. [Zugriff am 9 July 2025].

[120] E. Union, „Verordnung (EG) Nr. 1005/2009 des Europäischen Parlaments und des Rates vom 16. September 2009 über Stoffe, die zum Abbau der Ozonschicht führen (Neufassung) (Text von Bedeutung für den EWR)," Brüssel, 2009.

[121] E. Union, „Verordnung (EU) 2024/573 des Europäischen Parlaments und des Rates vom 7. Februar 2024 über fluorierte Treibhausgase, zur Änderung der Richtlinie (EU) 2019/1937 und zur Aufhebung der Verordnung (EU) Nr. 517/2014 (Text von Bedeutung für den EWR)," Brüssel, 2024.

[122] G. a. H. T. Dünnwald, Wärmepumpen, Düsseldorf, germany: VDI, 1996.

[123] M. e. a. Jesper, „Large-scale heat pumps: Uptake and performance modelling of market-available devices," *Renewable and Sustainable Energy Reviews ,* 2021.

[124] W. W. f. U. K. E. u. A. Blohm, „Daten des WGMN," Hamburg, 2024.

[125] Bundesministerium der Justiz und für Verbraucherschutz (BMJV), „Verordnung über den Zugang zu Gasversorgungsnetzen (Gasnetzzugangsverordnung - GasNZV) § 24 Standardlastprofile," 2025.

[126] K. Deutscher Wetterdienst and Biermann, „Beschreibung der Gasprognosetemperatur (GPT)," 2022.

[127] Bundesministerium der Justiz und für Verbraucherschutz, „Gesetz über die Elektrizitäts- und Gasversorgung," 2025. [Online]. Available: https://www.gesetze-im-internet.de/enwg_2005/index.html#BJNR197010005BJNE019605377. [Zugriff am 14 July 2025].

[128] Bundesministerium der Justiz und für Verbraucherschutz, „Gesetz zur Finanzierung der Energiewende im Stromsektor durch Zahlungen des Bundes und Erhebung von Umlagen (Energiefinanzierungsgesetz - EnFG)," 2025. [Online]. Available: https://www.gesetze-im-internet.de/enfg/__22.html#:~:text=%C2%A7%2022%20Umlageerhebung%20bei%20elektrisch,mit%20dem%20Netz%20verbunden%20ist.. [Zugriff am 14 July 2025].

[129] Bundesministerium der Justiz und für Verbraucherschutz, „Verordnung über die Entgelte für den Zugang zu Elektrizitätsversorgungsnetzen (Stromnetzentgeltverordnung - StromNEV) § 19 Sonderformen der Netznutzung," 2025. [Online]. Available: https://www.gesetze-im-internet.de/stromnev/__19.html. [Zugriff am 14 July 2025].

[130] Bundesministerium der Justiz und für Verbraucherschutz, „Verordnung über die Entgelte für den Zugang zu Elektrizitätsversorgungsnetzen," 2025. [Online]. Available: https://www.gesetze-im-internet.de/stromnev/index.html#BJNR222500005BJNE004308377. [Zugriff am 14 July 2025].

[131] Bundesministerium der Justiz und für Verbraucherschutz (BMJV), „Gesetz für die Wärmeplanung und zur Dekarbonisierung der Wärmenetze (Wärmeplanungsgesetz - WPG) § 4 Pflicht zur Wärmeplanung," 2025. [Online]. Available: https://www.gesetze-im-internet.de/wpg/__4.html. [Zugriff am 9 July 2025].

[132] Bundesministeriumder Justiz und für Verbraucherschutz (BMJV), „Gesetz zur Steigerung der Energieeffizienz in Deutschland 1 (Energieeffizienzgesetz - EnEfG) § 4 Energieeffizienzziele," 2025. [Online]. Available: https://www.gesetze-im-internet.de/enefg/__4.html. [Zugriff am 9 July 2025].

[133] Bundesminsterium der Justiz und für Verbraucherschutz (BMJV), „Gesetz zur Steigerung der Energieeffizienz in Deutschland 1 (Energieeffizienzgesetz - EnEfG) § 4 Energieeffizienzziele," 2025. [Online]. Available: https://www.gesetze-im-internet.de/enefg/__4.html. [Zugriff am 9 July 2025].

9 Appendix

A Process of Data Generation for District Heat Demand

To create new data series two class, 'SLP_simulation_conditions' and 'SLP' are used.

Table 4 shows the essential attributes of the objects of the class 'SLP_simulation_conditions'.[12]

Table 4: Overview of essential settings for the heat demand time series

Attribute	Description
demand_in_kWh_households	The annual district heat demand from households in kWh
demand_in_kWh_GHD	The annual district heat demand from commercial customers in kWh
demand_year	The year in which the heat consumption took place
KW_year	The year on which the KW-values for gas consumption are based on (should be the same as the weather year in an ideal case)
weather_year	The year from which the daily ambient temperatures are taken (should be the same as the demand year in an ideal case)
location	the location of the measurement station from where the weather data are taken

In Table 5 the essential attributes of the objects of the class 'SLP' are listed.

Table 5: Key attributes of a SLP object

Attribute	Description
code_long	Long abbreviation code for SLP according to the guidelines
name	Name of SLP used in the guidelines
type	Type of SLP according to the guidelines
A, B, C, D, T0, mh, bh, mw, bw	Profile parameters to calculate the function value h
dic_dayfactor	Dictionary containing the daily factors F_{day} for every day of the week
KW_year	Year in which the KW-values determining the consumption of the SLP has been recorded
dic_KW	Dictionary containing the KW-values of the SLP for every month of the year[13]

[12] The class objects contain additional attributes that offer further configuration options, but these were not used for generating the district heat consumption time series in this work, but also not removed afterwards.
[13] Here the use of an annual KW-value would be even more accurate

dic_df_hourly_factors	Dictionary containing data frames for every day of the week which in turn contain the hourly factors in percent

Utilizing the class ‘SLP_simulation_conditions’ and the class ‘SLP’ the data for the heat demand time series are generated according to the flowchart in Figure 68.

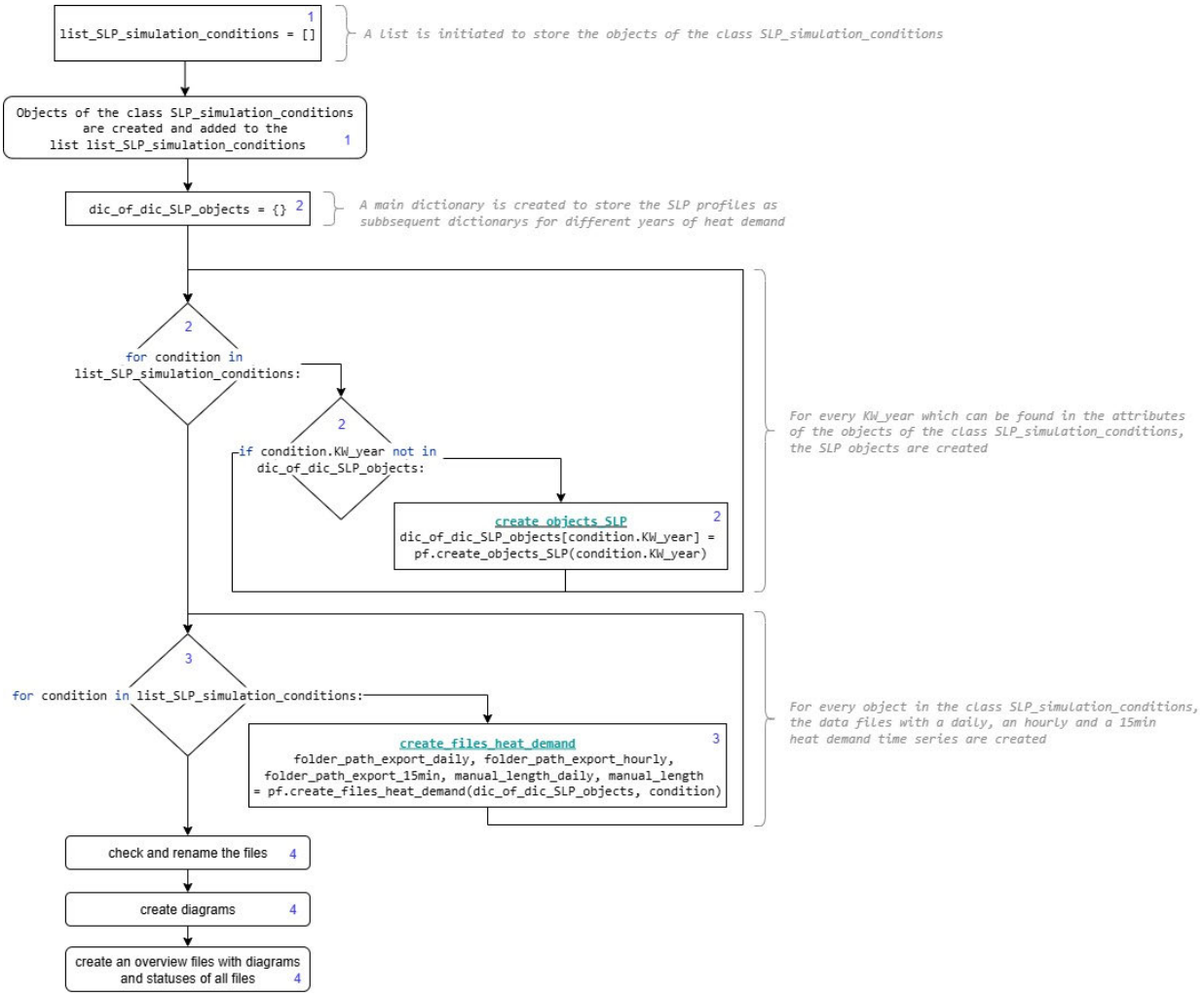

Figure 68: General structure to create heat demand time series

First the objects which describe the different simulation conditions are added to a list (step 1). Then the SLP objects which are relevant, that means they fit to the attribute ‘KW-year’ of at least one simulation condition object, are created with the function ‘create_objects_SLP’ (step 2). The function imports the parameters and KW-values of the SLP objects stored in Excel files and assigns them to the attributes of the SLP objects to be created. To better access the SLP objects, they are stored in a further memory structure. To do so a parent dictionary ‘dic_of_dic_SLP_objects’ is initiated, as shown in Figure 69.

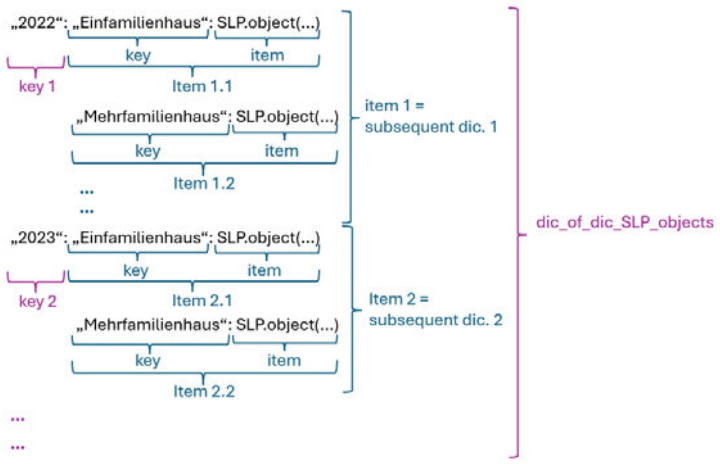

Figure 69: Memory structure to create multiple heat demand time series

The years which have been found in the attributes ‘KW_year’ of the objects for the simulation conditions are set as keys of the parent dictionary. The assigned item of every key is a subsequent dictionary which in turn contains all SLP objects as items. All items, SLP objects, of a subsequent dictionary fit to the relevant year which means to the key inside the parent dictionary. The SLP objects are stored as items of the subsequent dictionaries by setting their attribute ‘name’ as their key in the subsequent dictionary. Thus, every subsequent dictionary contains all SLPs as items for its corresponding year given in the key of the parent dictionary. After creating the SLP objects the data files containing the time series of the heat demand in a daily, hourly and 15-minute resolution can be generated for every simulation condition calling the function ‘create_files_heat_demand’ by iterating every object of simulation conditions (step 3). The data generation of the 15-minute district heat consumption time series for one object of simulation conditions due to the function ‘create_files_heat_demand’ is carried out as described above. The simplified process is illustrated in Figure 70.

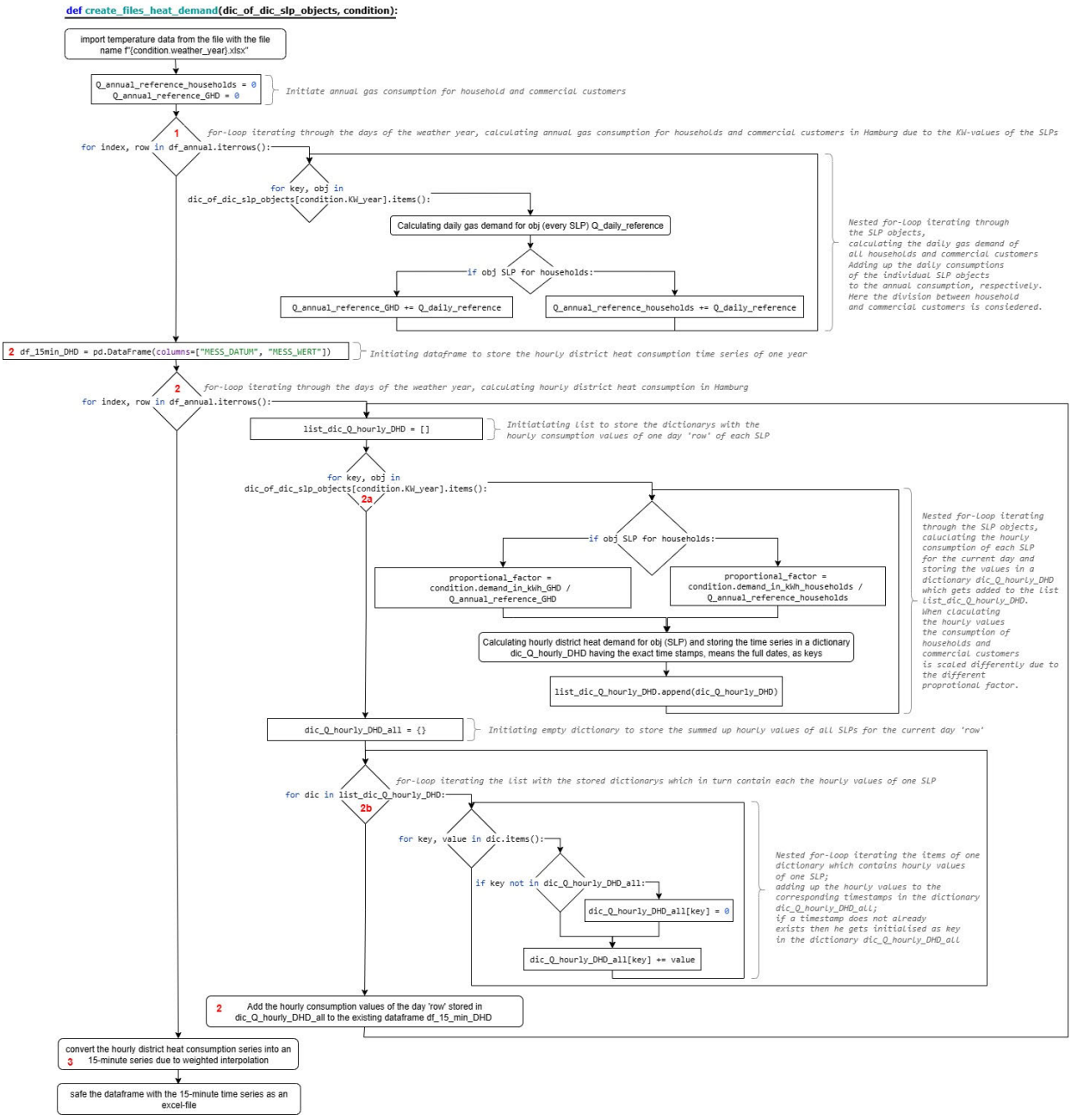

Figure 70: Generation of heat demand data time series